Constraining the Active Tectonic Deformation of Andaman-Nicobar Arc in the Background of December 26, 2004 Great Sumatra-Andaman Earthquake

Anil Earnest

Thesis submitted to the Faculty of Marine Sciences,
Cochin University of Science and Technology
in partial fulfillment of the requirements for the
degree of Doctor of Philosophy.

May 2007

Declaration

I, Anil Earnest, do hereby declare that the thesis entitled **"Constraining the active tectonic deformation of Andaman-Nicobar Arc in the background of December 26, 2004 Great Sumatra-Andaman Earthquake"**, is an authentic record of the doctoral research work carried out by me at Centre for Earth Science Studies (CESS), Kerala, Trivandrum, India, under the guidance of Dr. C.P. Rajendran, Scientist, CESS, in partial fulfillment of the requirements for the award of degree in Doctor of Philosophy from Cochin University of Science and Technology, Kerala, India, and no part of this work has previously formed the award of any other degree, diploma or associateship in any university or other institute of learning.

Trivandrum

May 29, 2007

Anil Earnest

Certificate

I hereby certify that the thesis entitled, **"Constraining the active tectonic deformation of Andaman-Nicobar Arc in the background of December 26, 2004 Great Sumatra-Andaman Earthquake"**, is a genuine research work done by Mr. Anil Earnest under my guidance and supervision. I further certify that this thesis or part thereof has not been the basis for the award of any degree or diploma.

Trivandrum
May 29, 2007

Dr. C.P. Rajendran
Scientist
Centre for Earth Science Studies
Trivandrum, Kerala
India – 695 031

Acknowledgements

I take this opportunity to express my sincere gratitude and thanks to my thesis supervisor Dr. C.P. Rajendran, Scientist, Centre for Earth Science Studies (CESS), under whose able guidance this research work was made possible and without which this thesis would not have come into existence. This work was inspired by a chance meeting with him during my graduation days at Cochin University of Science and Technology. Hope I emulated you well.

I am deeply indebted to Dr. Kusala Rajendran, Scientist, CESS, who guided me throughout the entire course work. You have inspired me a lot.

I am very grateful to Dr. M. Baba, Director, CESS, for the opportunity he gave me to carry out this work at CESS.

I am thankful to Dr. M. Radhakrishna, Reader, CUSAT for his timely advices as part of my doctoral commitee.

I express my sincere thanks to Dr. C.M. Harish, Scientist, CESS who introduced and taught me some of the analysis techniques and the processing methodologies involved in this work. I am most grateful to him for his patience and the time he offered.

I wish to place on record my gratitude to the whole team of scientists and staff of CESS for their support and helping hand in completion of this work at various stages.

I would like to express my heartfelt gratitude to Ms. Priya Rani, for her kind words and encouragement.

Words are not enough to express my gratitude and love to all my friends especially Mr. S.K. Arun, Dr. Girish Gopinath, Dr. Reji Srinivas, Dr. Ajith G. Nair, Dr. P.S. Sunil, Mr. Abin Philip, Mr. M.J. Jobin, Dr. K.R. Baiju, Mr. K.J. Thomson and Mr. V.T. Muralikrishana for being constant source of encouragement and for your kind prayers. Moments were there, without you people, I would have left this chapter closed very long back. I owe you people a lot!.

I would like to acknowledge Ms. Anu Rahul, for the constant support and help she offered. I hope this work will inspire you to greater efforts.

The entire work involved extensive field studies in the Andaman-Nicobar Islands. I am indebted to all who helped me in carrying out these field works, especially in the tsunami hit Nicobars. Due regards to Prof. P.M. Mohan, Mr. R. Devdas, Mr. G.M. Arun, Mr. Chandu Das and Mr. Sowik Banerjee for helping me out in some of the pre-earthquake surveys. Special thanks to Mr. M.K. Vellan, Assistant Engineer, Andaman Public Works Department. You have been very kind to me and helped me a lot in carrying out the work in Nicobars just after the tsunami.

Due thanks for Department of Science and Technology, Government of India, and CESS for funding this work. Special thanks to Prof. K.S. Valdiya, Jawaharlal Nehru Centre for Advanced Studies and Research, Bangalore for his special interest and support he offered for this work.

I like to place on record, my due thanks to the directors of Indian Institute of Geo-magnetism; Mumbai, Centre for Mathematical Modelling and Computer Simulation (C-MMACS); Bangalore, National Geophysical Research Institute; Hyderabad and National Transportation Planning and Research Centre (NATPAC);

Trivandrum for lending out their instruments at various stages of this study.

Also, I would like to place on record my gratitude to Dr. Gangan Pratap, Scientist in Charge, C-MMACS, Bangalore for allowing me to continue to work on this thesis after joining there.

Thanks to all GAMIT/GLOBK developers for providing it free of cost for research purpose. Special thanks to Prof. Tom Herring, MIT for sparing his valuable time, to answer some of my questions (Now I understand that most of them were very silly ones!). Due regards to Prof. Jeffrey Freymueller, University of Alsaka in helping me out in sorting out the problems related with the data processing, and for the fault dislocation models. Due regards to Prof. McCaffrey, Rensselaer Polytechnic Institute, New York for making his "DEFNODE" deformation modelling program and its tutorials freely available over internet.

Most of the figures in this thesis are created using GMT, an open source mapping and visualization software. Text processing and layout for this thesis are done using LaTeX.

And, last, but not the least, I thank my parents for their love, keen interest, encouragement and moral support they offered throughout this work.

Executive Summary

The Andaman-Nicobar Islands in the Bay of Bengal lies in a zone where the Indian plate subducts beneath the Burmese microplate, and therefore forms a belt of frequent earthquakes. Few efforts, not withstanding the available historical and instrumental data were not effectively used before the M_W 9.3 Sumatra-Andaman earthquake to draw any inference on the spatial and temporal distribution of large subduction zone earthquakes in this region. An attempt to constrain the active crustal deformation of the Andaman-Nicobar arc in the background of the December 26, 2004 Great Sumatra-Andaman megathrust earthquake is made here, thereby presenting a unique data set representing the pre-seismic convergence and co-seismic displacement.

Understanding the mechanisms of the subduction zone earthquakes is both challenging scientifically and important for assessing the related earthquake hazards. In many subduction zones, thrust earthquakes may have characteristic patterns in space and time. However, the mechanism of mega events still remains largely unresolved.

Large subduction zone earthquakes are usually associated with high amplitude co-seismic deformation above the plate boundary megathrust and the elastic relaxation of the fore-arc. These are expressed as vertical changes in land level with the up-dip part of the rupture surface uplifted and the areas above the down-dip edge subsided. One of the most characteristic pattern associated with the inter-seismic era is that the deformation is in an opposite sense that of co-seismic period.

This work was started in 2002 to understand the tectonic deformation along the Andaman-Nicobar arc using seismological, geological and geodetic data. The occurrence of the 2004 megathrust earthquake gave a new dimension to this study, by providing an opportunity to examine the co-seismic deformation associated with the greatest earthquake to have occurred since the advent of Global Positioning System (GPS) and broadband seismometry.

The major objectives of this study are to assess the pre-seismic stress regimes, to determine the pre-seismic convergence rate, to analyze and interpret the pattern of co-seismic displacement and slip on various segments and to look out for any possible recurrence interval for megathrust event occurrence for Andaman-Nicobar subduction zone. This thesis is arranged in six chapters with further subdivisions dealing all the above aspects.

Table of Contents

List of Tables

List of Figures

Chapter 1

General introduction

1.1 Introduction

The Andaman-Nicobar archipelago, arcuate melange of the Indo - Burmese collision, has been a source of many major earthquakes. However, the 2004 M_W 9.3 earthquake is unprecedented by breaking of the entire 1300 km long Sumatra-Andaman plate boundary (Stein and Okal, 2005; Ishii et al., 2005; Ni et al., 2005; Lay et al., 2005; Banerjee et al., 2005; Vigny et al., 2005; Meltzner et al., 2006). In this study, an attempt is made to investigate the active tectonic deformation of the Andaman-Nicobar subduction zone (5-15^{0}N and 92-98^{0}E) in the background of the Great Sumatra-Andaman earthquake.

1.2 Rationale

Subduction zones, regions on the earth where one tectonic plate slides under another (Fig. 1.1), are marked by a variety of earthquakes viz., inter-plate, megathrust, intra-plate and deep earthquakes (Fig. 1.2). These earthquakes differ in their occurrence in terms of time, space, size and mechanism (Venkataraman and Kanamori, 2004; Conrad et al., 2004). Shallow thrust subduction zone earthquakes release almost 90% of global seismic moment energy released annually (Kanamori, 1977). These earthquakes mainly occur on the plate interface at depths that vary from 5 to 50 km (Pacheco et al., 1993), are basically generated by the horizontal density contrasts within the plate due to the cooling and thickening of the oceanic

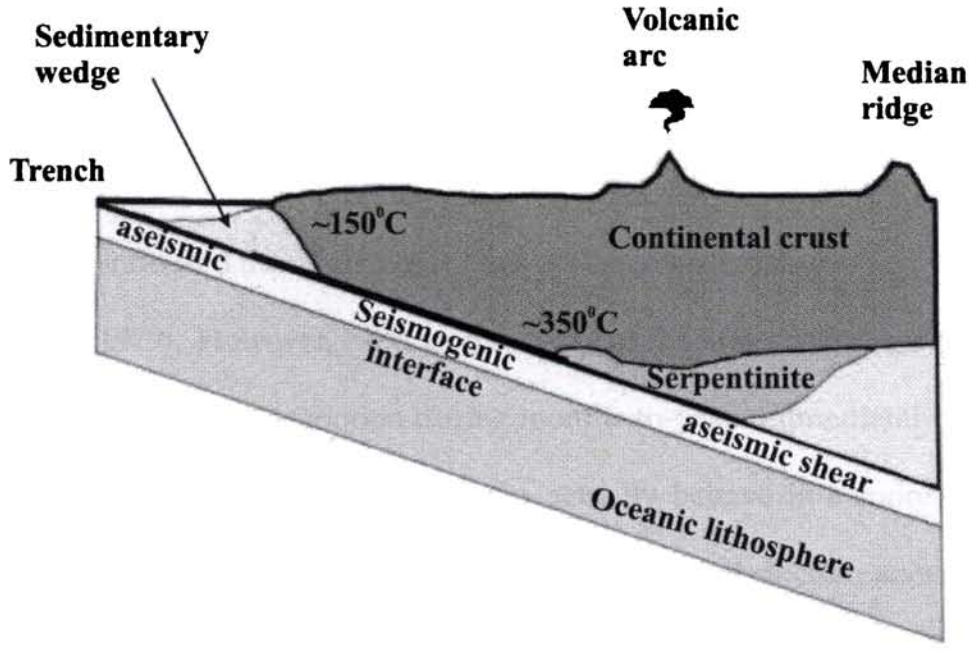

Figure 1.1: Schematic cross section of a subduction zone showing its first order geometry and features, modified from Burgmann, 2005.

lithosphere and negative buoyancy of the subducted oceanic lithosphere (Ruff and Kanamori, 1980; Stern, R.J., 2002). Major driving forces behind the subduction are the slab pull and the ridge push forces (Spence, 1987; Lallemand et al., 2005) (Fig. 1.3).

To a first order approximation, subduction zone features a locked zone (5-10 to 30-50 km in depth), that is bounded up-dip and down-dip by portions of the fault that deform aseismically (Savage, 1983). The inter-seismic phase is marked by the gradual sinking of the subducting slab, increasing the extensional stresses at depths and leading to shortening of the upper colliding plate that manifest as a coastal uplift (Fig. 1.4.a). Finally, the stress originating due to the ridge push and slab pull forces, exceeds the strength of the locked interface, resulting in an earthquake. Co-seismically the region near the plate boundary is uplifted and the

arc-ward edge of the subducting slab drags down resulting in coastal subsidence (Plafker, 1972) (Fig. 1.4.b).

Observations from some of the subduction zones decades before and after earthquakes, have indicated the robustness of this earthquake deformation cycle (Thatcher and Rundle, 1979). However, exponential decay of the aftershocks and the long-term transient post-seismic motion during months-to-years immediately after the earthquake indicate that subduction zones actually behave in a more complex manner. It has also been noted that the rupture in the subduction zones are not always segment specific. There are earthquakes that break shorter segments and those that break through major portions of the plate boundary (Fig. 1.5). Thus longer segment of a subduction zone may rupture in a single megathrust earthquake, instead of smaller rupture segments spaced out in time (Kanamori and Mcnally, 1982).

The extent and termination of rupture are restricted and controlled by invariant physical properties of the fault zone such as geometric and/or material heterogeneity along the arc (Schwartz, 1999) which form the basis of the theory of seismic asperites (Kanamori and Brodsky., 2004). Asperites are the unbroken portions of high strength within a fault that breaks during an earthquake (Lay et al., 1982). An alternative way to explain these earthquakes was given by Aki (1979) who introduced the concept of barriers as regions within a fault plane that arrests rupture. The asperites and barriers vary spatially and temporally along the strike, and dip reflecting variations in strength along the seismogenic zone (Kelleher and McCann, 1976).

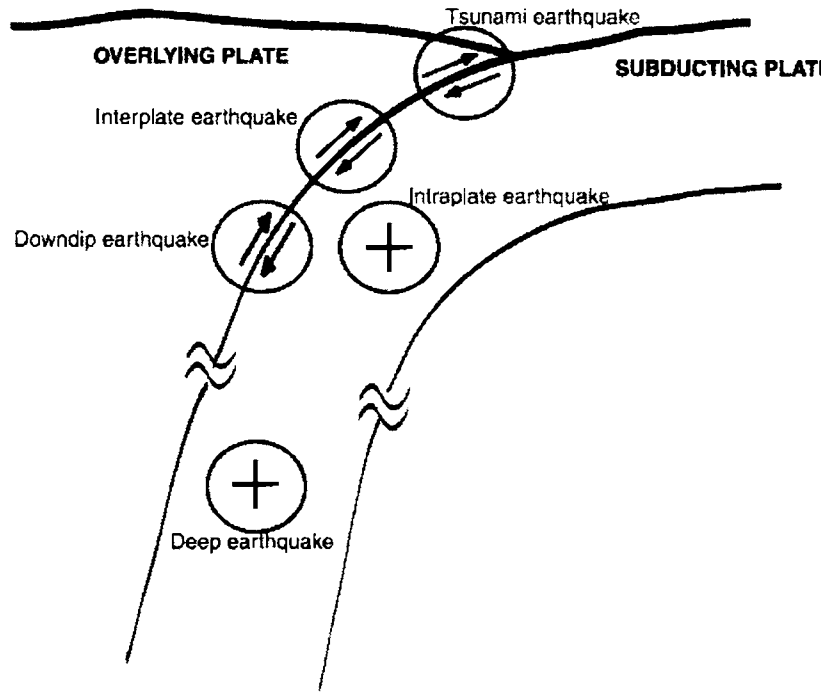

Figure 1.2: Cartoon showing different types of subduction zone earthquakes relative to the subducting slab (Venkataraman and Kanamori, 2004).

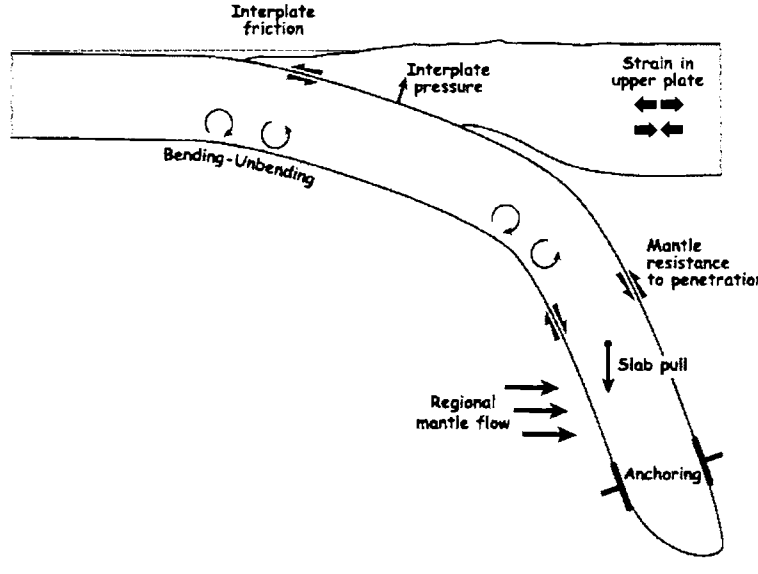

Figure 1.3: Major forces acting in a subduction zone, modified from Spence, 1987 and Lallemand et al., 2005.

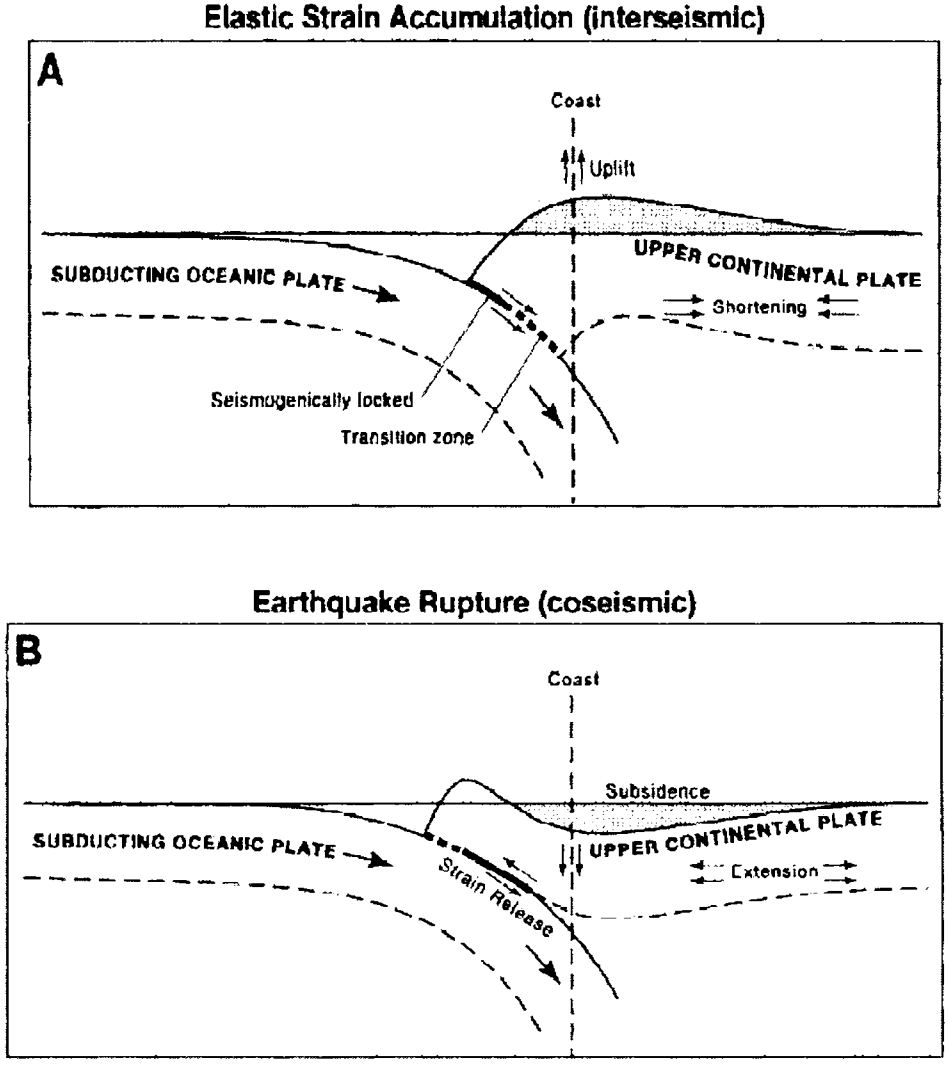

Figure 1.4: Subduction zone earthquake deformation cycle - A) The cycle begin with the inter-seismic strain accumulation in the upper plate above a locked part of the plate boundary. B) Accumulated strain is released through slip on the locked zone during the co-seismic part of the cycle. During large earthquakes region nearest to the plate boundary is uplifted; and the arc-ward of the zone suddenly subsides (Plafker, 1972, Ando, 1975, Nelson et al., 1996).

1.3 The problem

How do thrust earthquakes release the accumulated plate motion is a question that is scientifically challenging and important for assessing earthquake hazards. In many subduction zones, thrust earthquakes display characteristic patterns in space and time. For example, large earthquakes have occurred in the Nankai trough area of southern Japan approximately every 125 years since 1498 with similar fault areas (Anto, 1975). In some cases the entire region had slipped at once; in others, slip was divided into several events over a few years. Given such repeatability, it seems likely that a segment of a subduction zone that has not slipped for some time constitutes a seismic gap and is due for an earthquake (Fig. 1.5). Partial and complete rupture of plate boundary zones, over a time window, puts forth a question on recurrence of such mega event generation, and still remains an enigma.

If the stress rate is constant and known, and both the failure stress and the final stress remain unchanged for successive earthquakes, the displacement and recurrence time of future events will be identical and predictable. This first approximation called the uniform earthquake model is bound by the elastic rebound theory (Reid, 1910). It assumes a perfect periodicity, where the strain accumulates during a long inter-seismic phase until a yield point is reached, where upon energy is released (earthquake) as the locked surface suddenly slips (Fig. 1.6.a). The time predictable model (Shimazaki and Nakata, 1980; Murray and Segall, 2002) assumes that if the failure stress remains constant then the time to next earthquake

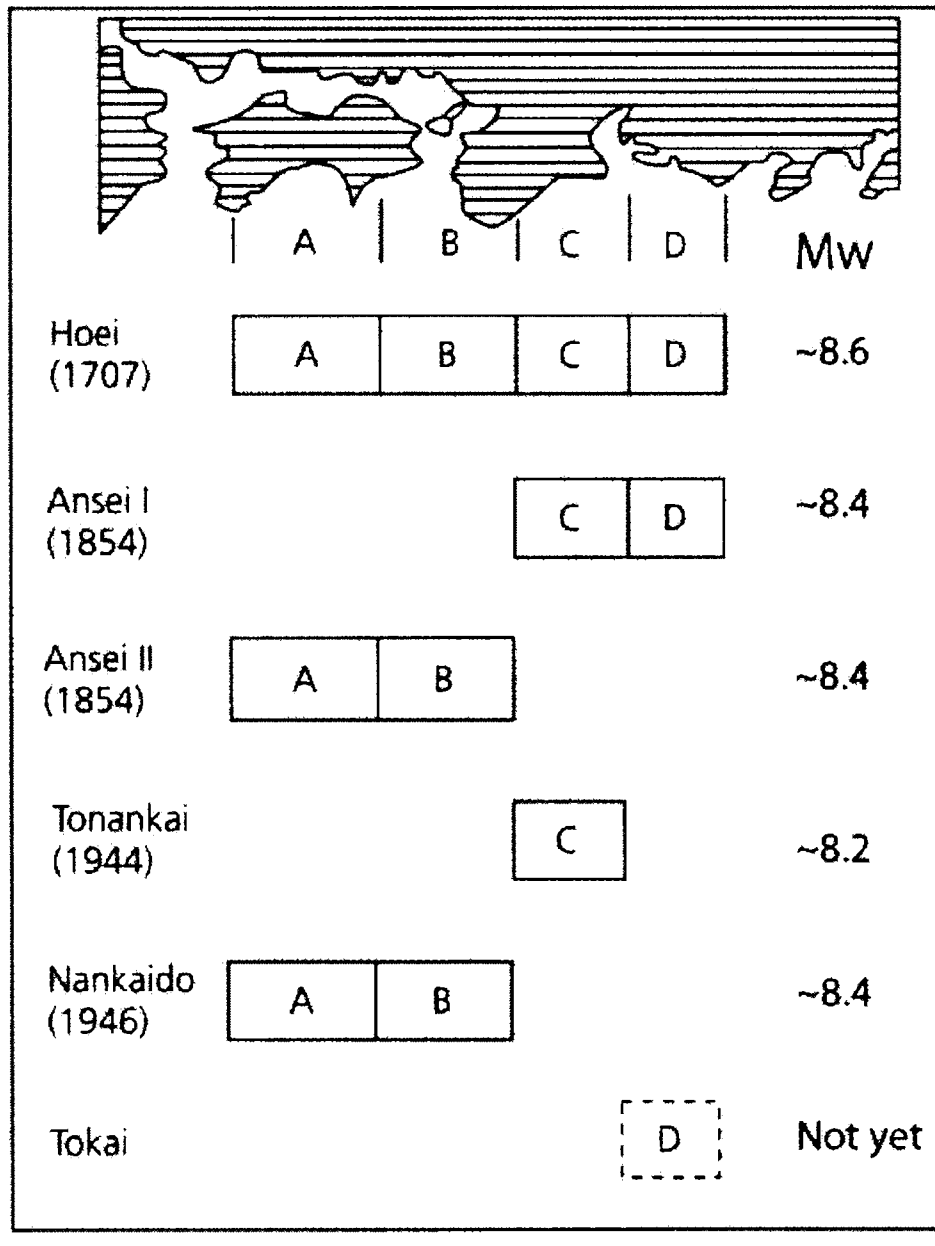

Figure 1.5: History of earthquakes along the Nankai trough. The region is divided into four rupture zones (A-D). In some earthquakes the entire region has slipped at once; in others, slip was divided into several events over a few years. Given such repeatability, it seems likely that a segment of a subduction zone that has not slipped for some time constitutes a seismic gap and is due for an earthquake (Shimazaki and Nakata, 1980).

can be calculated based on the stress drop of the preceding event (Fig. 1.6.b). The slip predictable model (Shimazaki and Nakata, 1980) makes the opposite assertion that the earthquakes start at variable stress state, but falls to a constant base level. In this model, slip of the next earthquake can be predicted, but not the time (Fig. 1.6.c).

Although the model by Shimazaki and Nakata (1980), makes a good approximation of the earthquake process in a region undergoing constant and uniform deformation, real life scenario varies. It is an interesting question whether these recurrences are controlled by any of the variants of these characteristic earthquake model, and whether an ideal form of earthquake cycle can be formed when its stress and slip histories are known. At some places where data are available for a long period of time, a combination of these models seem to work as in Nankai trough (Scholz, 1990) (Fig. 1.5).

Large subduction thrust earthquakes produce perceptible deformation of the Earth's crust. Pre- and post-earthquake geodetic observations can be used to infer the fault geometry and slip distribution on the fault plane. Deformation modelling is normally based on two dimensional models (Savage, 1983) or 3D analytical models (Okada, 1985; Gomberg et al., 1998) and numerical finite element models (Wang, et al., 2003). In the simplest 2D model, a subduction zone is modelled as a thrust fault or edge dislocation embedded in an elastic half-space.

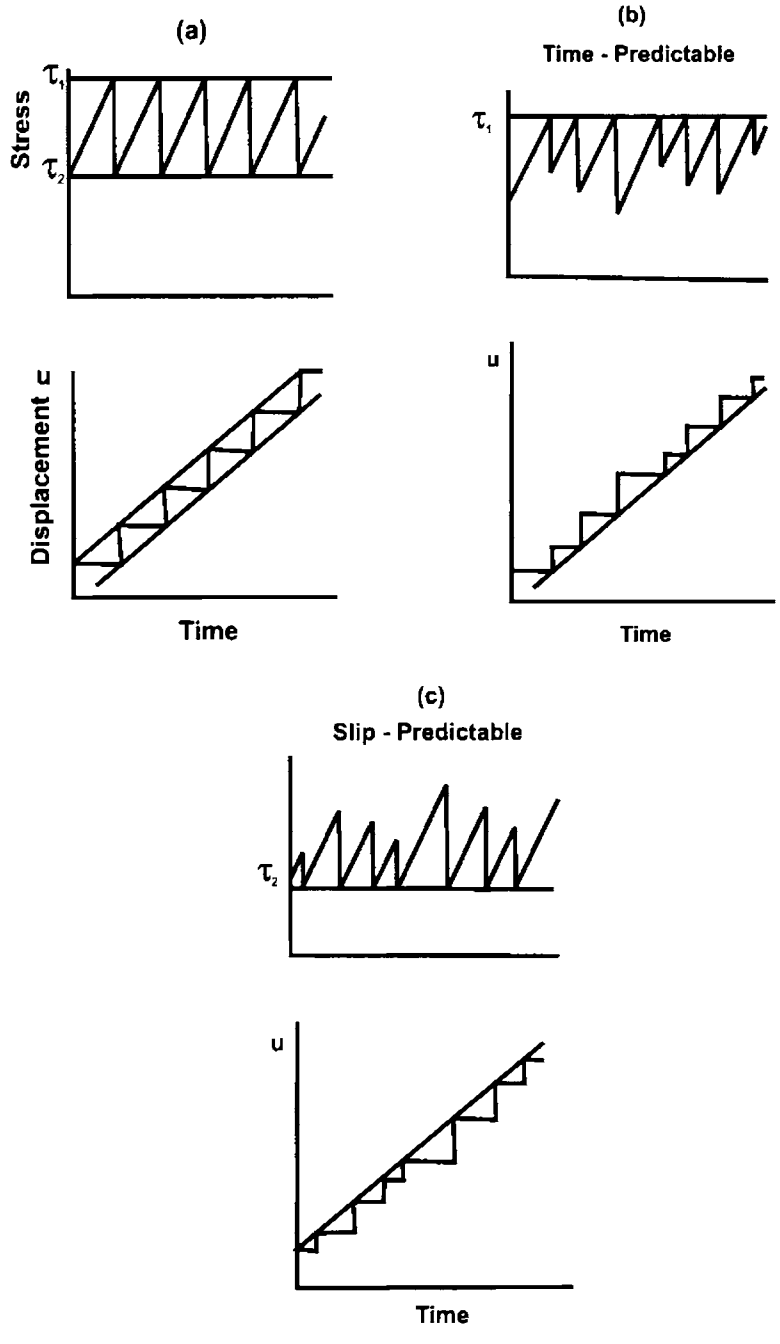

Figure 1.6: Various scenarios for buildup and release of stress on a fault - earthquake recurrence models: (a) Reid's perfectly periodic model showing regular stick-slip faulting where the slip will be the same for each event and recurrence interval constant. (b) time-predictable model, where the failure stress remains constant and the time to next earthquake can be calculated from the stress drop of the preceding event. (c) slip-predictable model, where the earthquakes start at variable stress state, but falls to a constant base level. Here the slip of the next earthquake can be predicted, but not the time (Shimazaki and Nakata, 1980).

1.4 Objectives

The study is taken up with the following objectives;

i) Assess the pre-seismic stress regimes along the arc.

ii) Determine the pre-seismic convergence rate along the arc.

iii) Analyze and interpret the pattern of co-seismic displacement and slip on various segments along the arc.

iv) Look out for any characteristics that would address the problem of megathrust event recurrence along the Andaman-Nicobar subduction zone.

1.5 Organization of the dissertation

The thesis has been arranged in six chapters with further subdivisions. The first chapter is introductory, stating the problem, necessity and scope of the study. This chapter also describes the objectives of this study and an overall structure of the thesis.

Chapter 2 reviews the related literature relevant to the present study, together with general background on the tectonic setting of the Andaman-Nicobar arc. This chapter also includes a review of the December 26, 2004 Great Sumatra-Andaman earthquake and the available literature on this event.

Chapter 3 highlights the methodology adopted for the work. It involves description of data acquisition surveys, data analysis techniques and processing methodology.

Chapter 4 deals with pre-seismic constraints from this study before the December 26, 2004 Sumatra-Andaman earthquake. This includes, spatio-temporal analysis of the available seismicity and associated focal mechanism data. Major stress regimes associated with Andaman-Nicobar subduction zone are also discussed. Results from the geodetic global positioning system (GPS) campaigns carried out for this work in the Andaman-Nicobar Islands from May, 2002 to September 2004 are presented. The most significant result discussed in this chapter is the along-arc pre-seismic convergence rate for Andaman-Nicobar Islands with respect to India.

Chapter 5 discusses near source observations from the Andaman-Nicobar region, using instrumental as well as observational data. Post-earthquake measurements were begun on January 13, about 3 weeks after the main-shock. Over the next three weeks, five of the eight GPS sites were re-surveyed and observations of relative sea level changes, ground shaking effects (such as liquefaction), and investigation of tsunami deposits were made. Features discussed, serve as proxies of co-seismic elevation changes, which are used along with the GPS data.

A summary and the major conclusion drawn are given in chapter 6 followed by references cited. A list of publications and meeting abstracts that came out of this study is given as Annexure. These sections are followed by appendices on the global positioning system (GPS), GPS data observables, GPS error budget, the GAMIT/GLOBK data processing software and how the various GPS antennas used in this study are calibrated.

Chapter 2

Background

2.1 Introduction

The Burmese-Andaman-Sunda arc defines the 5500 km long boundary between the Indo-Australian and Eurasian plates, from Myanmar to Sumatra and Java to Australia. The plate boundary separates the north east moving Indian plate from the southeast Asian plates that includes Burma and Sunda microplates (Fig. 2.1). Global plate tectonic reconstructions suggest that the Indian plate converges obliquely toward the Asian plate at a rate of 54 mm/yr (DeMets et al., 1994a) at N22^{0}E. The effect of oblique convergence has resulted in the formation of a sliver plate between the subduction zone and a right lateral fault system, which has evolved as the Sumatra Fault system in the southern part of the subduction zone and the Sagaing Fault in the Myanmar, as well as the opening of the Andaman Sea (Curray, 2005).

Varying degrees of tectonism, seismic and volcanic activity occur along this subducting margin. The Andaman-Sunda section of the subduction zone had produced many large earthquakes in the past, some of which have also generated destructive tsunamis. Significant historical earthquakes occurred in this region are the 1679 (M ~7.5) in the west coast of North Andamans; 1797 (M ~8.4), 1833 (M 9.0), 1861 (M 8.5), 1907 (M ~7.8), 1935 (M_W 7.7) from Sumatra region; 1881 (M_W 7.9) off Car Nicobar and 1941 (M_W 7.7) off Middle Andaman (Fig. 2.3). While

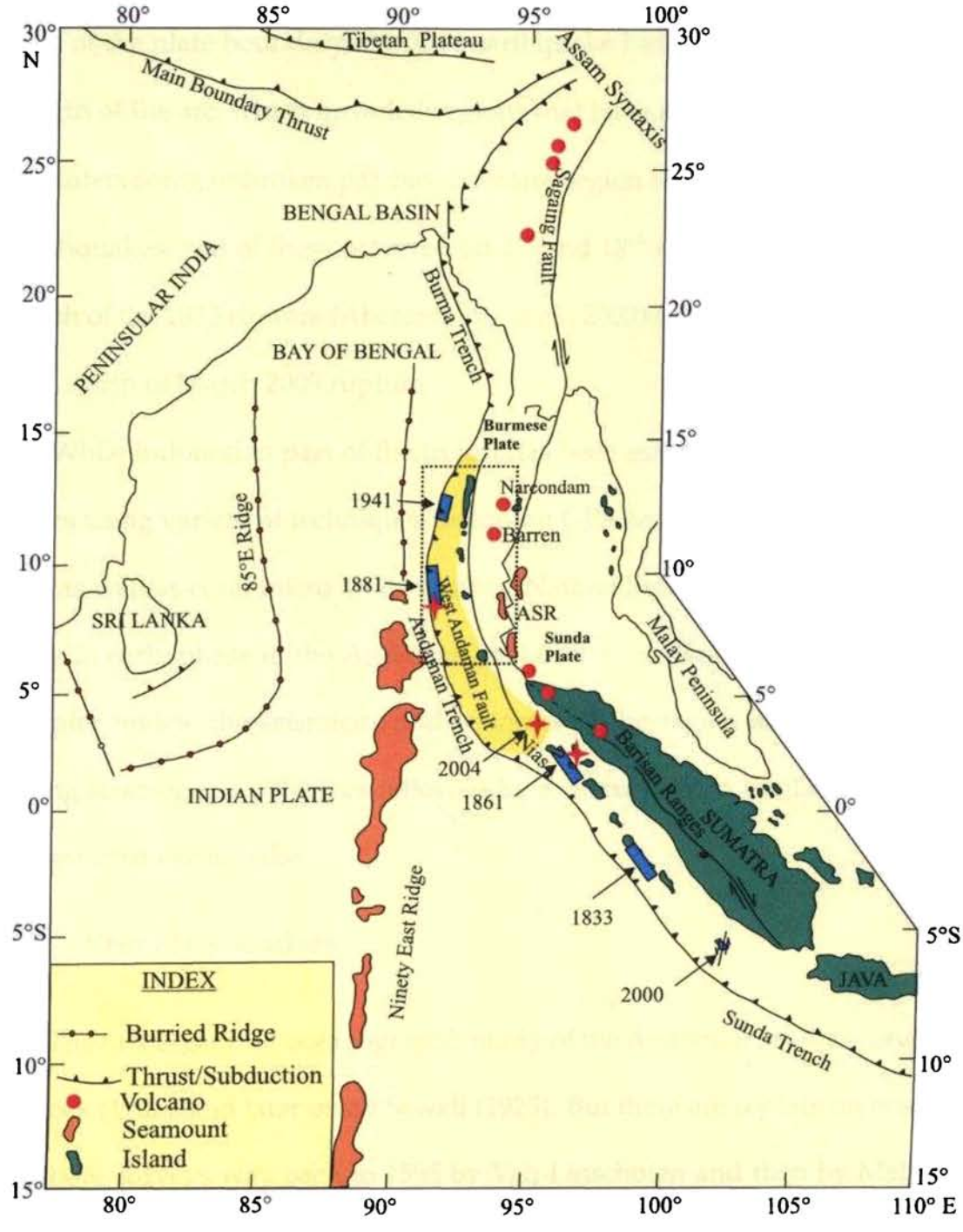

Figure 2.1: Map showing the major tectonic segments of Andaman-Sumatra subduction zone. Area of interest for this thesis lies in a zone between 5-15^{0}N and 92-98^{0}E. Rupture area for 2004 earthquake is marked in yellow, historic rupture areas also marked. (modified from Kayal, 2004.)

these large earthquakes have ruptured only a few hundreds of kilometers (200-300 km) of the plate boundary, the 2004 earthquake has ruptured more than 1300 km length of the arc, which included regions that have ruptured in the past as well as the intervening unbroken patches. Sumatra region has also witnessed three recent earthquakes; two of these occurred on 4^{th} and 18^{th} of June 2000 (M_W 7.8), located south of the 1833 rupture (Abercrombie et al., 2003) and the third one on 2002 (M_W 7.3), north of March 2005 rupture.

While Indonesian part of the trench has been extensively studied in the recent years using variety of techniques including GPS based ground deformation studies, as well as coral micro atolls studies (Natawidjaja et al., 2004), similar work is only in early phase in the Andaman part of the arc (Rajendran et al., 2007). This chapter review the seismicity and tectonics of the region and evaluates the on-going seismogenic processes followed by a discussion on the December 26, 2004 megathrust earthquake.

2.2 Previous studies

The first organized oceanographic study of the Andaman Sea was conducted by Alcock (1902), and later on by Sewell (1925). But there are reports on onshore and offshore surveys way back to 1595 by Van Linschoten and then by Mallet (1895) on the Barren Island volcano. Study of the geology and origin of the Andaman-Nicobar ridge started with Rink (1847), who suggested that this ridge had been formed of sediments uplifted from deep ocean floor. Hochstetter (1869) pointed out that the same ridge extended southward as the outer arc ridge off Sumatra and

Java. Wegner (1966) was the first to postulate a rift origin of the Andaman Sea. First systematic geophysical survey of the Andaman Basin was conducted by Weeks et al., (1967) as part of the International Indian Ocean Expedition, onboard U.S Coast Guard ship *Pioneer*. They carried out marine magnetic, gravity and limited sub-bottom seismic profiles, and using these data they suggested that the Barisan range of northern Sumatra extends into the Andaman Sea to 10^0N.

The earlier available reference to the geology of the islands is made by Helfer (1840), who described the rocks of Ritche's archipelago. Later, Rink (1847) divided the rocks of the Nicobar into three groups namely, 1) brown coal formation, 2) igneous rock and 3) older alluvium. Ball (1870) recorded the geology of the vicinity of Port Blair and correlated these rocks with that of the Nicobars. According to him the sedimentary rocks of the South Andaman are cross-cut by serpentine intrusions. Tipper (1911) mapped parts of North Andaman Island and Nicobar. During 1959 and 1960 a team led by C. Karunakaran of Geological Survey of India, conducted investigations for sulphur on the Barren and Narcondam Islands and mapped parts of South Andaman Island. The central Andaman Sea is 100-200 km wide trough and marked by steep and elongated sea valleys and sea mounts such as the Nicobar Deep, Barren-Narcondam volcanic islands, Invincible bank, Alock and Sewell sea-mounts (Rodolfo, 1969). Geological expeditions of scientific interest were initiated by Survey of India way back to 1957 (Bandyopadhaya et al., 1971). Fitch (1972) brought out that the NE movement of India was resolved or partitioned into two large components: dextral strike-slip on the Sagaing Fault (5 cm/yr) and high rate normal subduction along the Sunda-Andaman trench (4

cm/yr).

The western base of the Andaman-Nicobar trench is filled with sediments of Bay of Bengal (Curray et al., 1979). The structure along the arc in the Andaman-Nicobar region is dominated by east dipping nappes having folding, while intense folding is observed off Sumatra (Weeks et al., 1967; Curray et al., 1979). Curray et al., (1979) proposed the existence of an independent sliver plate absorbing the oblique motion of India with respect to southeast Asia. Eguchi et al., (1979) inferred collision of the Ninety-east ridge with the Sunda trench in the middle or late Miocene. They also reported that the ridge-trench collision transmitted compressional stresses into the back-arc area and collision of India with Eurasia exerted a drag on the back-arc region causing opening of the Andaman Sea.

Post-world war II work in the Andaman Sea, Burma and Sumatra which contributes to the understanding the Andaman Sea includes papers by Brunnschweiler (1966, 1974), Peter et al., (1966), Weeks et al., (1967), Aung Khin and Kyaw win (1968, 1969), Rodolfo (1969a, b), Frerichs (1971), Mitchell and Mckerrow (1975), Paul and Lian (1975), Curray et al., (1979, 1982), Bender (1983), Chatterjee (1984), Roy and Chopra (1987), Mukhopadyay (1984, 1992), Polachan and Racey (1994), Sieh and Natawidjaja (2000), Genrich et al., (2000) and many others. Recently, Pal et al., (2003) came out with the geodynamic evolution of the outer-arc fore-arc belt of the Andaman Islands.

2.2.1 Seismicity and tectonics

The seismicity and tectonics of Andaman-Nicobar region was analyzed by many and led to many conclusions on the processes that control the subduction. The regional seismicity pattern itself reflects different tectonic regimes within this Island arc system, namely the thrust dominated subduction front, the strike-slip faulting along the west Andaman transform and the extensional processes within the Andaman spreading center. Sinvhal et al., (1978) analyzed the time-space seismicity evolution and the associated neotectonics and reported a seismic gap north of the Andamans. This paper also deals greatly with the mechanism associated with the 1941 Middle Andaman earthquake. Uyeda and Kanamori, (1979) related the back-arc spreading activity in the Andaman Sea to leaky transform tectonics. The geometry of the Wadati-Benioff zone has been studied in detail for the Andaman region by many workers (Verma et al., 1976; Uyeda and Kanamori, 1979; Mukhopadhyay, 1984; Mukhopadhyay and Dasgupta, 1988; Mukhopadhyay, 1988; Ni et al., 1989; Gupta et al., 1990; Mukhopadhyay and Krishna, 1991). Gravity and seismicity data along the Burmese-Andaman arc suggests the presence of a subducted slab (Verma et al., 1978; Gupta et al., 1990). Srivastava and Chaudary (1979) analyzed epicentral data from USGS for a period of 1917-1974, and constrained the dip of the subducting interface (Fig. 2.2). A geodynamic perspective of the region was put forth by Surendra Kumar (1981) using the epicentral data as well as the available focal mechanism data. From marine magnetic anomaly studies Liu et al., (1983) identified a fossil spreading ridge beneath the Nicobar fan.

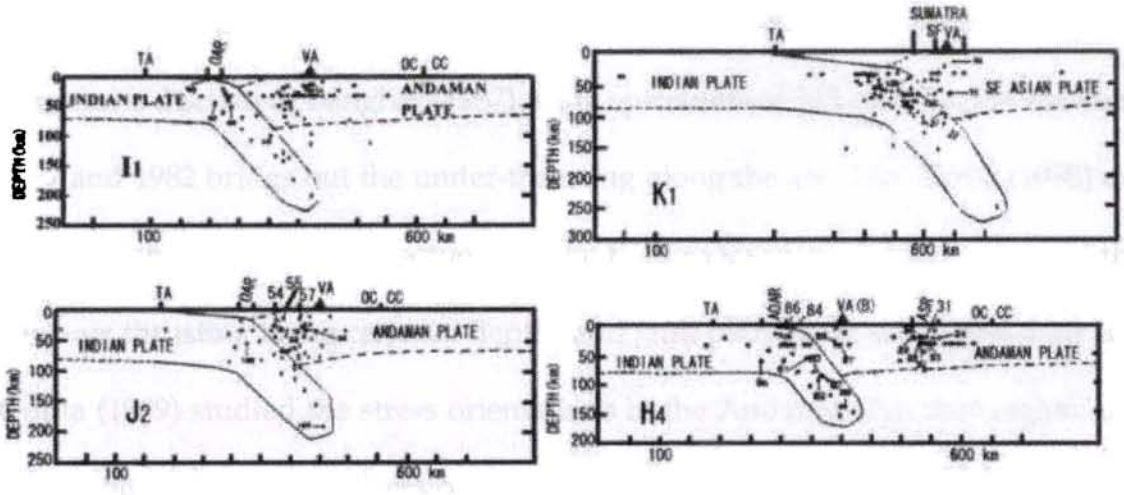

Figure 2.2: Dipping subducting interface (Benioff zone) at various segments of Andaman-Nicobar arc using epicentral data from USGS for a period of 1917-1974 (Srivastava and Chaudary, 1979).

Curray et al. (1982) inferred that the Andaman Sea and the central lowlands of Burma are parts of a single structural province. Chandra (1984) inferred segments that divide the major tectonic regimes in the Burmese-Indonesian arc based on several lines of evidence, which include change in trend and offset in arcs, bathymetry and sedimentation, faulting in the region, change in composition and trend of the line of volcanoes, spatial distribution of earthquakes and change in dip of Benioff zone. Mukhopadhayay (1984) studied extensively on the shallow earthquakes at the Andaman spreading ridge and reported evidence for extensional stress within the subducting lithosphere, and reported the under-thrusting of Indian lithosphere below the Burma plate down to a depth of 200-220 km. Further, he observed that some of the north-south faults developed on the main islands are seismically active. Hamilton (1979) reported that the subduction is more penetrative (~600 km) under the Sunda arc further south.

The decoupled transcurrent movement of the Burmese sliver plate is presented

in detail by Maung (1987) wherein the opening up of Andaman basin in the mid Miocene is discussed. Banghar (1987) using epicenters of 345 earthquakes between 1967 and 1982 brings out the under-thrusting along the arc. McCaffrey (1988) extensively studied the active tectonics of the Eastern Sunda and Banda arcs and the back-arc thrusting using centroid depths and fault plane solutions. Rajendran and Gupta (1989) studied the stress orientations in the Andaman-Nicobar region and found the maximum compression in the region is NE-SW to N-S, compatible with the motion of the Indian plate. They reported the along-arc variations in the stress orientations. Surendra Kumar (1981) used gravity data in addition to seismicity information to better constrain the geometry of the subduction zone.

Using micro-earthquake survey data Harjono et al. (1991) studied the transtensional Sunda strait and stress tensors for the area were computed and confirmed that the Sunda strait is an extensional tectonic regime as a result of the northwestward movement of the Sumatra sliver plate along the Semango Fault Zone. Guzman-Spezilae and Ni (1993) studied the opening up of the Andaman Sea, and suggested that the strain due to the opening of the Andaman Sea spreading system is seismic. The subduction azimuth varies from frontal/normal subduction in the Java to oblique subduction in the Sumatra - Andaman region (McCaffrey, 1988; Malod et al., 1995).

Crustal evolution and sedimentation history of the Bay of Bengal studied by Rao and Kumar (1997) pointed out that Sumatra-Andaman arc is an intermediate stress subduction zone with relatively few large magnitude events. A detailed study on the neotectonics of the Sumatran Fault was conducted by Sieh

and Natawidjaja (2000) which brought out many new insights into this 1900 km long fault. Radhakrishna and Sanu (2002) using focal mechanism data of shallow earthquakes from this region identified major tectonic segments along the arc and inverted these mechanisms for the stress tensors there. Shallow seismicity and available source mechanisms in the Andaman-west Sunda arc and Andaman sea region suggest distinct variation in stress distribution pattern both along and across the arc in the overriding plate. They inferred that the oblique plate convergence, partial subduction of 90^0E ridge in north below the Andaman trench and the active back-arc spreading are the main contributing factors for the observed stress field within the overriding plate in this region. In the background of spurt of seismicity in North Andamans, Rajendran et al. (2003) and Kayal et al. (2004) analyzed the spatio-temporal evolution of seismicity and the volcanism associated (Fig. 2.4) with the archipelago. Rajendran et al. (2003) reported that this area has entered into a phase of renewed activity and suggested an association with the down-dip extension of the subduction earthquakes.

Using multi-beam swath bathymetry, magnetic and seismological data Kamesh Raju et al. (2004) and Kamesh Raju (2005) brought out a three phase tectonic evolution of the Andaman basin. They presented that the current full rate spreading at Andaman Sea (Raju et al., 2004) is about 38 mm/yr, 327^0 relative to the present north (Curray, 2005). Using data sets from decades long oceanographical surveys and other geophysical studies, Curray (2005) gives a detailed information on the Andaman spreading, its evolution, and in addition an overall review of the tectonics.

An estimation of the relative motion between the plates is of significant importance in studies quantifying the deformation within the Indian Ocean and understanding the relative high level of seismicity there (Gordon et al., 1990). New constraints have been obtained decades later from seismology and GPS measurements, after the pioneering efforts of Fitch (1972) and Curray (1979) using early global plate kinematic models. Modern day geodetic techniques have become increasingly prominent in studies of plate boundary deformation. Using GPS data collected in Bangalore (IISC) and at several global GPS sites, Freymueller et al. (1996) found agreement between the present day Indian plate motion with that predicted by NUVEL-1A (DeMets et al., 1994a). Later on analysis by Chen et al. (2000) and Shen et al. (2000) suggest that the motion of Bangalore is 5-7 mm/yr slower than NUVEL-1A. A significant motion of a large Sundaland block (Sumatra, Java, Vietnam, China, Borneo) with respect to Eurasia was discovered by Chamot-Rooke and Le Pichon (1999); Simones et al. (1999); Michel et al. (2001). Paul et al. (2001) estimated the convergence of 14 mm/yr between India and Port Blair from a single campaign mode control point at CARI, Port Blair and forms the first GPS geodetic observations from this Island archipelago. According to this study, CARI samples only 50% of the India/Andaman convergence due to the unknown degree of coupling there, and this makes it difficult for an independent estimate of the full Andaman velocity. A velocity of 20 mm/yr was established across Sagaing Fault (Vigny et al., 2003) using GPS.

Strain rate field from Andaman Sea region was studied by Kreemer et al., 2003 and obtained new constraints on the partitioning of the compression along the

Sumatra-Andaman trench and the extension along the spreading segments. They predicted the direction of extension, as it occurs along the spreading segments, and showed that it is consistent with earthquake slip vectors ~N30^{0}W. They also reported that there is a significant component of right-lateral shear in agreement with the seismotectonics indicated by the focal mechanisms. Bird (2003) compiled from the available deformational rates and fault locations, proposed a pole of rotation for the Burmese plate with respect to the Sunda plate as 103^{0}E, 13.9^{0}N, 2.1^0/Ma.

2.2.2 Significant pre-seismic earthquakes

The Andaman-Nicobar section of the Sunda-Andaman plate boundary has produced many large and destructive earthquakes in the past (Table 2.1 and Fig. 2.3). Among the earlier earthquakes, those in 1847 (7.5<M<7.9), 1881 (M_W 7.9) and 1941 (M_W 7.7) are significant (Bilham et al., 2005). An earthquake also occurred in the Arakan coast of Burma on April 2, 1762 (Chhibber, 1934) from the description of felt effects in northern part of the Bay of Bengal and Arakan, it appears that the event was close to the Irrawady delta. Another large earthquake is reported to have occurred in the North Andaman on January 28, 1679 (Iyengar et al., 1999). Felt reports from the Burmese coast as well as parts of the east coast of India (Temple R. C., 1911) suggest this to be comparable to the 1941 earthquake in magnitude and rupture extent (Rajendran et al., 2007). According to Hochstetter (1866) the 1847 earthquake happened near to Kondul Island, an island in between the Little Nicobar and Great Nicobar, with an aftershock duration of 5 weeks, which makes it comparable to 1941 and 1881 earthquakes. Location of the earthquake is still

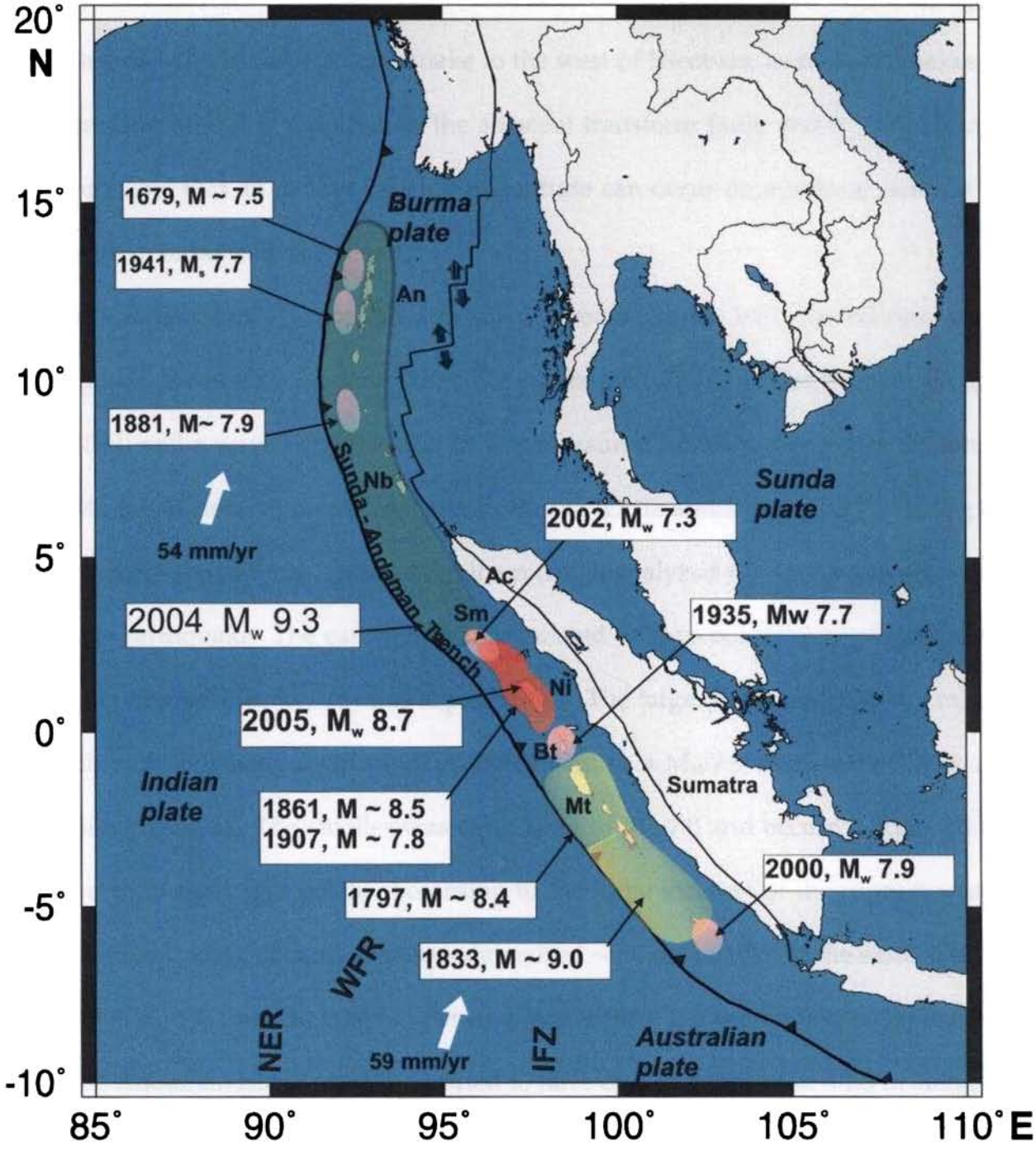

Figure 2.3: Siginificant earthquakes and their rupture areas along the Sunda-Andaman plate boundary. An, Andaman islands; Nb, Nicobar islands; Sm, Simuleue island; Bt, Batu island; Mt, Mentwai island; Ac, Aceh province; Ni, Nias island; NER, Ninety East ridge; Sfz, Sumatran fault zone); WFR, Warton fossil ridge; IFZ, Investigator fracture zone. Filled arrows represent Indian and Australian plate velocities and direction (DeMets et al., 1994). Modified from Briggs et al., 2006.

speculative, as there is no other source of information. Bilham et al. (2005) rejects the idea of a strike-slip earthquake to the west of Nicobars, as no earthquakes exceeding M_W7.2 is reported on the adjacent transform fault, and it is much more probable that an event of such a magnitude can occur on a reverse fault on the west of or beneath the islands.

Oldham (1884) compiled a detailed account on the 1881 Car Nicobar earthquake. It caused a tsunami surge not exceeding 0.75 cm at Car Nicobar (Rogers, 1883) and a wave height of 0.25 m was measured from the tide gauge stations at Madras (Chennai) on the east coast of India (Ortiz and Bilham, 2003). Using the tsunami travel times, Oritz and Bilham (2003) analyzed the source mechanism of this earthquake. The earthquake is calculated to have occurred near and west of car Nicobar with two reverse slip ruptures. The larger measured 150x60 km, and dipped 25^0E with a slip of 2.7 m equivalent to a M_W7.9 earthquake (Oritz and Bilham, 2003). The smaller was equivalent to M_W7.0 and occurred some 50 km north of the larger patch. According to them the location of the rupture was so close to Car Nicobar, its western edge raised $\sim$ 50 cm relative to the eastern shore. June 26, 1941 earthquake happened a year before the occupation of Japanese in the Andaman Islands and is reported to have caused an uplift of $\sim$1.5 m along the western margin of the middle Andaman and subsidence of the same magnitude along the eastern margin, an observation not validated by any direct measurements (Jhingran, 1953). There are no reports of any tsunami impact either from the Andaman-Nicobar Islands or from the east coast of India (Rajendran et al., 2007). The event affected the middle and south Andaman regions, including the town of

Port Blair. The central watch tower of the cellular jail in Port Blair collapsed along with a hospital and other masonry structures. There are also eyewitness accounts on the subsidence of Ross Island, subsequent to this earthquake. Using the available aftershock extent information Bilham et al. (2005) infer the rupture extend between 11^0N and 13^0N and computes a slip of 3 m on a 50 km wide 150 km long down-dip rupture.

The M 8.7 earthquake of 1833, is reported to have ruptured about 550 km segment of this arc; it also generated a tsunami (Natawidijaja et al., 2004). Natawidijaja et al., (2006) re-estimated the 1833 magnitude to 8.9-9.0 based on the rupture extent they measured based on the emergence and subsidence of the coral microatolls there. Briggs et al., (2006) fixed the magnitude to M 9.0 (see, Fig. 2.3). Another great earthquake of 1861 (M 8.5) broke a segment north of the equator, also triggering a tsunami. The 1833 and 1861 earthquakes and the attendant tsunamis occurred before the introduction of harbour tide gauges in most parts of the world and no tidal gauge data exist for these events. However, better documentation exists for the 31^{st} December 1881 earthquake which caused run-up in eastern coast of India. This earthquake is also the oldest for which slip geometry has been inferred. See, Table 2.1 for major siginificant pre-seismic earthquakes from Andaman-Sumatra subduction zone.

2.2.3 Volcanism

Subduction along the Andaman-Sumatra trench system has given rise to a discontinuous belt of submarine volcanic seamounts. The andesitic volcanoes of Bar-

Table 2.1: Significant Pre-seismic earthquakes that occurred in recent and historic times in and around the Andaman-Nicobar region. Rupture areas and earthquake locations, where-ever available are plotted in Fig. 2.3. [1]Iyengar et al., 1999, [2]Imperial Gazetteer of India, 1909, [3]Oritz and Bilham, 2003, [4]Bapat et al., 1983, [5]NEIC, USGS, [6]Rajendran et al., 2003.

Date	Latitude	Longitude	Magnitude	Region
28/Jan./1679	12.50	92.50	7.5[1]	M/N.Andamans
31/Oct./1847	07.30	94.75	$7.5 < M < 7.9$	Kondul[2],[3]
31/Dec./1881	09.25	92.70	7.9[3]	Off Car Nicobar
16/Nov./1914	12.00	94.00	7.2[4]	S-W of Barren Island
28/Jun./1925	11.00	93.00	6.5	Little Andamans[5]
01/Aug./1929	10.00	93.00	6.5	Car Nicobar[5]
09/Dec./1929	04.90	94.80	7.2[4]	Sumatra
19/Mar./1936	10.50	92.50	6.5	Little Andaman[5]
14/Sep./1939	11.50	95.00	6.0	East of Car Nicobar[5]
26/Jun./1941	12.00	92.50	7.7[4]	West of M. Andaman
08/Aug./1945	11.00	92.50	6.8	North of Little Andaman[5]
23/Jan./1949	09.50	94.50	7.2[4]	East of Car Nicobar
17/May./1955	06.70	93.70	7.3[4]	East of Great Nicobar
14/Feb./1967	13.70	96.50	6.8	Andaman Sea[5]
20/Jan./1982	06.95	94.00	6.2	Great Nicobar[5]
20/Jan./1982	07.12	93.94	6.1	Great Nicobar[5]
13/Sep./2002	13.08	93.11	6.4	South East of Digilipur[6]

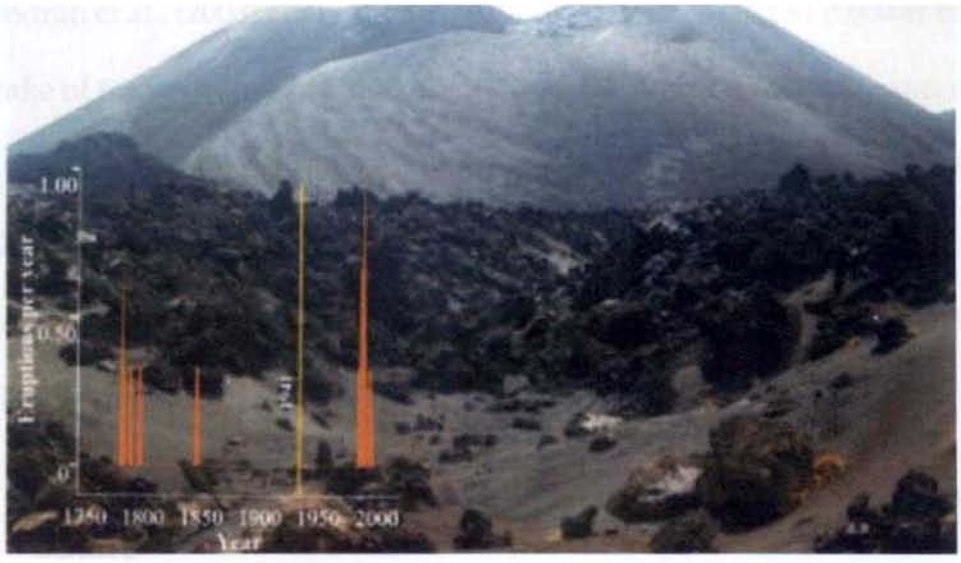

Figure 2.4: Cone of Barren Island volcano as on May, 2002 (view from west). See Fig. 2.1 for location. Inset shows the composite eruption rate, smoothened using a moving average filter, shows an accelerated eruption ~50 years after the 1941 earthquake. (Rajendran et al., 2003).

ren and Narcondam Islands are prominent among them; the Narcondam being now extinct, but barren is still marked by an active volcano and lie on the neogene inner volcanic arc. It erupted in March, 1991 after lying dormant for about two centuries (see Fig. 2.4-inset for eruption history). The first known historical eruption was on 1787 when a cinder cone grew in the center of pre-historical caldera. Intermittent eruptions were there on 1832, 1991 and 1995. Presently the island is just 3 km across, with a reported maximum elevation of ~400 m (Haldar et al., 1992). Further south, this volcanic chain is represented by the Barisan range in Sumatra, and in North, the trend is correlated with the chain of vlocanoes in Burma (Curray et al., 1982). Global observations on earthquake-volcano interactions, suggest large-scale eruptions following large earthquakes over periods of 7-50 years at dis-

tances of 30-150 km, and 30-50 years at distances upto 1000 km (Hill et al., 2002). Rajendran et al., (2003) analysed the eruption history of Barren (Haldar et al., 1992) in wake of the spurt of earthquake activity in the North Andamans and suggested a 50 -year correlation may be appicable to the Barren Island volcano, located within the 250 km of the 1941 epicentre (Fig. 2.4, inset). Recently Kumar et al., (2006) reported a minor eruption of Barren volcano on May, 2005 using remotely sensed satellite imageries.

2.3 26 December, 2004 M_W 9.3 Great Sumatra-Andaman earthquake

The 26 December main-shock rupture began at 3.36^{0}N, 96.0^{0}E at a depth of 30 km at 00:58:53 GMT (National earthquake information centre (NEIC), United States geological survey (USGS)). Harvard moment tensor solution suggests thrusting on a shallowly dipping plane (8 ^{0}), striking 328^0. It ruptured a 1300 km long plate boundary north-westward along the Sunda trench and the Andaman trench and caused static offsets as far as 4000 km away from the epicenter (Banerjee et al., 2005). The aftershock zone extends to nearly 15^{0}N. Distribution until the beginning of March 2005 suggests little change in the extent of the aftershock zone (Fig. 2.5). One notable feature is the absence of aftershock activity north of about 15^{0}N latitude, a zone that has not generated much earthquakes in the past.

Significant vertical displacements of the sea floor were responsible for a tsunami that propagated throughout the world's oceans (Bilham, 2005). Tsunami runup heights were measured at ~25 m near Banda Aceh region of Sumatra (Borrero,

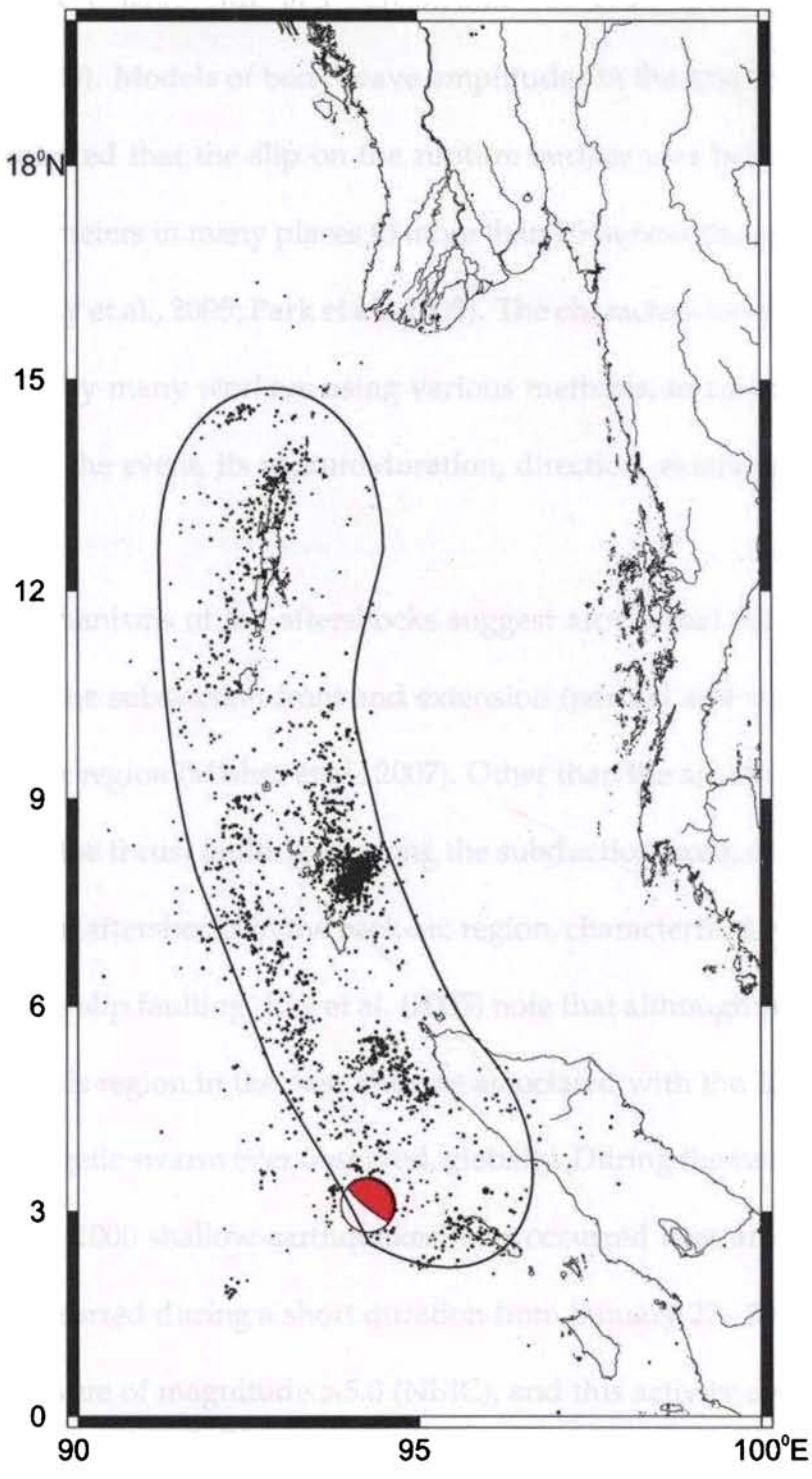

Figure 2.5: Location of December 26, 2004 earthquake shown by centroid moment tensor (CMT) solution beach ball, and aftershocks (black dots) till 1st March, 2005. Epicentral data source: NEIC, USGS, CMT: Harvard University CMT database. Extent of rupture zone can be clearly marked by the extent of aftershocks.

2005), 6 m in Thailand (Titov et al., 2005), and 3-12 m along the coast of Sri Lanka (Liu et al., 2005). Models of body-wave amplitudes in the first few minutes of the rupture indicated that the slip on the rupture surface was hetrogenous, varying from several meters in many places to more than 20 m near the epicenter (Ammon et al., 2005; Lay et al., 2005; Park et al., 2005). The characteristics of this earthquake were studied by many workers using various methods, to constrain the moment magnitude of the event, its rupture duration, direction, extent and the associated mechanism.

Focal mechanisms of the aftershocks suggest arc-normal compression (thrust faults) along the subduction front and extension (normal and strike-slip faulting) in the back-arc region (Mishra et al., 2007). Other than the arc normal compression expressed by the thrust faulting all along the subduction front, one notable feature is the cluster of aftershocks in the back-arc region, characterized by normal and occasional strike-slip faulting. Lay et al. (2005) note that although such swarms have occurred in this region in the past, the one associated with the 2004 earthquake is the most energetic swarm ever observed, globally. During the two months that followed, nearly 1000 shallow earthquakes have occurred here among which about 600 events occurred during a short duration from January 27–30, 2005 and nearly 100 of them were of magnitude >5.0 (NEIC), and this activity continued there till September 2005. This region is a transition area between the Sumatra Fault and developing Andaman back-arc spreading center. This high aftershock activity along the back-arc ridge-transform faults indicates accompanying slip partitioning along that boundary (Engdahl et al., 2007). According to them, most of these swarm

earthquakes were characterized by shallow depth right-lateral strike-slip, but also including a number of normal faulting mechanisms oriented perpendicular to the predominant strike-slip faults in the region along a linear trend. There is a marked transition in the distribution of aftershocks at $\sim 5.5^0$N and it broadly corresponds to changes in the physical properties of the plate interface (Kennet and Cummins, 2005). Also, this transition corresponds to the second region of significant slip in many main-shock rupture models (Ammon et al., 2005; Ishii et al., 2005).

Various modes of rupture mechanisms were put forth by many including single and multi segmented rupture, involvement of slow slip in the northern segment and the varying rupture dimensions along the arc. Some common features of almost all rupture models are, a rupture of $\geq$1300 km along the Sumatra-Andaman megathrust, with rapid slip concentrated in the southernmost 500 km (Ammon et al., 2005; Lay et al., 2005; Banerjee et al., 2005; Chlieh et al., 2007; Rhie et al., 2007). Ammon et al., (2005) suggests the possibility of slow slip in the first 50-60 sec of rupture in the southern region near the epicenter. Several studies have required a slower rupture velocities for the northern segment of the rupture, with periods greater than 600 sec (Banerjee et al., 2005; Lay et al., 2005; Stein and Okal, 2005; Tsai et al., 2005; Singh et al., 2006). Some studies, agian using various seismic and geodetic datasets, have found that the slow slip and low rupture velocities in the norhtern region are not necessary to explain the data (Ishii et al., 2005; Tsai et al., 2005; Vigny et al., 2005; Banerjee et al., 2007; Chlieh et al., 2007).

The centroid moment tensor of the 26 December, 2004 Sumatran event was of point source mechanism and of moment magnitude of (M_W) 9.0 (Dziewonski et al.,

1981). The magnitude of the earthquake has been a matter of energetic debate, with most estimates falling in the range of M_W 9.0-9.3. Stein and Okal (2005) estimated a moment of 10^{23} Nm (M_W 9.3) based on normal mode excitation, although Banerjee (2005) argue that this is overestimated because they assumed a point source with too large a dip angle. Ammon et al., (2005) have produced three different model slip distributions, each of which has M_W 9.0-9.2. Park et al., (2005) using normal mode spectral data find that a model with M_W 9.1. Braitenberg and Zadro (2007) compare the free oscillation amplitudes of 1960 Chile and 2004 Sumatra-Andaman earthquake and give a direct comparison that Sumatra-Andaman event was smaller than the Chilean event by a factor between 1.5-3.0. Using an extension of the empirical Green's function, Choy and Boatwright (2007) demonstrated that the second half of the rupture radiated less high-frequency energy than the first half of the rupture. The rupture process of the Sumatra-Andaman earthquake lasted for approximately 500 sec. The moment energy release by the rupture processes took place in the first 250 sec, with some minor patches of high frequency release up to 8 min after the onset of *P* (Lomax, 2005; Kruger and Ohrnberger, 2005 and Ishii et al., 2005). Several finite fault inversions (Ammon et al., 2005) using low frequency surface wave data derived moment rate functions that had similar durations of 500-600 sec. Seismic rupture models which based entirely on analysis of body waves were unable to resolve the rupture in the northern segment because of the mixing of the arrivals from that segment with the secondary phases arriving from the intial phases of the rupture (Stein and Okal, 2005). All the authors argued that the major source of additional moment release from a slow slip in the northern

segment of the aftershock zone (Stein and Okal, 2005; Ammon et al., 2005; Bilham, 2005; Lay et al., 2005a). Tsai at al. (2005) estimated a similar magnitude using a CMT modelling aproach, with 5 distributed point sources along the length of the rupture. Later, doubts have been cast on the slow slip hypothesis, as many later analyses showed that almost entire seismic energy release is from normal speed seismic rupture (Ishii et al., 2005; Neetu et al., 2005). The published models show a wide variation in features such as the depth and overall length of significant rupture.

The largest earthquake to follow the great event (M_W 8.6) occurred on 28 March. This earthquake had a similar mechanism as the 26 December earthquake, showing predominantly thrusting on a shallow-dipping (7^0) fault plane. The rupture was about 300 km long, as defined by the extent of aftershocks. However, this one did not generate a huge tsunami like the December earthquake. It has been suggested that the March earthquake did not breach the sea floor, resulting in the transfer of lesser energy to the water column. Further, the earthquake occurred under relatively shallow water, displacing lesser volume of water.

Chapter 3

Methodology

3.1 Introduction

The adopted techniques and methodology for this study to constrain the active tectonic deformation happening at the Andaman-Nicobar arc are briefly detailed in this chapter. These include spatial and temporal analysis of the epicentral data, analysis of the earthquake focal mechanism data, satellite gravity data, bathymetry data and the global positioning system (GPS) data. This chapter also briefly deals with the data acquisition techniques and processing schema adopted for analysis of GPS data sets.

3.2 Spatio-temporal analysis

The epicentral data made used for this study is from NEIC of USGS. Data span is from 1^{st} January, 1973 to 25^{th} December, 2004, for the pre-earthquake analysis. For aftershock studies data sets from 26^{th} December, 2004 to 1^{st} March, 2005 are made use of (for Fig. 2.5). Spatial span of the epicentral data sets are from 0-20^0N and 90-100^0E, of magnitude M$\geq$4.0 and without any depth limitation . Spatial analysis of the epicentral data helps in delineating the major zones of deformation and their spread. To map along-arc variations in the dip of the Benioff zone, depth wise distribution of epicentral data is made use of. For temporal analysis the same data set is made use of.

3.3 Stress orientation computation

CMT solutions for the same spatial spread and period of M≥4.9 was made use for the pre-earthquake analysis. Specific CMT solutions were downloaded for December, 2004 and March, 2005 events for plotting. To deduce the stress directions using focal mechanisms, the orientation of three principal stresses S_1, S_2, S_3 (the maximum, intermediate and minimum compressive stresses) in different modes of faulting was considered. It was assumed that one of the three principal stresses corresponds with the vertical stress S_v, induced by overburden. Thus in areas of normal faulting, S_v corresponds to S_1 (in the vertical plane), implying that S_H and S_h (maximum and minimum principal stresses) are less than the overburden effect. In areas of strike-slip faulting, it is assumed that S_v is the intermediate principal stress, S_2, and in regions of thrust faulting, S_v corresponds to the least principal stress, S_3. It was further assumed that P- and T-axes loosely correspond to S_1 and S_3.

There are limitations in inferring the directions of S_1 and S_3 from P- and T-axes (McKenzie, 1969). McKenzie (1969) noticed that in general P- and T-axes may lie anywhere in the dilatational and compressional quadrants of the focal planes and may not be the actual and assumed directions of S_1 and S_2. However, these errors can be minimized by averaging groups of P- and T-axes (Zoback and Zoback, 1987).

From the cluster of P- and T-axis orientations, the mean direction was calculated by simple arithmetic average. The average P-axis orientation from the focal

mechanisms was assumed to be the direction of maximum horizontal stress (S_H in regions of strike-slip and thrust faulting). In regions of normal faulting, the direction perpendicular to the T-axis was assumed to the direction of S_H.

3.4 Geodetic constraints using GPS

Geodetic measurements provide very accurate determinations of positions of points on the surface of the Earth. When measured over a few years, the change in positions of points are representative of strain accumulation in a region. The rapid growth of usage of GPS devices over the last decade has occurred primarily because of comparatively low cost and high accuracy of GPS receivers.

3.4.1 GPS Data acquisition

GPS measurements presented in this study started as an initiative to model the crustal deformation associated with the Andaman-Nicobar arc. First set of measurement was made during May, 2002 by establishing and collecting campaign mode GPS control points and data at Port Blair (PBLR), Havelock Island (HVLK) and Barren Island (BRRN). These points are made up of threaded steel bolts, embedded in cement concrete basement except BRRN, where it's on a base rock exposure. During 2003 field work, three more points were added at Diglipur (DGLP) in the North Andamans, Car Nicobar (CARN) and Chatham (CHAT), Port Blair. The first two locations are on cement concrete basement with nail marks serving as the point and the third one on a Naval hydrographic survey benchmark with a copper plate description. During the September, 2004 field campaign, two more points

were added, one at Campbell Bay (CBAY), Great Nicobar and another one at Hut Bay (HBAY), Little Andamans, where both the points are nail marks embedded in cement concrete basement (See Fig. 3.1). The spatial spread of all these points are between 6.85^0N and 13.05^0N latitude, covering $\approx$ 800 km of the 2004 rupture zone. Occupation history of these points is listed on Table 3.1., and receiver and antenna details are listed in, Table 3.2. Some of the points were not occupied in subsequent surveys due to entry restrictions and/or logistical problems. The four character site codes used for data analysis are listed in, Table 3.2 as station codes.

3.4.2 GPS Data analysis

There are many variety of data analysis strategy for GPS regional campaigns, and there has been an evolution of strategies with the deployment of continuously running stations. The basic aim of the analysis is to determine the motions of sites in a network relative to each other and within a global reference frame. The most straight forward approach to the analysis of regional data is to take all of the available GPS data, both in the region and globally, and to perform an analysis of all the data simultaneously, estimating all the parameters. The parameters include the orbital elements for each satellite arc, changes in Earth orientation parameters, tropospheric delays, clock offsets and initial phase biases. From this analysis, a global coordinate system can be determined using the global stations, and the motions of the regional sites will then be given in this global frame. However such a direct approach is not feasible because of large number of parameters that would need to be estimated. To avoid the problem of excessive number of parameters, the above

scheme is modified with no change to the final results, by processing the GPS data in subsets and then combining the geodetic parameter estimates in a second analysis. The results will be identical provided there are no correlations between the non geodetic parameters in subsets.

One way to form subsets is to process each day of GPS data separately and to carry-forward the parameters for station positions in the further analysis viz., Earth orientation parameters and possibly the orbital information from satellites. Even this level of analysis can become large with number of continuously tracking GPS receivers. One mode of simplification is to use the orbital parameters and Earth orientation parameters determined by other analysis centers. The generation of such products is one of the main purposes of IGS (IGS – International GNSS (Global navigational satellite system) service for geodesy.). When these products are used, only the regional data and data from some global sites need to be used.

In the analysis of regional networks, it is important to maintain a well-defined coordinate system to which the regional site positions are referred. The important aspects of coordinate system are its translation and rotation. The precise method for maintaining this system depends on the tectonic problem being addressed. In nearly all cases, the rotational origin of the network is best defined by the global rotation of the Earth. The collected observation files are converted to RINEX (RINEX - Receiver independent exchange format.) for quality check and analysis. For this study, GPS data processing was done using GAMIT/GLOBK (King and Bock, 2005, Herring, 2005).

Analysis was done using an elevation cutoff angle of 15 degrees. Latest realiza-

tion of the international terrestrial reference frame ITRF00 (ITRF00 - International terrestrial reference frame, year of realization 2000.) (Altamimi et al., 2002) was used for reference frame definition. An elevation dependant antenna model was used, with direct hight to the antenna reference point (ARP) serving as the reference. IGS station data (station character code in parenthesis) of Bangalore (IISC), Kumuing (KUNM), Lhasa (LHAS), Singapore (NTUS), Coco Island (COCO), Dego Gracia (DGAR) were used (Fig. 3.1). First, the daily positions of the stations were computed and the baseline estimates between the stations were computed for each day as a loosely constrained solution.

The non-fiducial orbit was estimated in a global solution that included only loosely constrained site positions, so it is internally precise but in no particular reference frame. Each daily solutions are transformed into the IGS-2003 realization of the ITRF00 reference frame using all common sites in the daily solution weighted by the joint uncertainty in the model position at the epoch of the solution and the daily solution uncertainty. After transformation, the typical 3D-RMS misfit with the sites used to realize the ITRF00 frame is 6-7 mm. Here no attempt is made to remove common mode errors by defining a regional reference frame.

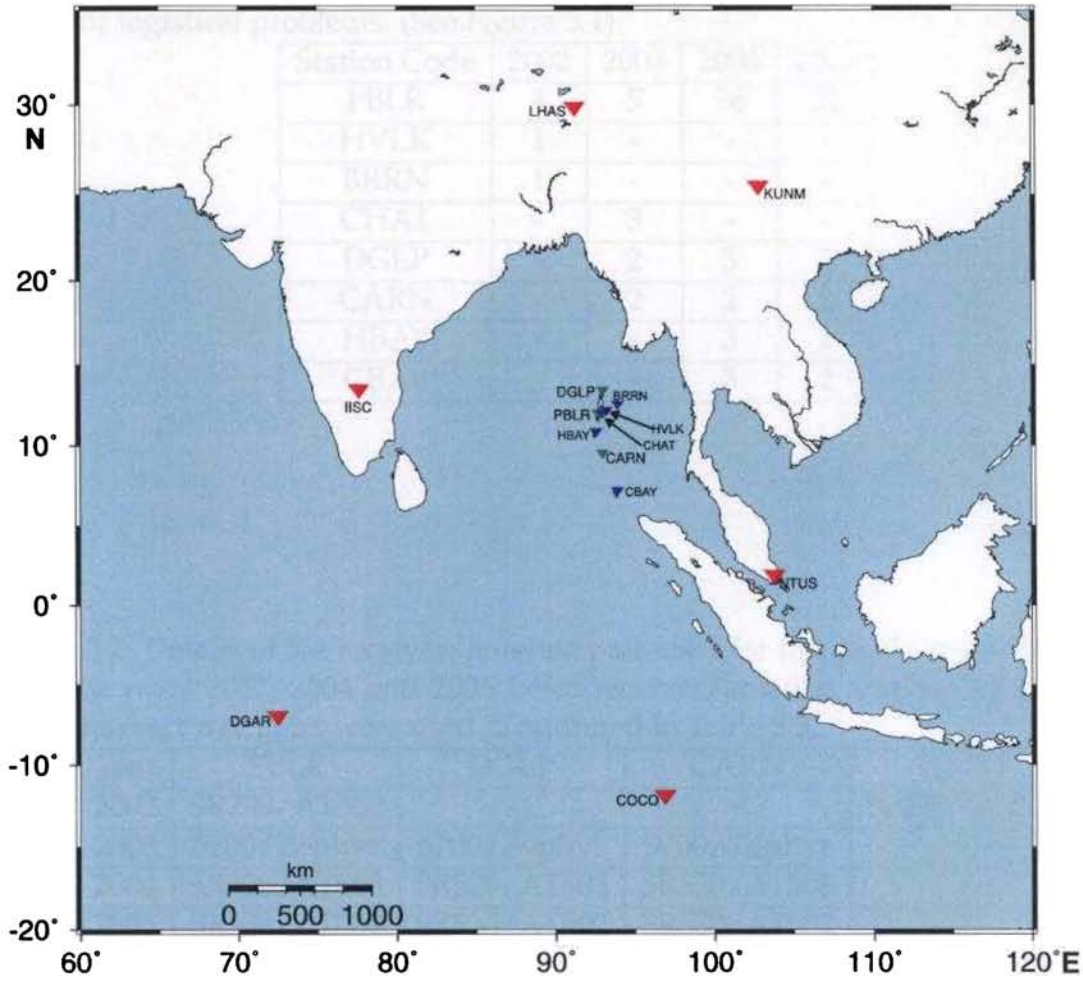

Figure 3.1: GPS control points used in this study to constrain the tectonic deformation of the Andaman-Nicobar arc. Red inverted triangles are international geodetic stations. Remaining blue and green ones are established in the islands as part of this study. Station data sets from green inverted triangles were used for preseismic velocity computation. Among the blue inverted triangles, except HBAY and CBAY remaning were not reoccupied after December 26^{th} earthquake due to entry restrictions or logistical problems. See table 3.1 for occupation history

Table 3.1: Occupation history of the stations with number of days occupied at each point, established at Andaman-Nicobar Islands till 2005 as part of this work. Some of the control points are not re-occupied in susequent surveys due to entry restrictions or logistical problems. (See Figure 3.1)

Station Code	2002	2003	2004	2005
PBLR	4	5	26	22
HVLK	1	-	-	-
BRRN	1	-	-	-
CHAT	-	3	-	-
DGLP	-	2	3	2
CARN	-	2	2	2
HBAY	-	-	3	2
CBAY	-	-	3	2

Table 3.2: Details of the receiver/antenna pair used for this study at each location. For the years 2002, 2004 and 2005 Leica receiver/antenna and for 2004 Trimble antenna/receiver pairs were used. Continued in Table 3.3.

Year	PBLR	DGLP	CARN	BRRN
2002	SR299/AT302	-	-	SR299/AT302
2003	5700/Zephyr	5700/Zephyr	5700/Zephyr	-
2004	SR520/AT503	SR520/AT503	SR520/AT503	-
2005	SR530/AT502	SR530/AT502	SR530/AT502	-

Table 3.3: Details of the receiver/antenna pair used, continuation of Table 3.2.

Year	HVLK	CHAT	HBAY	CBAY
2002	SR299/AT302[1]	-	-	-
2003	5700/Zephyr[2]	5700/Zephyr[2]	-	-
2004	-	-	SR520/AT503[3]	SR520/AT503[3]
2005	-	-	SR530/AT502[4]	SR530/AT502[4]

Chapter 4

Pre-seismic deformational constraints

4.1 Spatio-temporal analysis of pre-seismic earthquakes

The Spatial distribution of instrumentally recorded earthquakes (January 1, 1973 to December 25, 2004) coincides with the major tectonic segments of the Andaman-Nicobar arc (Figures 4.1.A, 2.1 and 2.3). Inner side of the arc shows considerable and distinct seismicity along the West Andaman Fault (WAF), Andaman Spreading Ridge (ASR) and the volcanic arc (See, Figure 2.1 for locations.).

Loci of earthquakes mostly follow a NNE trend, the western arm representing the fore-arc setting as well as the volcanic arc consisting of Barren and Narcondam Islands. The eastern arm that branches off at about 11^0N is characterized by shallow seismicity associated with the back-arc extension in the ASR as discussed later. The reduced level of seismicity and formation of a gap north of the archipelago is evident and has been reported (Sinvhal et al., 1978; Rajendran and Gupta, 1989). Similarly there is a lack of any significant cluster of near trench earthquakes in the Sumatra-Andaman boundary during this period. If ASR earthquakes are not taken into account, this can be assumed due to a pre-seismically locked trench-ward plate interface and a seismogenic plate interface away from the trench. Such pre-seismic quiescence is not uncommon for subduction zones. For example, inter-plate earthquakes are not usually observed along the shallowest (<10 km) portions of the subduction megathrust pre-seismically (Byrne et al., 1988; Scholz, 1998; Pacheco et

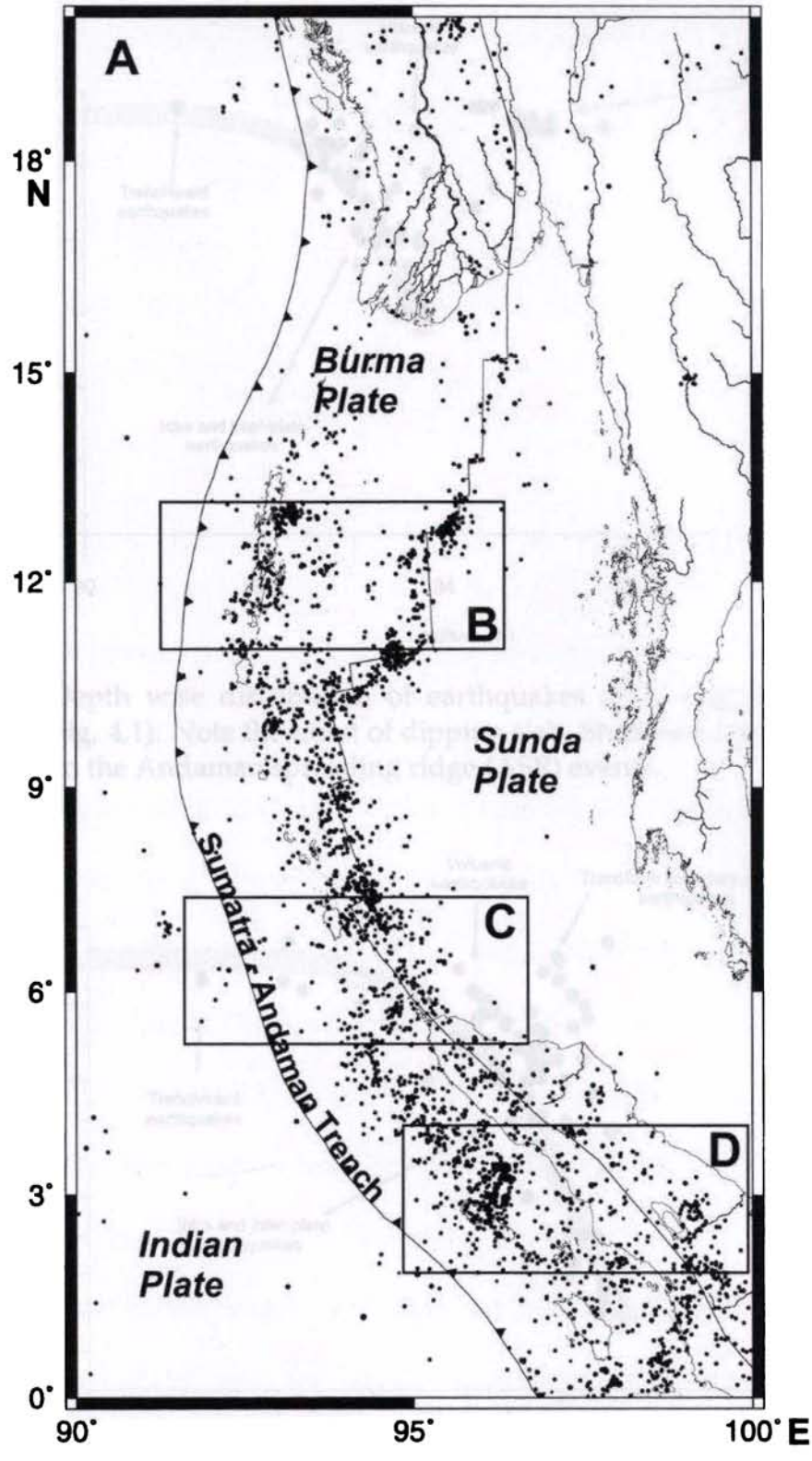

Figure 4.1: A) Spatial distribution of Andaman-Nicobar seismicity, M≥4.0, for a period of January 1, 1973 to December 25, 2004, Data Source: USGS, NEIC database. B-D) zones marked for depth analysis.

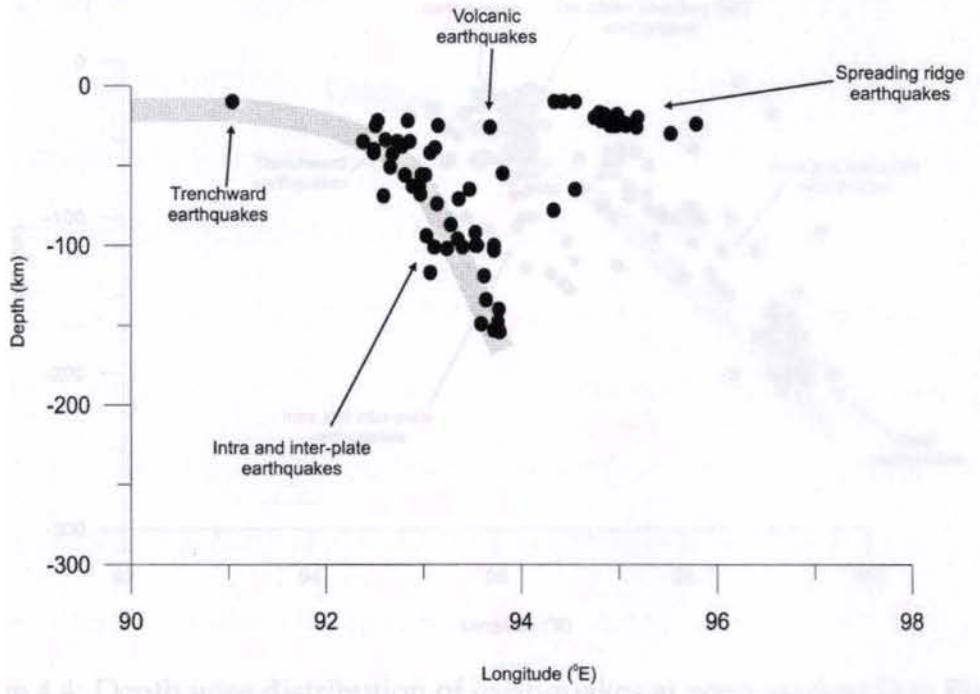

Figure 4.2: Depth wise distribution of earthquakes at 12 degree north (zone marked B in Fig. 4.1). Note the trend of dipping slab. Shallow earthquakes east of 94^0E are due to the Andaman spreading ridge (ASR) events.

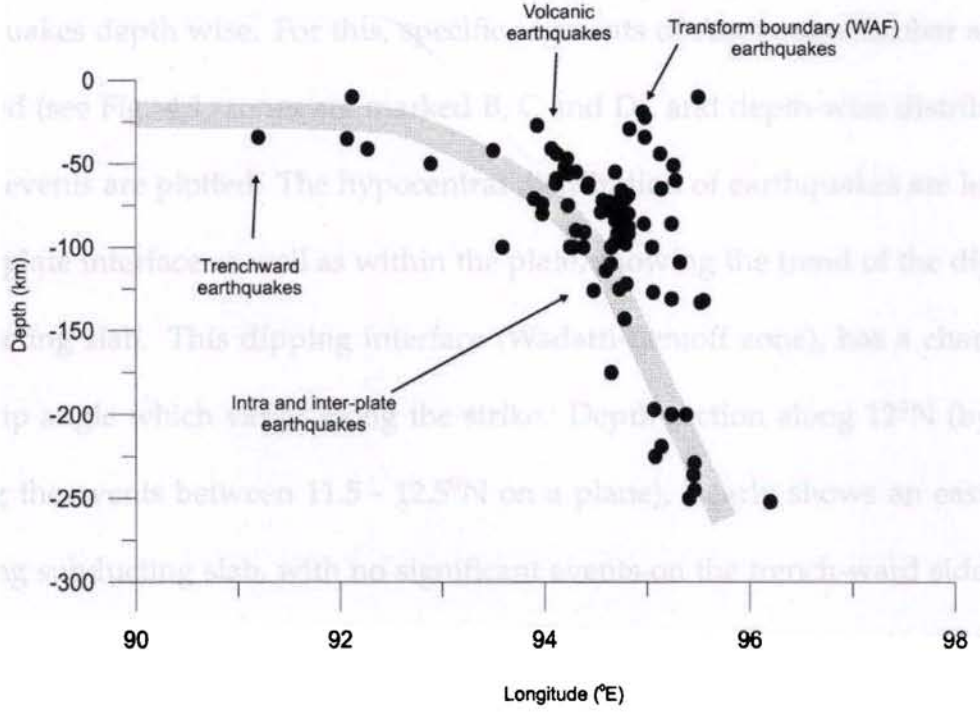

Figure 4.3: Depth wise distribution of earthquakes at zone marked C in Fig.4.1

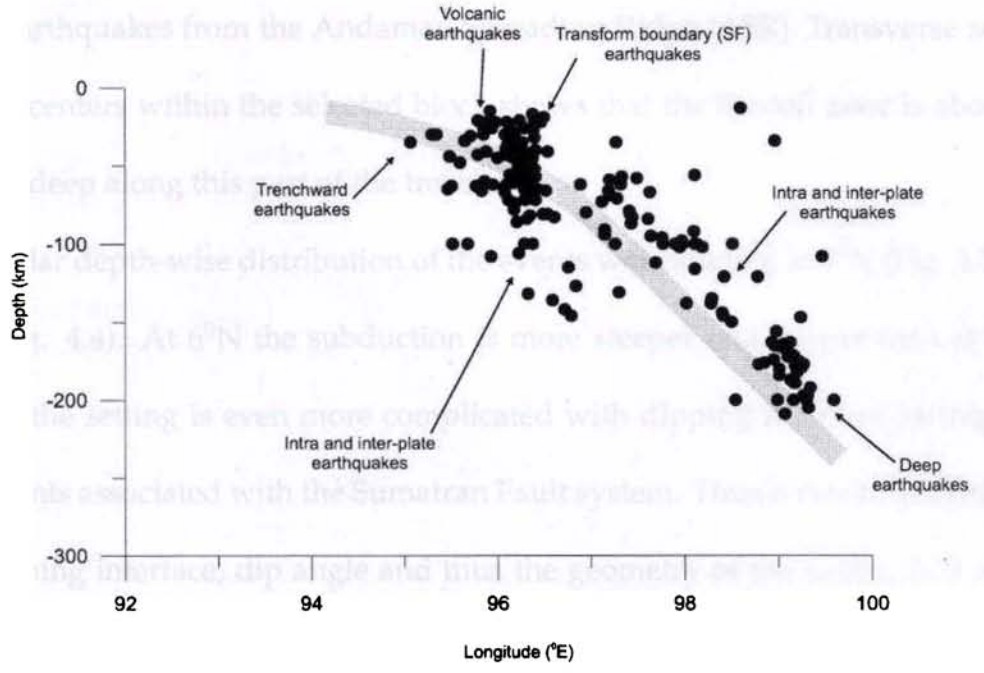

Figure 4.4: Depth wise distribution of earthquakes at zone marked D in Fig.4.1

al., 1993; Hyndman et al., 1997).

A better way to validate this assumption is to analyze the spatial distribution of earthquakes depth wise. For this, specific segments of Andaman-Nicobar arc are selected (see Fig. 4.1, zones are marked B, C and D), and depth-wise distribution of the events are plotted. The hypocentral distribution of earthquakes are located at the plate interface as well as within the plate, showing the trend of the dipping subducting slab. This dipping interface (Wadatti-Benioff zone), has a characteristic dip angle which varies along the strike. Depth section along 12^0N (by projecting the events between 11.5 - 12.5^0N on a plane), clearly shows an eastward dipping subducting slab, with no significant events on the trench-ward side, dipping at about 30-35^0 (Fig. 4.2). Towards the back-arc regions intermediate/deeper events associated with the volcanic arc are found, followed by shallow spreading

ridge earthquakes from the Andaman Spreading Ridge (ASR). Transverse section of hypocenters within the selected block shows that the Benioff zone is about 85-130 km deep along this part of the trench.

Similar depth-wise distribution of the events were studied at 6^0N (Fig. 4.3) and 3^0N (Fig. 4.4). At 6^0N the subduction is more steeper and deeper than at 12^0N. At 3^0N the setting is even more complicated with dipping interface earthquakes and events associated with the Sumatran Fault system. Thus it can be inferred that the dipping interface, dip angle and thus the geometry of the subduction setting of the Andaman-Nicobar changes along strike. From north to south its dip angle becomes more steep and penetration of the downgoing slab becomes more deep. The maximum hypocentral depth is at 260 km, near the southern segment of the study area. The youthfulness of the subduction zone along this part is evident also from the presence of large and great earthquakes in this area (See, Figure 4.8).

A comparison made on the bathymetry and hypocentral depths along the same profile defines the above discussed trend of downgoing slab beneath the archipelago. To map the trend of the dipping plate interface and better 3-D visualization of the trench geometry along the arc (Fig. 4.5) cross-section of the gridded data sets of bathymetry and hypocentral distribution are made use. Gridded topography data is from ETOPO-5 (National Ocean and Atmospheric Administration (NOAA), 1988) and the epicentral data is from USGS, NEIC database of events $M \geq 4.0$. A wire-frame surface map of the gridded hypocentral data created shows the spatial variation of the hypocentral depths on a surface.

A wire-frame plot of the gridded bathymetry data set along the 12^0N (Fig. 4.5),

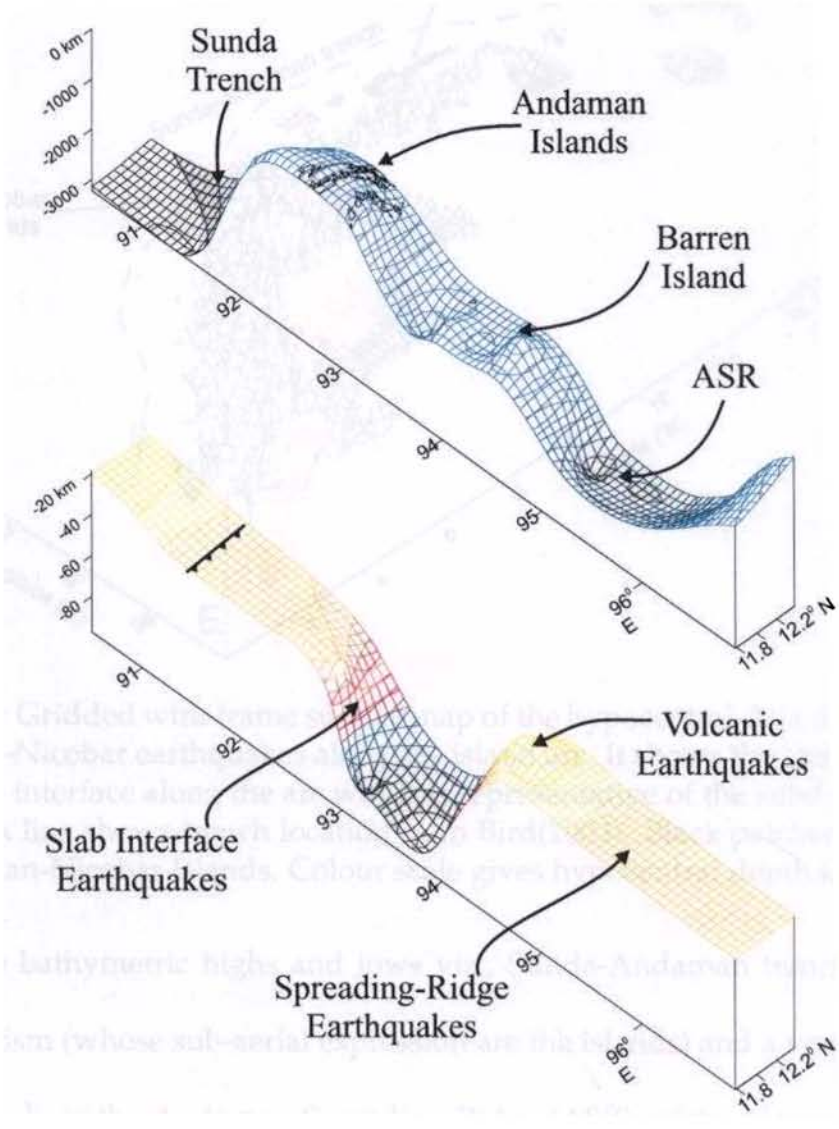

Figure 4.5: Upper panel shows the wire-frame surface topographic section along 12^0N, showing the trench, accretionary prism (Andaman Islands), volcano (Barren island), and the Andaman spreading center. Lower panel corresponds to the gridded wire-frame surface map of the hypocentral data along the same profile, showing the trend of the dipping Benioff zone, volcanic earthquakes, and shallow speading ridge earthquakes. Gridded topography data is from ETOPO-5 from National Ocean and Atmospheric Administration (NOAA) and the epicentral data is from USGS, NEIC database of events M$\geq$4.0.

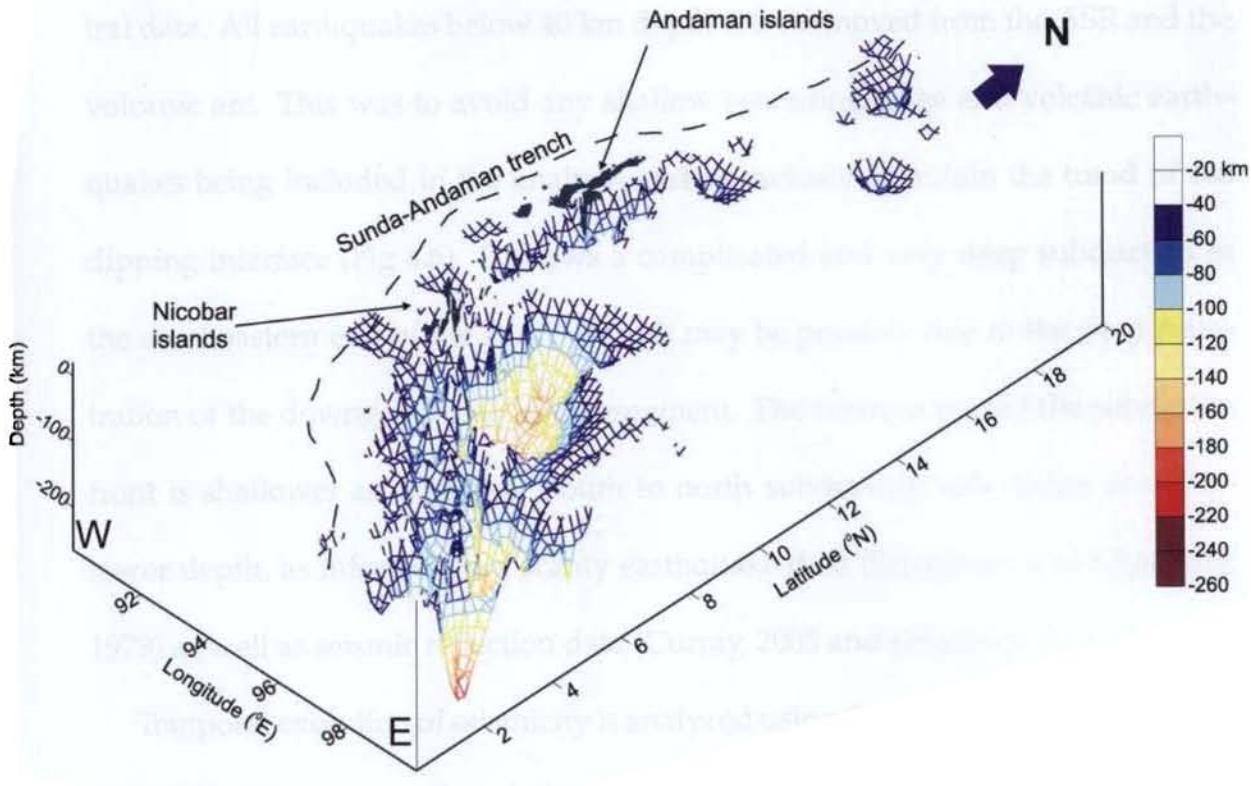

Figure 4.6: Gridded wire-frame surface map of the hypocentral data distribution of Andaman-Nicobar earthquakes along the island arc. It shows the trend of the dipping plate interface along the arc which is representative of the subduction geometry. Black line shows trench location from Bird(2003). Black patches are location of Andaman-Nicobar Islands. Colour scale gives hypocentral depth information.

shows the bathymetric highs and lows viz., Sunda-Andaman trench, the accretionary prism (whose sub-aerial expression are the islands) and a very deep back-arc basin where the Andaman Spreading Ridge (ASR) exists. Comparing with a gridded wire-frame plot of the hypocentral distribution along the same section shows the spatial extent of the earthquakes and the trend of the dipping slab beneath the accretionary wedge. Also seen are the presence of very shallow volcanic arc earthquakes beneath the Barren Island and the spreading ridge earthquakes beneath ASR.

Similar wire-frame surface map along the arc was made with the gridded hypocen-

tral data. All earthquakes below 40 km depth were removed from the ASR and the volcanic arc. This was to avoid any shallow spreading ridge and volcanic earthquakes being included in the analysis and to exclusively obtain the trend of the dipping interface (Fig 4.6). It shows a complicated and very deep subduction in the southeastern end of the study area. It may be possibly due to the deep penetration of the downgoing slab in this segment. The western part of the subdution front is shallower as expected. South to north subducting slab occurs at a shallower depth, as inferred from scanty earthquake data (Srivastava and Chaudary, 1979) as well as seismic reflection data (Curray, 2005 and references therein).

Temporal evolution of seismicity is analyzed using the earthquakes M≥4.9 from the NEIC database mentioned above, for the region within 0-14^{0}N and 92-100^{0}E, which defines the area of interest of this study. Annual frequency of earthquakes during this period consist of ~700 events of M≥4.9 among which 43 events are of M≥6.0 (Fig. 4.7). Among these events twelve are of M≥6.5 and three are of M≥7.0 (Fig. 4.8). Maximum event magnitude reported during this period was M 7.6, an event occurred near the trench-ward side of the north western Sumatra.

The temporal pattern of seismicity does not suggest any particular pattern. It has been suggested based on some of the worlds better studied subduction zones that a period of quiescence follows major earthquakes (Ohtake et. al., 1981). The spatial distribution of M≥6.0 events along arc generally suggests that most parts of the subduction front have been generating earthquakes (Fig. 4.8). Some earthquakes in the southern (1861) as well as the northern part of the subduction zone (1881, 1941 and 1679) have caused larger ruptures. Admittedly, the sampled data

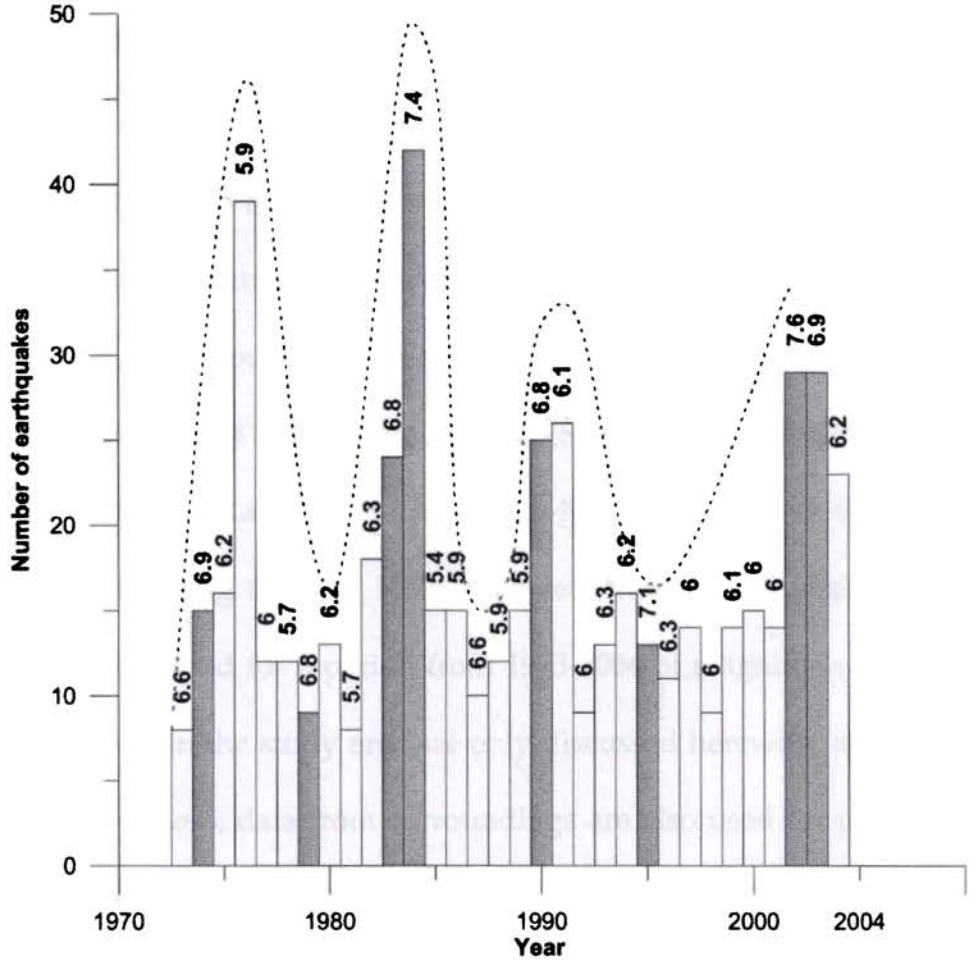

Figure 4.7: Temporal pattern of Andaman-Nicobar seismicity from 1973-2004 for the events M≥4.9. Maximum magnitude of earthquake reported is marked above for the particular year. Data Source: USGS, NEIC database.

time span window is very small, compared with the time scales of continental deformation. However, based on the available data one may note that no part of this subduction zone (except in the northern portions) has remained free of earthquakes.

4.2 Tectonic segmentation based on focal mechanism data and the major stress regimes.

A subduction zone is expected to feature near trench shallow thrust faulting earthquakes, shallow strike-slip earthquakes at the back-arc transforms, shallow normal earthquakes around the spreading ridge and deep normal fault earthquakes in the down-dip side of the downgoing plate (Spence, 1987). Analysis of the available focal mechanisms around the Andaman-Nicobar arc shows the variations in tectonic activity along the arc. Here, data sets from Harvard centroid moment tensors were analyzed for a period from 1973-2004 of magnitude 4.9 and above. Mechanisms within the study area are only discussed herewith, although for the sake of completeness, data from surroundings are also used for plotting. Mechanisms are scaled for magnitude and depth by size and colour respectively (Fig. 4.9).

Focal mechanisms of the major earthquakes along the Sumatra-Andaman trench are consistent with the under-thrusting along the megathrust fault. As already discussed, there is a lack of significant trench-ward earthquakes during this period of analysis (1973-2004). During this period only one event is located on the trench line east of Nicobar with a thrust faulting mechanism. Trench-ward earthquakes

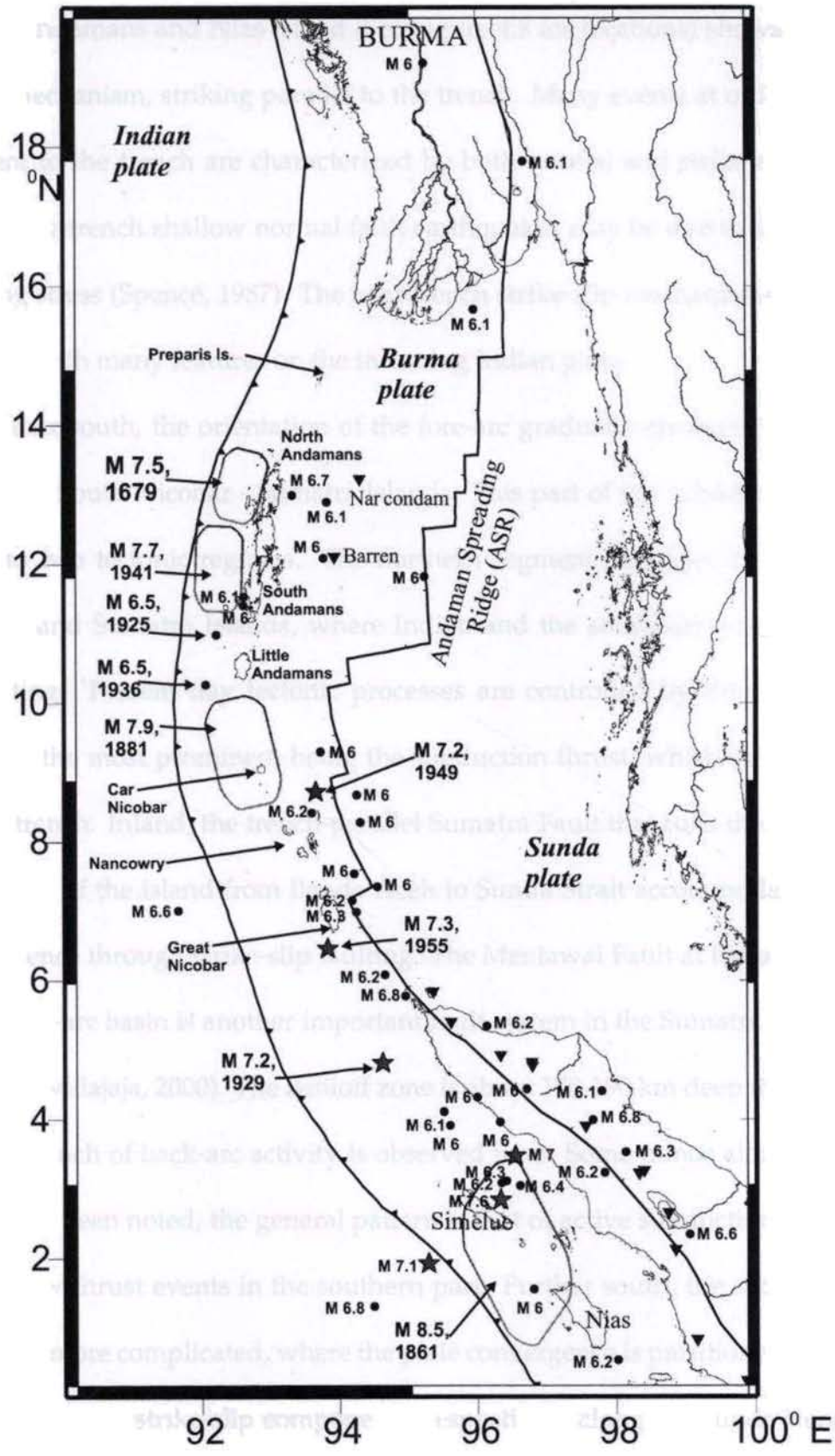

Figure 4.8: Significant pre-seismic earthquakes of M≥6.0 along the Andaman-Nicobar arc.

east of Andamans and Nias Island (See Figure 4.8 for locations) shows consistent thrust mechanism, striking parallel to the trench. Many events at or immediately adjacent to the trench are characterized by both normal and strike slip faulting. These near-trench shallow normal fault earthquakes may be due to the intra-slab bending stress (Spence, 1987). The near-trench strike-slip mechanisms may be associated with many features on the incoming Indian plate.

Further south, the orientation of the fore-arc gradually changes from NNE to NW-SE in South Nicobar - Sumatra Islands. This part of the subduction zone belongs to two tectonic regimes. The northern segment corresponds to the Great Nicobar and Sumatra Islands, where Indian and the southeast Asian plates are interacting. Present day tectonic processes are controlled by three major fault systems, the most prominent being the subduction thrust, which outcrops in the Sunda trench. Inland, the trench-parallel Sumatra Fault that runs through the entire length of the island from Banda Aceh to Sunda Strait accommodates oblique convergence through strike-slip faulting. The Mentawai Fault at the outer margin of the fore-arc basin is another important fault system in the Sumatra region (Sieh and Natawidajaja, 2000). The Benioff zone is about 170-190 km deep in this section and not much of back-arc activity is observed here. Some minor along-arc variations have been noted, the general pattern is that of active subduction dominated by shallow thrust events in the southern part. Further south, the subduction geometry is more complicated, where the plate convergence is partitioned as dip-slip and right lateral strike-slip components, respectively along the Sunda trench and the Sumatran Fault.

Away from the trench to the east, thrust earthquakes of <40 km, with its striking parallel to the arc can be seen. It is followed to east towards back-arc by 40-80 km deep thrusting events (coloured green in Fig. 4.9) primarily associated with the series of the thrust faults in the Andaman subduction zone. Among these, the West Andaman Fault (WAF) is the most prominent. This fault appears to be continuous from the west of Sumatra to east of Nicobars and Andamans. Along the WAF earthquakes with normal mechanisms appear forming another plane of seismicity.

Deeper events of varying mechanisms (coloured blue in Fig. 4.9) are seen among which most may be associated with the Sunda-Andaman volcanic arc. Along the Sumatran Fault (SF), strike -slip events of <40 km can be seen which extends towards north to the Andaman Spreading Ridge (ASR). The ASR earthquakes show typical shallow strike-slip and normal mechanisms. Earthquakes in the 7 to 15^0N show distinct characteristics of the back-arc spreading. The orientation of the normal faulting earthquakes are consistent with the small ocean spreading features in Andaman marginal sea. The Andaman Sea basin is considered to be complex back-arc spreading center, categorized as a pull apart or rip off basin rather than a typical back-arc extensional setting (Curray, 2005).

The transition region between north of SF and south of ASR shows a cluster of shallow and intermediate predominant strike-slip and normal mechanisms and deeper normal mechanisms. This part of the arc exhibits more complex pattern and segregation into clusters of thrust, normal and strike-slip earthquakes (Dasgupta et al., 2003). These mechanisms represent the tectonic features accommo dating the right lateral oblique convergence along the WAF and SF and the slip partitioning

happening there due to the obliqueness in subduction. Along the Sumatra Subduction zone, plate convergence is partitioned into dip-slip and right lateral strike-slip components, the former being accommodated by the slip on the subduction interface and the latter by the Sumatran Fault (Fitch, 1972; Curray, 2005).

The P- and T-axes inferred from earthquake focal mechanisms provide a first order approximation of the stress. The maximum horizontal stresses inferred from the focal mechanisms in the segments discussed above were analyzed as a function of depth. The average P-axis orientation from the focal mechanisms was assumed to be the direction of maximum horizontal stress (S_H in regions of strike-slip and thrust faulting). In regions of normal faulting, the direction perpendicular to the T-axis was assumed to the direction of S_H. The figures 4.10 and 4.11 show the P- and T-axes inferred from the focal mechanism solutions available for the area. The rose diagram showing the orientations of mean S_H and S_h within 40 km depth are shown in Fig. 4.10. The same parameters for the earthquakes deeper than 40 km are shown in Fig. 4.11.

Around the Andaman Islands (Fig. 4.10.a), the direction of S_H is N-S to NE-SW. Two shallow normal faulting earthquakes are reported from this area, which may be representative of deformation within the upper plate structures or volcano deformation. In the zone of shallow seismicity at the northern segment of ASR (Fig. 4.10.b), the mean stress direction is in the NNE-SSW direction, whereas below this segment (Fig. 4.10.c) the trend is in NNW-SSE direction, which is also reported by Rajendran and Gupta (1989). These are associated with the ocean floor spreading and the right lateral motion, and is consistent with the reported opening up of the

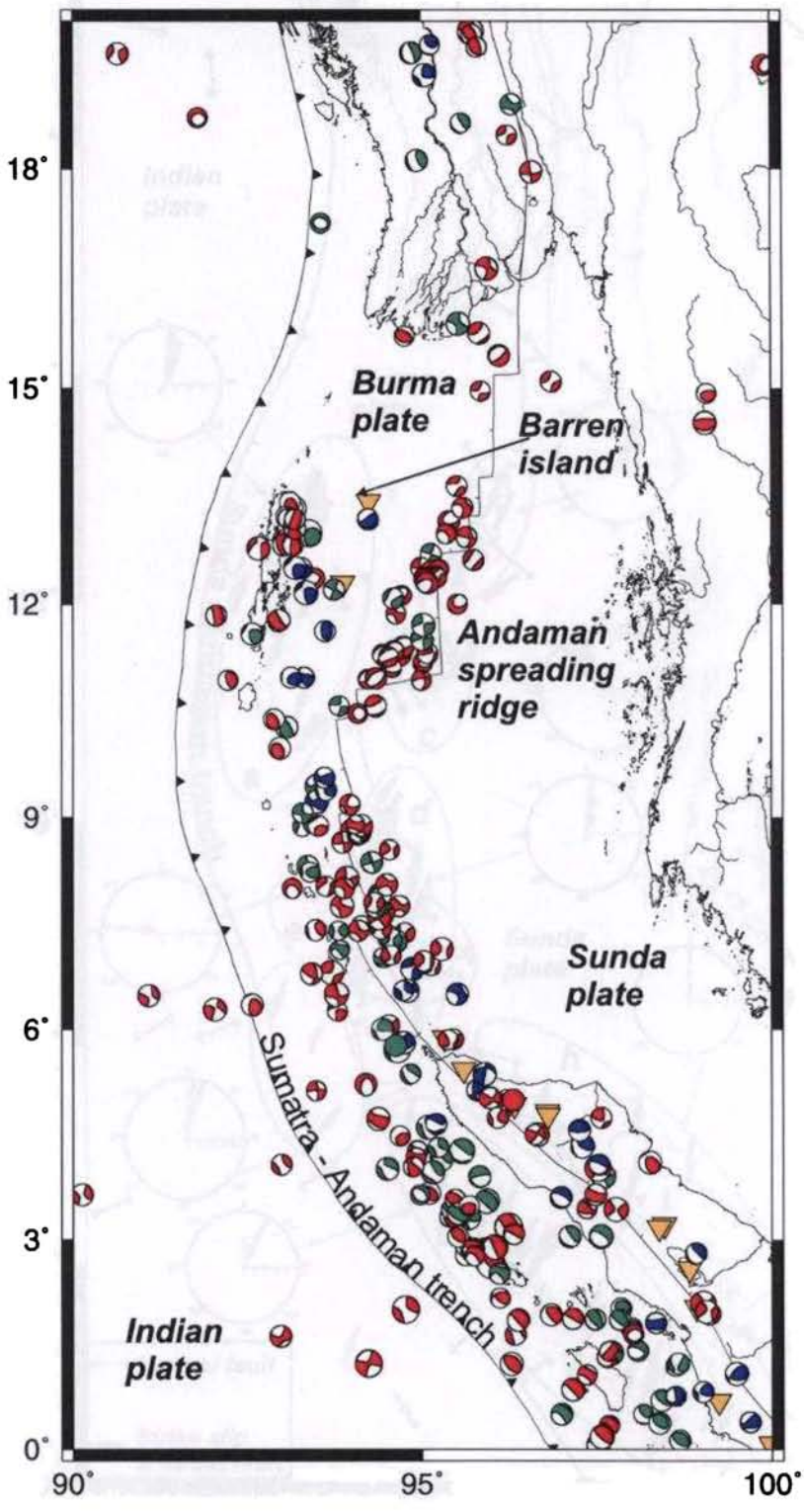

Figure 4.9: Centroid moment tensor solution mechansims of M>4.9 earthquakes (1973-2004) from Harvard CMT catalogue. Events are size wise scaled for magnitude and colour wise scaled for depth. Red - 0 to 40 km, green - 40 to 80 km and blue - 80 to 300 km deep. Plate boundary locations are from Bird(2003). Inverted yellow triangles are volcanoes.

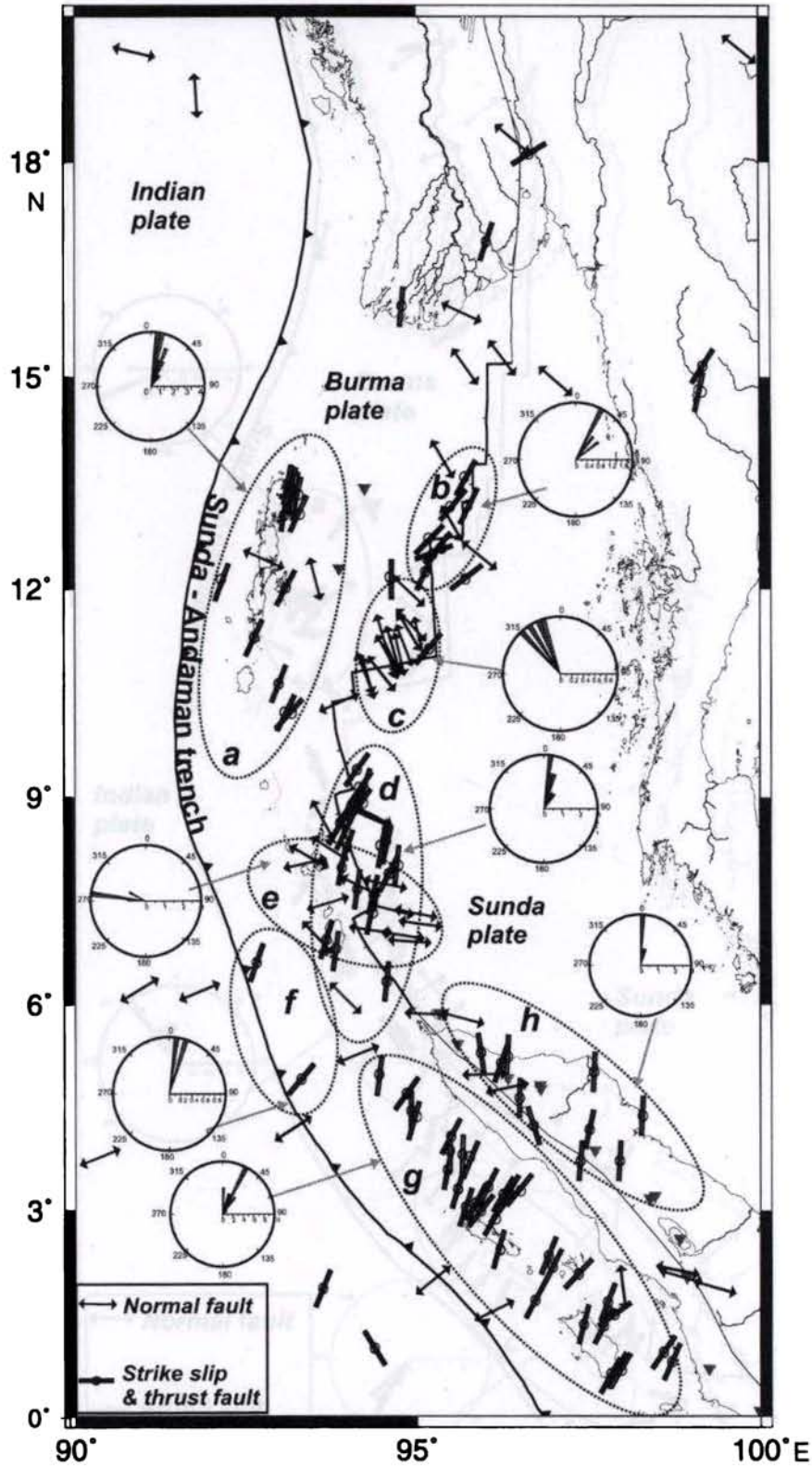

Figure 4.10: The directions of P- and T-axes and type of faulting derived form focal mechanisms of the earthquakes with hypocentral depth less than 40 km. The direction of the lines indicates the orientation of P-axis for strike slip and thrust faulting and T-axis for normal faulting. Rose diagrams show S_H and S_h (maximum and minimum horizontal stresses) for different tectonic regimes (marked by dashed areas).

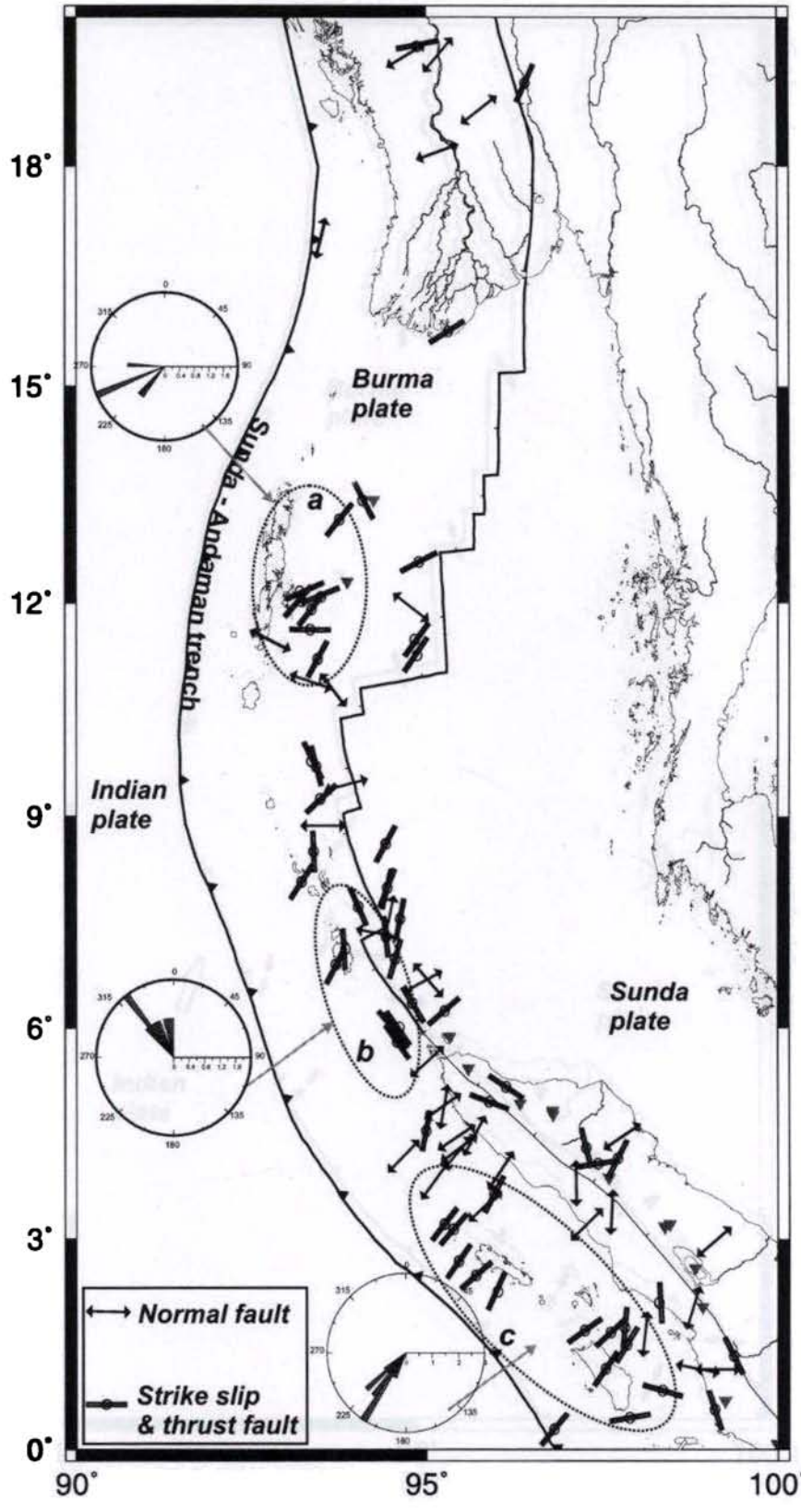

Figure 4.11: The directions of P- and T-axes and type of faulting derived form focal mechanisms of the earthquakes with hypocentral depth greater than 40 km. The direction of the lines indicates the orientation of P-axis for strike slip and thrust faulting and T-axis for normal faulting. Rose diagrams show S_H and S_h (maximum and minimum horizontal stresses) for different tectonic regimes (marked by dashed areas).

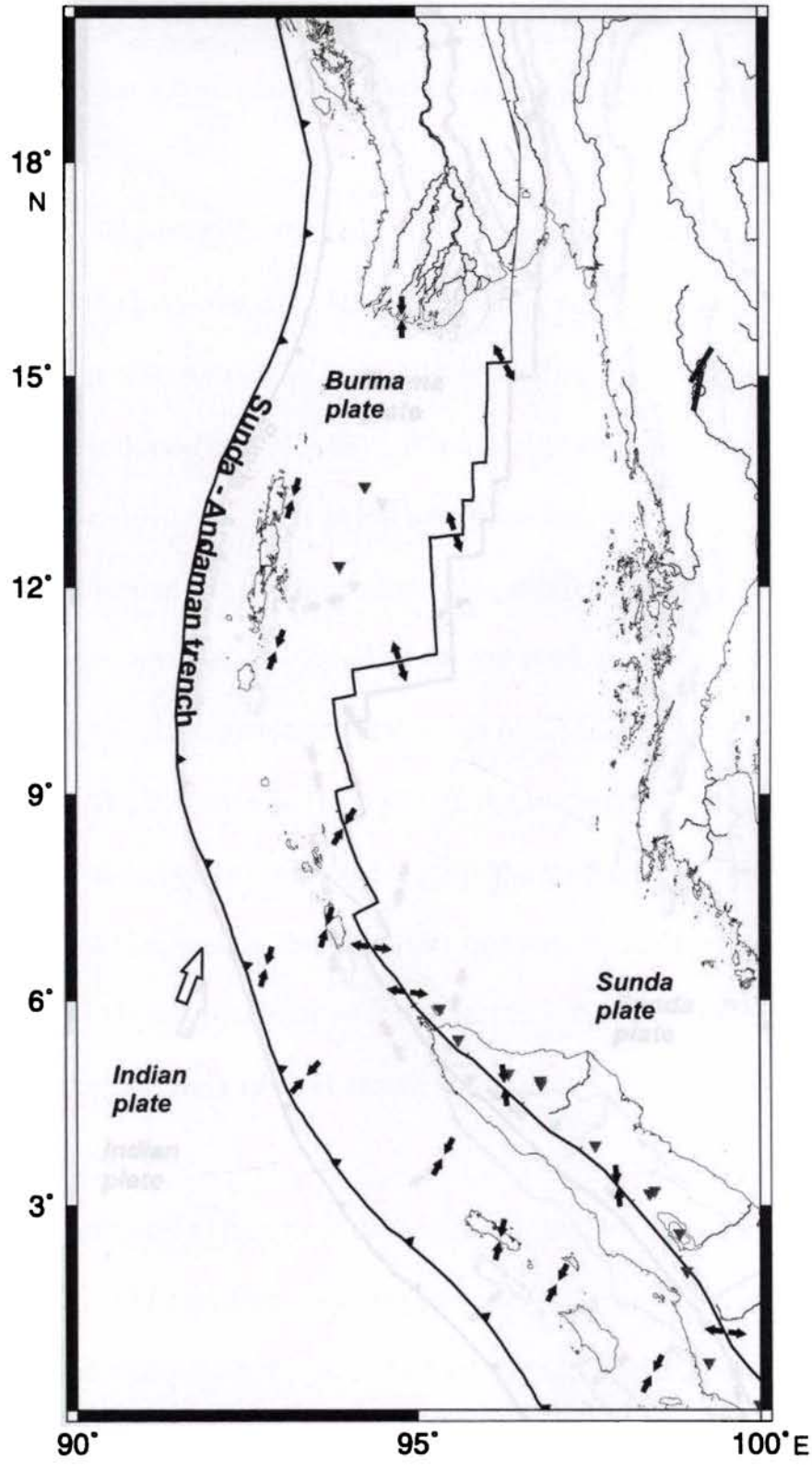

Figure 4.12: Generalized stress map of the Sumatra-Andaman region within 40 km depth. Converging arrows indicate compressions and diverging arrows indicate extension.

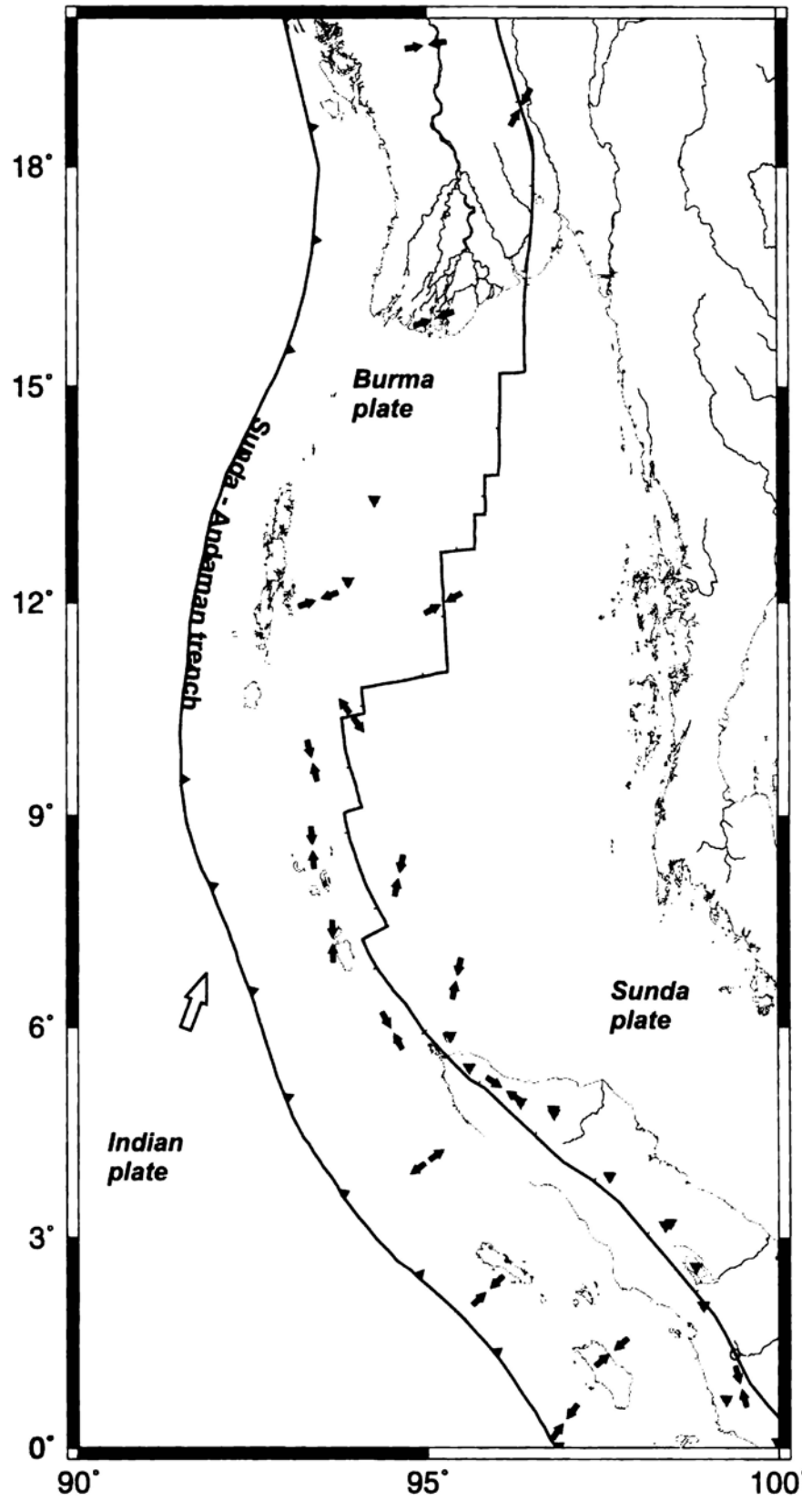

Figure 4.13: Generalized stress map of the Sumatra-Andaman region of >40 km depth. Converging arrows indicate compressions and diverging arrows indicate extension.

Andaman sea region by Curray, (2005) and Raju, (2004). Figures 4.10.d and 4.10.e show similar stress orientations but they are oriented towards N-E to NWW-SEE direction.

A segment very near to the trench shows S_H oriented towards NNE-SSW (Fig.4.10.f), consistent with the plate velocity vector azimuth there (DeMets et al., 1994a). North western segment of Sumatra (Fig. 4.10.g) shows typical trench-ward under-thrusting with a stress orientation of NNW-SSW. It is a typical signature (Lu et al., 1997) of the near trench extensional stress in the bent plate due to the earthquakes that occur below the plane of the bending subducting lithosphere. East of this zone the stress orientations are mainly controlled by the right lateral SF and its northern extension. The major S_H orientation is towards NNE-SSW.

At a greater depth (>40 km) (Fig. 4.11.a), the major stress orientation changes to E-W compression. Fewer number of earthquake mechanisms in ASR shows consistent stress orientations like the shallower portions there. Segment - b, shows a NW-SE trend of stress, consistent with the deeper WAF right lateral motion. Segment - c, shows the trend of near trench compression in the deeper portions of North Western Sumatra.

Spatial distribution of the stress field and their variations with depth are summarized in Fig. 4.12 and Fig. 4.13. Trench-ward, the Sumatra-Andaman region shows a general sense of compression in NE-SW to N-S direction at the shallower portions. In the ASR region, the general trend of stress (S_h) is in NNW-SSE. In a transition zone between the ASR and SF, the stress orientations (S_h) change to E-W direction. In intermediate depths, the trend of (S_H), east of Sunda-Andaman trench

is NE-SW to N-S (Fig. 4.13).

4.3 Geodetic constraints on the pre-seismic convergence along the arc

4.3.1 Pre-earthquake velocities

Pre-earthquake GPS surveys were carried out in the Andaman-Nicobar Islands as part of this study and were part of a broader study of geomorphic features in the islands, and a total of 8 sites were surveyed prior to the earthquake in measurement campaigns in 2002, 2003, and 2004 (Earnest et al., 2005). The final pre-earthquake campaign was carried out in August 2004 over a period of about 4 weeks, and was 4-5 months before the December 26^{th} mainshock. A site in Port Blair was surveyed in each campaign, and sites in Diglipur (North Andaman) and Car Nicobar were surveyed in both 2003 and 2004. The other 5 sites were surveyed only once prior to the earthquake. Each GPS survey at a site involved the collection of 2 or more days of data, with each days data generally covering a full 24-hour span. The Port Blair site, PBLR was surveyed continuously for the duration of each survey.

Pre-earthquake velocities were estimated using daily GPS solutions spanning between 4^{th} May, 2001 and 11^{th} September, 2004. Coordinate repeatability were tested (See figs. 4.14 to 4.16), and station velocity is measured in the ITRF00 frame (Fig. 4.17 and Table 4.1 for details). Convergence between India is computed by fixing the IISC point (Fig. 4.18 and Table 4.2 for details).

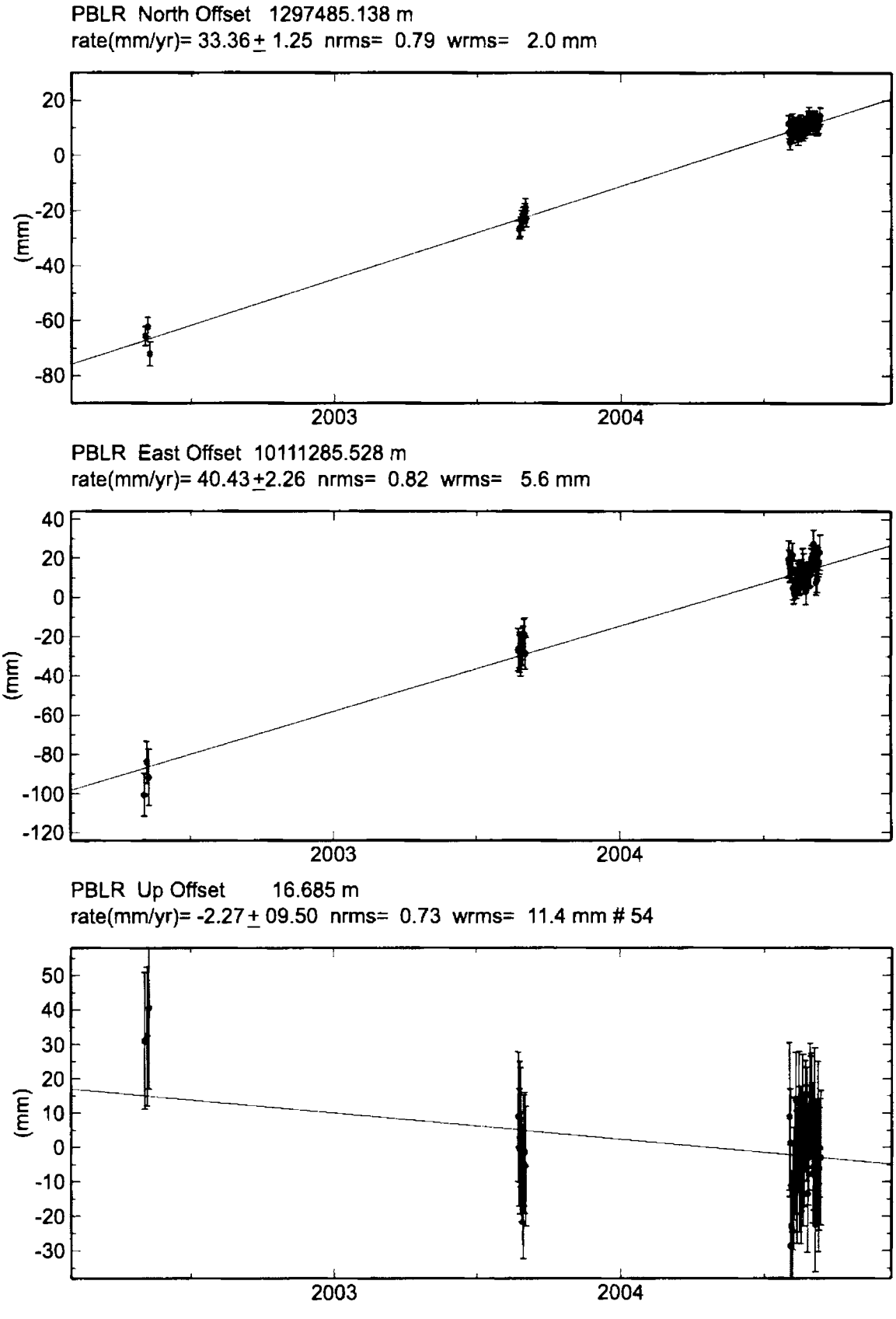

Figure 4.14: Time series plot of PBLR, Port Blair GPS point from 2002-2004 in ITRF00 reference frame.

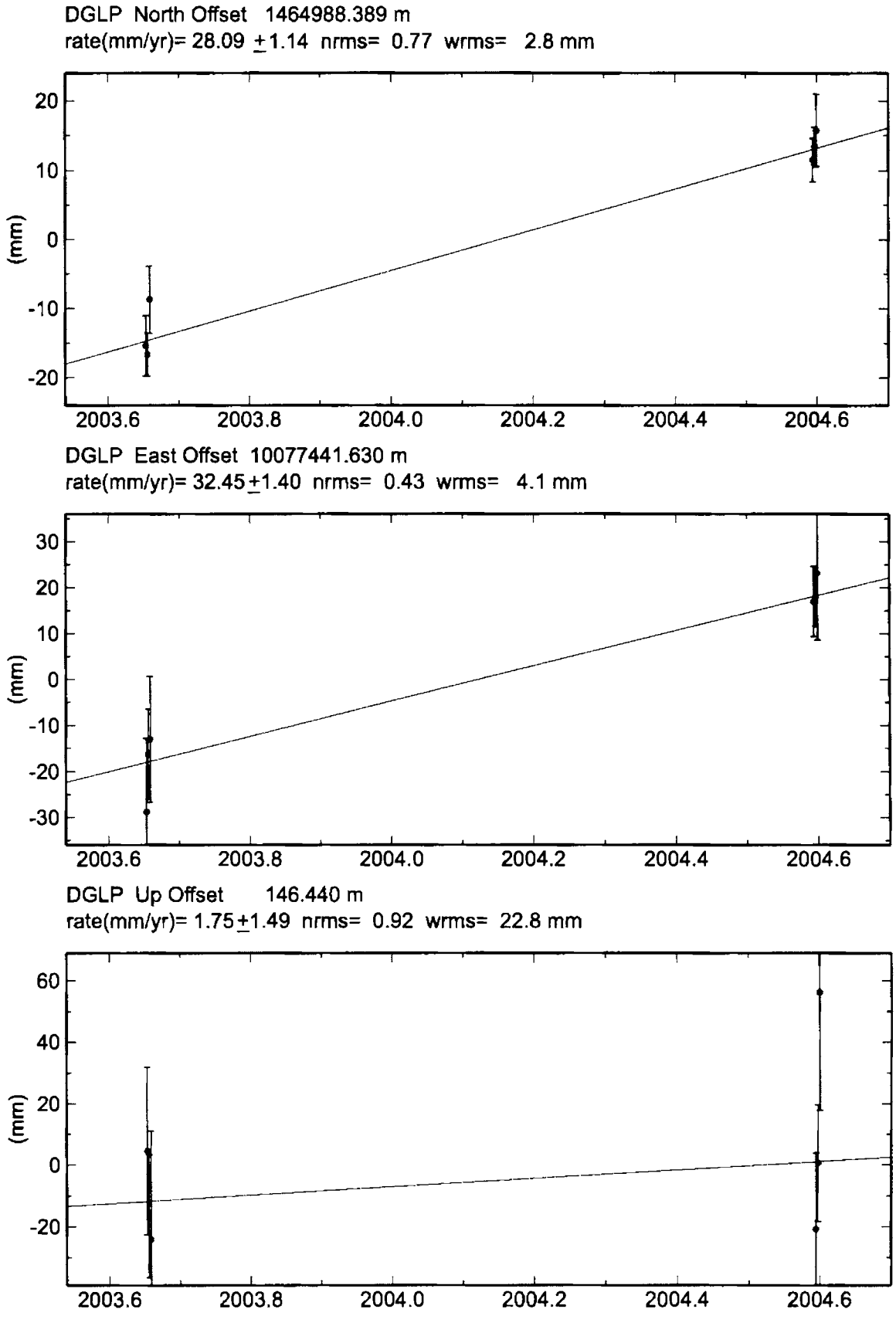

Figure 4.15: Time series plot of DGLP, Diglipur, North Andamans GPS point from 2003-2004 in ITRF00 reference frame.

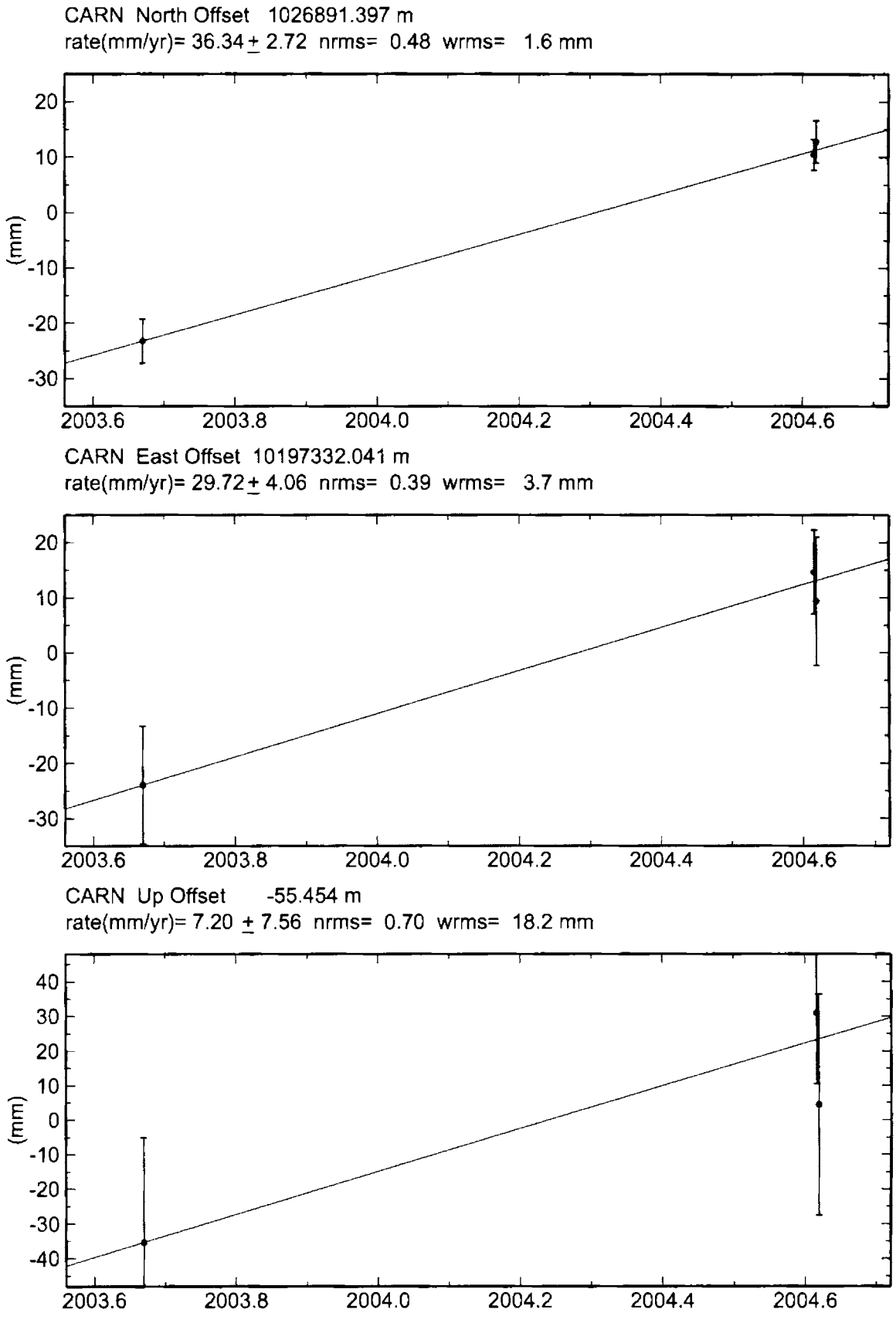

Figure 4.16: Time series plot of CARN, Car Nicobar GPS point from 2003-2004 in ITRF00 reference frame.

Table 4.1: Computed absolute velocity(mm/yr) of the control points in ITRF00 reference frame.

Station Code	East	E-sigma±	North	N-sigma±
PBLR	40.43	0.08	33.36	0.05
DGLP	32.45	0.21	28.09	0.12
CARN	29.72	0.41	36.34	0.53

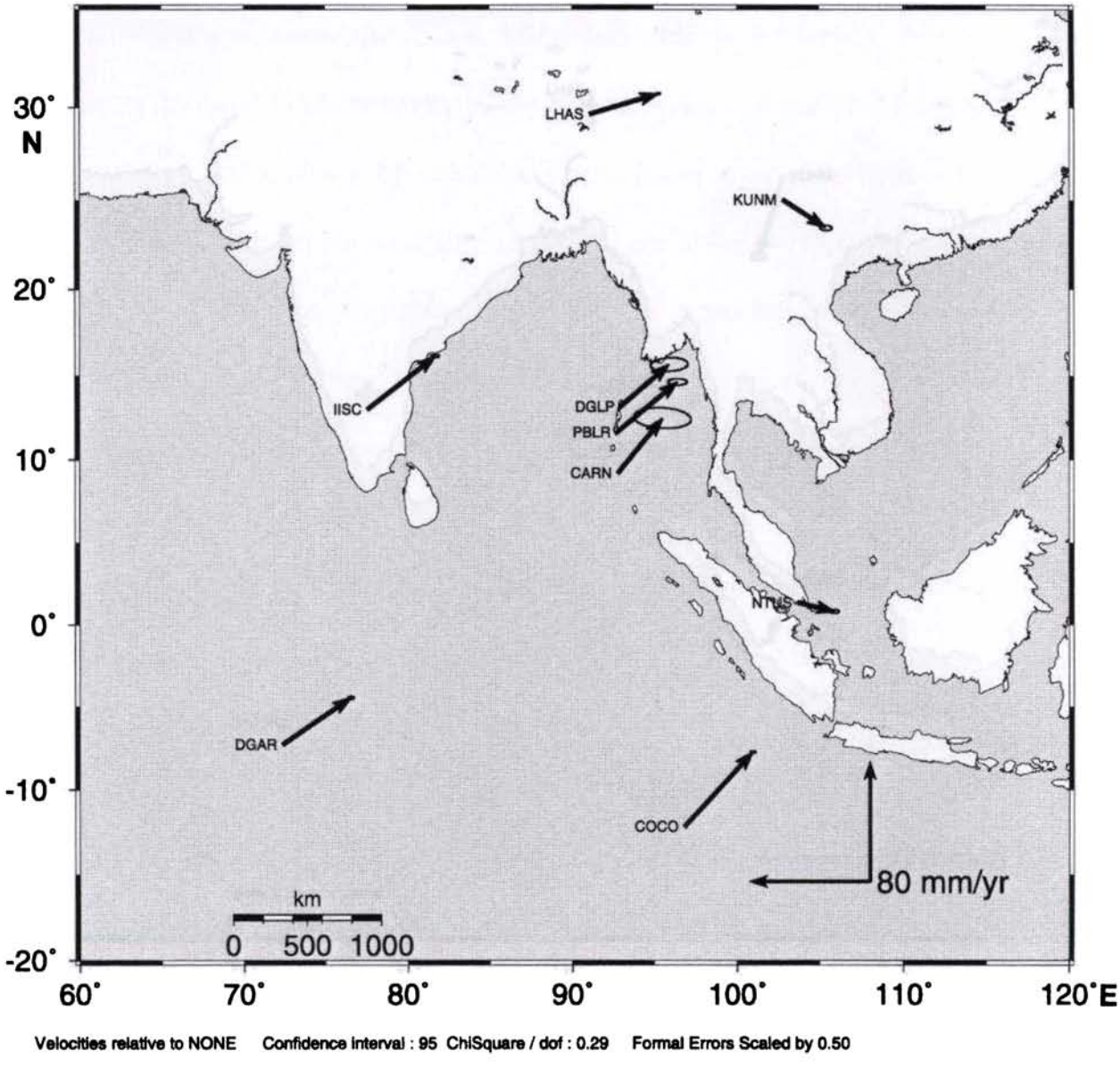

Figure 4.17: Absolute velocity vectors of the campaign and IGS stations used in this study. The frame of reference is ITRF00.

Table 4.2: Computed relative velocity(mm/yr) of the control points with respect to IISC, Bangalore.

Station Code	East	E-sigma	North	N-sigma
PBLR	-4.99	1.38	-1.91	0.03
DGLP	-12.97	2.21	-7.18	0.12
CARN	-15.70	2.87	1.07	0.19

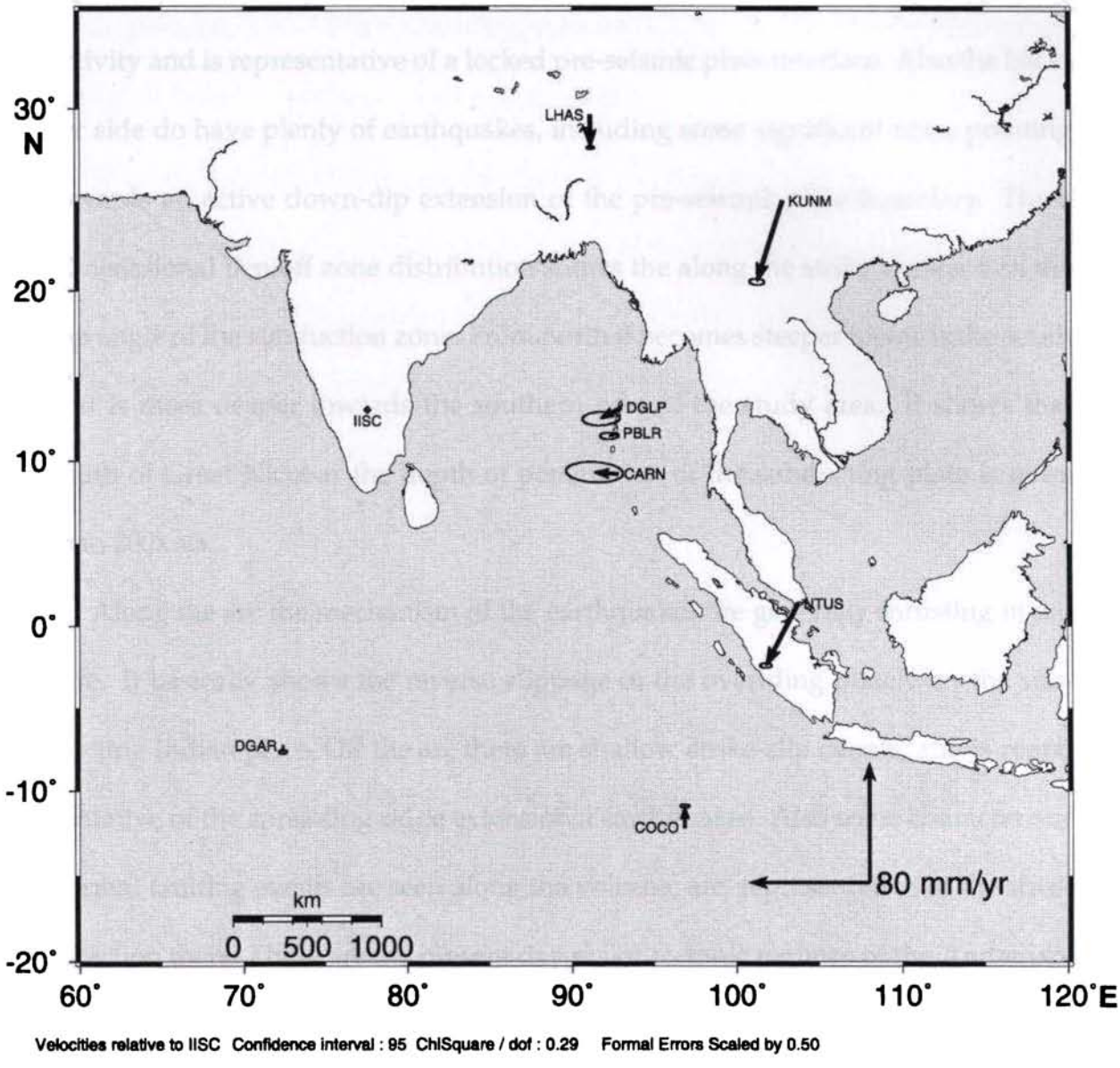

Figure 4.18: Relative velocity vectors of the campaign and IGS stations used in this study. The frame of reference is ITRF00. Velocity vectors are computed with respect to IISC, Bangalore.

4.4 Discussion

Temporal analysis of pre-seismic earthquakes shows that there is an ambient and consistent seismicity level with occassional M>6.0 earthquakes. But it does not show any precursory signal towards the 2004 megathrust occurrence. But spatial spread of earthquakes shows that the trenchward side is devoid of seismic activity and is representative of a locked pre-seismic plate interface. Also the back-arc side do have plenty of earthquakes, including some significant ones, pointing towards an active down-dip extension of the pre-seismic plate boundary. Three dimenssional Benioff zone distribution shows the along the strike variation in the dip angle of the subduction zone. From north it becomes steeper towards the south and is more deeper towards the southern part of the study area. It shows that south of Great Nicobar the depth of penetration of the subducting plate is more than 200kms.

Along the arc the mechanism of the earthquakes are generally thrusting in nature. It basically shows the reverse slippage of the overiding plate over the subducting Indian plate. Off the arc there are shallow strike-slip events, and is representative of the spreading ridge extensional earthquakes. Also some characteristic normal faulting events are seen along the volcanic arc, representative of the stress direction there. These are the present day major tectonic regimes of the Andaman-Nicobar subducting environment. The Sumatra-Andaman trench region shows general sense of compression in NE-SW to N-S direction at the shallower portions. In the ASR region, the general trend of stress is in NNW-SSE. In a transition zone

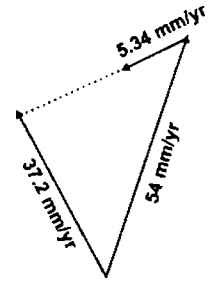

Figure 4.19: Vector closure diagram for the Port Blair segment. 54 mm/yr ($N22^0E$) and 37.2 mm/yr (320^0) are the Indian plate velocity with respect to eurasia (DeMets et al., 1994a) and Andaman spreading velocity (Curray, 2005) respectively. Present day Port Blair convergence velocity computed in this study samples only 15% of expected full rate convergence of ~40 mm/yr.

between the ASR and SF, the stress orientations change to E-W direction. In intermediate depths, the orientation of stress, east of Sunda-Andaman trench is NE-SW to N-S. The trend of P-axis is generally N-S, suggesting that the entire area is subjected to compression in relation to the nearby Himalayan syntaxis consistent with the observations of Le Dain et al., (1984) and Guzman Speziale and Ni, (1993).

GPS observations prior to the earthquake show nearly pure convergence across the Andaman Trench, consistent with the previous and independent GPS results of Paul et al., (2001). The sites in the Andaman Islands move westward relative to India. Only one site, Port Blair(PBLR), has a velocity significantly different from zero, because the other sites have only two pre-earthquake surveys one year apart and have large uncertainties. However, the estimated velocities of Diglipur (DGLP) and Car Nicobar (CARN) are consistent with that of PBLR. Port Blair converges with India at a rate of 5.34 $\pm$ 1.38 mm/yr oriented almost due west. This estimate is slower than the 14 mm/yr estimate of Paul et al., (2001). Diglipur (DGLP) shows a velocity of 14.82 $\pm$ 2.21 mm/yr and Car Nicobar (CARN) shows 15.73 $\pm$

2.87 mm/yr. This suggests that the Andaman Trench is part of a purely slip partitioned plate boundary, with the strike-slip component of India-Sunda relative plate motion being taken up on the transform fault in the Andaman Sea or on the West Andaman Fault, and the convergent component on the Andaman Trench. In this respect the Andaman Trench is similar to Sumatra, which also exhibits almost full strain partitioning between the subduction zone and Sumatra Fault (McCaffrey et al., 2000). Thus there is no reason to expect a significant strike-slip component to the co-seismic displacements along the Andaman segment, except in the northernmost Andaman Islands where here is a significant bend in the trench.

Some of the differences may be due to reference frame, as Paul et al., (2001) defined an India-fixed frame by subtracting the motion of India from the NNR-NUVEL1A plate motion model (DeMets et al., 1994b) from their ITRF96 velocities. This assumes that the ITRF96 velocities are in the same frame as NNR-NUVEL1A (DeMets et al., 1994b), which is not true, although the ITRF is approximately aligned with the NNR frame. In addition, the motion of India in NUVEL1A is now known to be biased, due to the diffuse plate boundaries in the Indian Ocean (Gordon et al., 1998). Thus their reference frame is different from this study and direct comparison of velocities may be misleading. Unfortunately, the analysis strategy of Paul et al., (2001) (fixing several sites to their ITRF96 coordinates) makes it difficult to place their velocities into the latest ITRF without a re-analysis.

The azimuths of convergence of Port Blair (PBLR), Diglipur (DGLP) and Car Nicobar (CARN), with respect to India (IISC) are probably representative of the motion of the Burmese sliver along the arc. These velocities are not representative

of the full Andaman-Nicobar velocity, due to the unknown degree of seismic coupling there. The predicted NUVEL-1A convergence rate of Indian plate along this margin is 54 mm/yr along N22^{0}E (DeMets et al., 1994a). Locally, due to the back-arc rifting process opening up of the Andaman sea in the ASR occurs in a direction of 327^0 (Fig. 4.10.c) from present day north with a magnitude of 37.2 mm/yr (Raju et al., 2004 and Curray, 2005). Assuming, uniform subduction without any locking along the various segments of the arc, yields an Indo/Andaman convergence vector of ~40 mm/yr almost due west. A vector closure model (Fig. 5.12) based on these assumptions and arc-normal convergence predicts that in the pre-earthquake period PBLR should move toward India at 85% of the Burma-India convergence rate. Elastic deformation from the locked shallow megathrust causes eastward motion of only 15% of the total convergence rate. Similarly, DGLP and CARN samples only 37% and 37.5% respectively of the India/Andaman convergence.

Chapter 5

Co-seismic deformational constraints

5.1 Introduction

The Sumatra-Andaman earthquake caused significant ground-level changes, which includes uplift as well as subsidence. Documenting these features is important, because they may act as a process in the search for similar occurrences from past earthquakes. Here, the effects of co-seismic deformation in some selected regions along the arc are presented. The most devastating effect of the earthquake was the large tsunami that inundated most parts of the islands (among other regions); thick deposits of sand have been left by these waves in many parts of the islands. Considerable vertical changes were observed all along the arc, some sites showing evidence of subsidence, whereas others registering uplift. This earthquake generated co-seismic deformation features such as elevated coastal terraces, uplifted coral beds, ground fissures, sandblows, and other liquefaction features resulting from severe ground shaking. The earthquake caused significant ground-level changes, uplift as well as subsidence, some of which were mapped from aerial surveys (Mallick and Murthy, 2005) as well as by ground investigations (Earnest et al., 2005; Kayane et al., 2007; Rajendran et al., 2007).

5.2 Ground level changes

Notable uplift was observed in regions in the northern part of the rupture zone, such as Diglipur and also along the western margins of the the islands. This is

manifested mostly in the form of elevated shore lines and coastal terraces, uplifted coral beds and emerged mangrove swamps, and receded water marks showing the pre-earthquake survival levels of mussels and barnacles attached to rock exposures and man made pillars. About 50 km north of Diglipur, in the Landfall Island rise in ground level was evidenced by the emergence of the the coral bed surrounding the island and the uplift of the mangrove swamps, with their roots appearing about 0.65 m above the post-earthquake water level (Fig. 5.1.a). In Ariel Bay, east coast of Diglipur, the uplift of the coast had caused recession of sea by about 60-80 m from the previous shoreline (Fig. 5.1.b). Extent of this recession of the sea was observed till Kalipur coast, about 8 km south of Ariel Bay as part of this study. Another evidence for the rise in land comes in form of lines of barnacles occurring 60-70 cm above the present day sea level, on the pillars of the pier near Ariel Bay (Fig. 5.1.c).

Change in elevation of land >50 cm was also evident at Mayabandar, about 80 km south of Diglipur, where line of mussels occur >50 cm above the post-earthquake high tide (Rajendran et al., 2007). The beaches of Avis Island, located on the north-eastern margin of middle Andaman were uplifted by ~80 cm, as evident from the raised beaches. An overall rise in the land level around North Andaman Island is evidenced by dried up mangrove creeks and raised beaches. Co-seismic ground uplift appears to have progressed to the northern limits of the islands, the farthest observed at Landfall Island. Based on remote sensing data, Meltzner et al., (2006) have reported minor uplift of 20-30 cm at Preparis Island, ~80 km north of Landfall Island, marking the northern boundary of the 2004 event rupture termination (See Figure 4.8 for location).

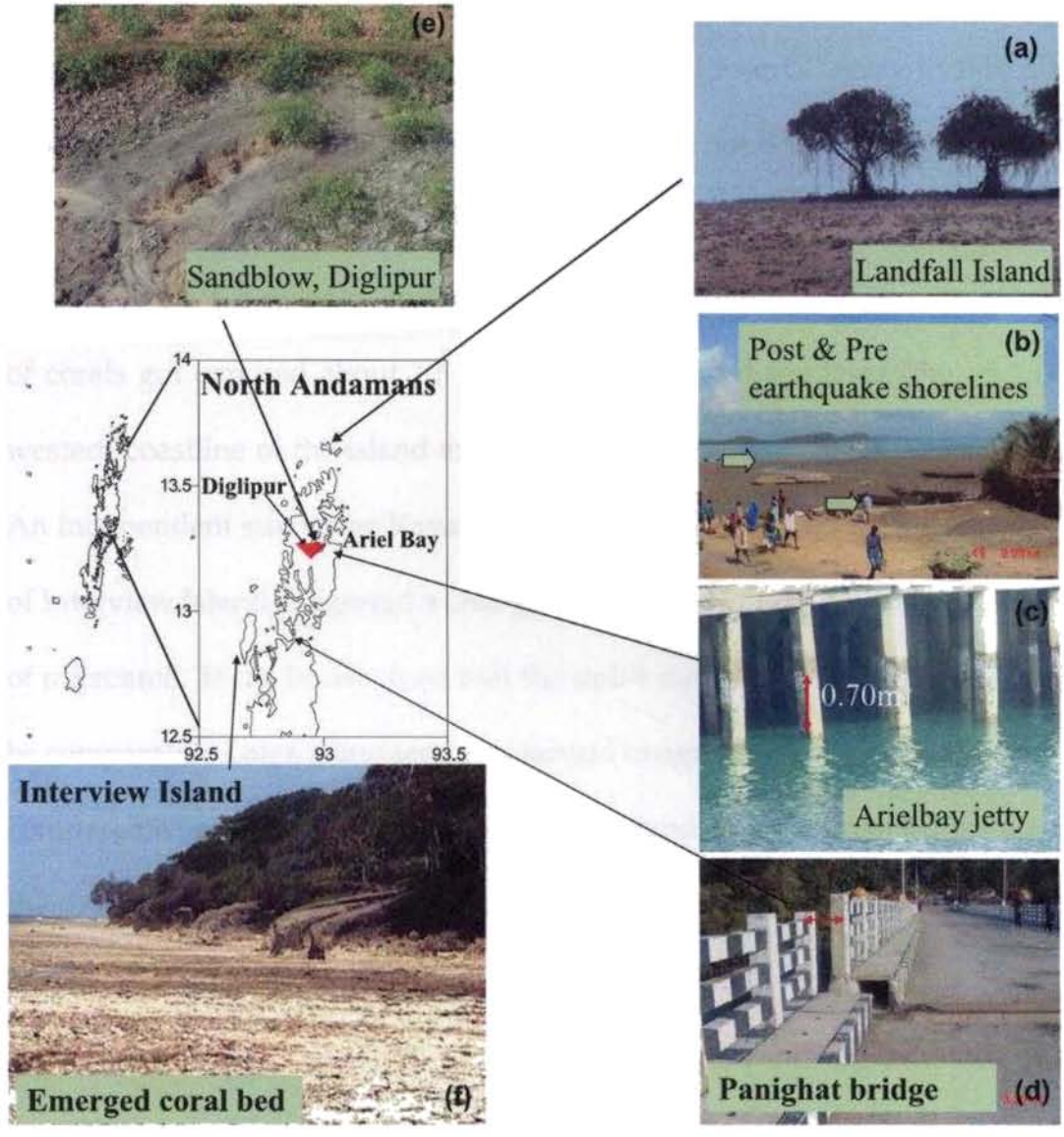

Figure 5.1: Co-seismic deformational features observed, as part of this study, in and around North Andamans. Respective locations are marked by arrows on the map. a) emerged coral bed and mangrove swamp at Landfall Island. b) Receded post-earthquake shoreline at Ariel Bay c) Pre-earthquake line of barnacles on a pillar at Ariel Bay jetty. d) Co-seismic lateral shift on the span of the bridge connecting North Andaman and Middle Andaman. e) Co-seismic sandblow feature seen near Magar Nalla, Diglipur. f) uplifted coral bed in the western margin of Interview Island.

The Indian Coast Guard reported new beaches and elevated coral beds along the western part of the North Sentinel Island, and reported a 1 m uplift along its western coast (Fig. 5.2.e). Being a Sentineli tribal reserve, entry to this island is prohibited, and thus the features from there were not documented as part of this study. However, evidence of uplift along the western margin of Interview Island was observed. Co-seismically, the entire western coastline and its adjacent patches of corals got exposed about 1.5 m above the present sea level (Fig. 5.1.f). The western coastline of the island extended about 500-600 m from the previous one. An independent survey by Kayanne et al., (2007) conducted on the western coast of Interview Island suggested a change in elevation of 1.53 m based on emergence of microatoll. It can be assumed that the uplift reported from Sentinel Island may be comparable. Later, using remotely sensed images, Meltzner et al., 2006 reported comparable uplift values for North Sentinel Island. Aerial surveys done soon after the earthquake have reported uplift of $\sim$1 m, along the western Andaman coast, based on raised watermarks (Mallik and Murthy, 2005).

While most parts of Middle and North Andaman showed evidence of uplift, Port Blair, located on the eastern margin of South Andaman generally subsided. A demonstrative evidence of subsidence here is displayed by the pre- and post-earthquake tide gauge record from Port Blair (Fig. 5.2.c). At this station operated by the National Institute of Ocean Technology (NIOT), Chennai; diurnal sea-level changes after the earthquake were observed $\sim$ 1 m above the pre-earthquake datum, indicating subsidence along its eastern fringes (Fig. 5.3). Sipighat area in Port Blair shows tell-tale evidence of submergence like flooding even during low tides.

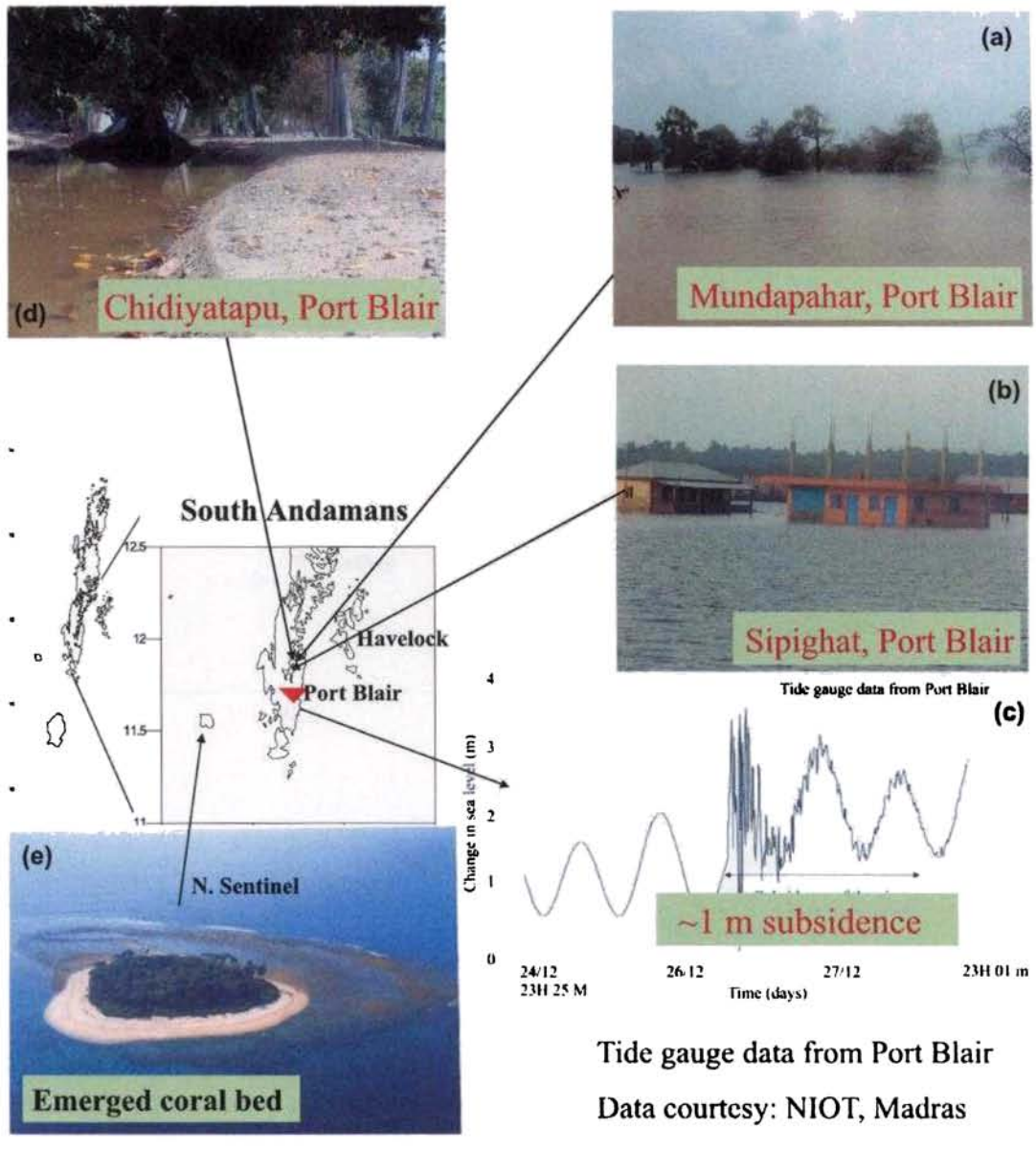

Figure 5.2: Co-seismic deformational features observed, as part of this study, in and around South Andamans. Respective locations are marked by arrows on the map. a) Submerged mangrove forest at Mundapahar beach, Port Blair. b) Flooded Sipighat, Port Blair even during low tides. c) tide guage record at Chatham observatory run by NIOT. d) tsunami soil deposits land inward at Chidiyatapu beach, Port Blair. e) Aerial view of the uplifted western coast of North Sentinel Island (photo courtesy: Indian Coast Guard)

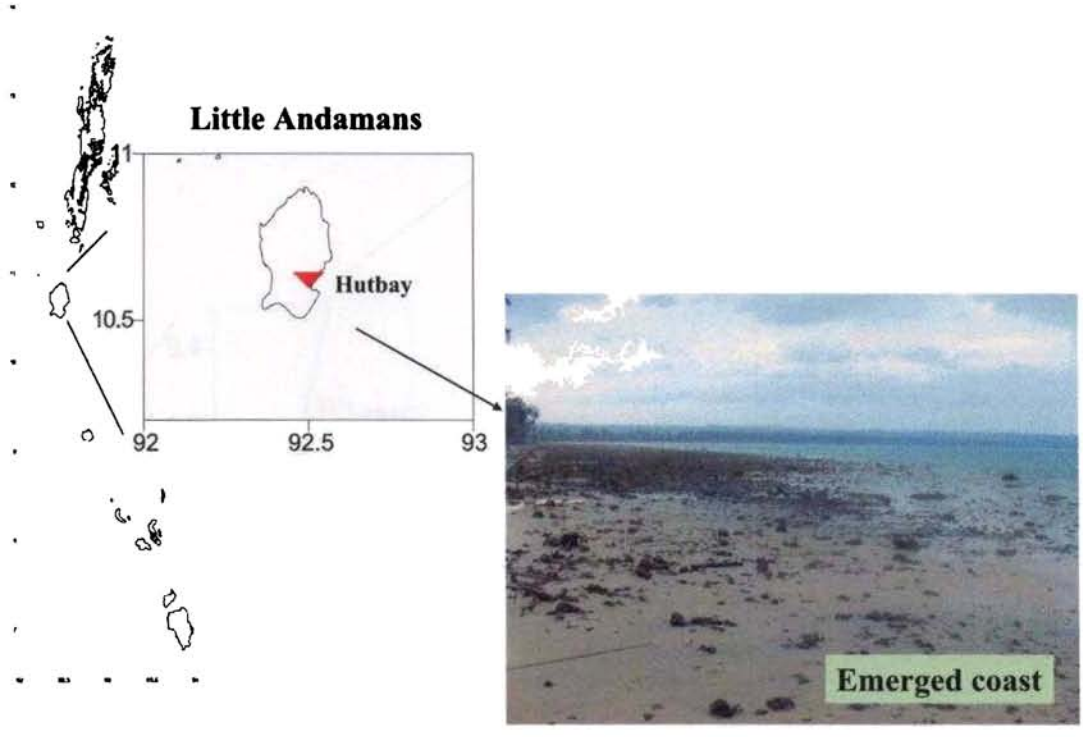

Figure 5.3: Co-seismically Hut Bay emerged $\sim$ 0.35 m as evident from the emerged beaches there. Location of Hut Bay marked by arrow. No other field observations available due to entry restrictions being an Onge tribal reserve.

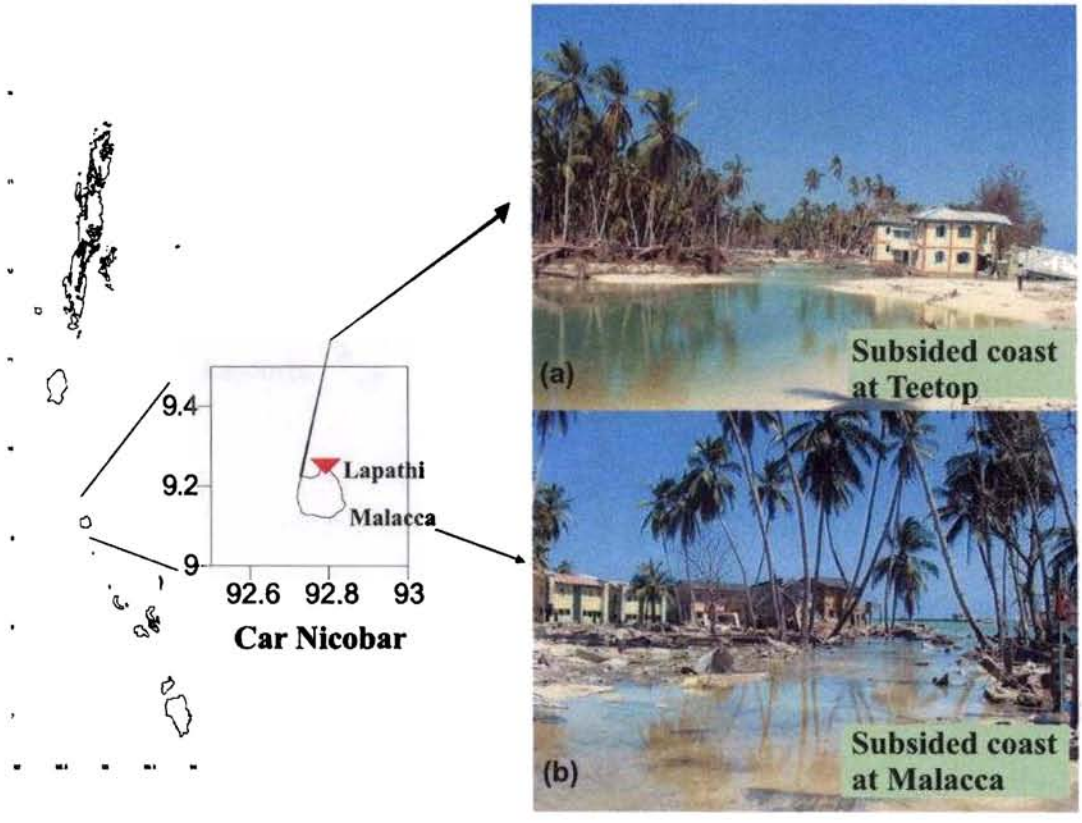

Figure 5.4: Co-seismic deformational features observed, as part of this study, in Car Nicobar. Respective locations are marked by arrows on the map. a) subsided coastline at Teetop, north western coast of Car Nicobar. b) subsided coastline at Malacca, east coast of Car Nicobar.

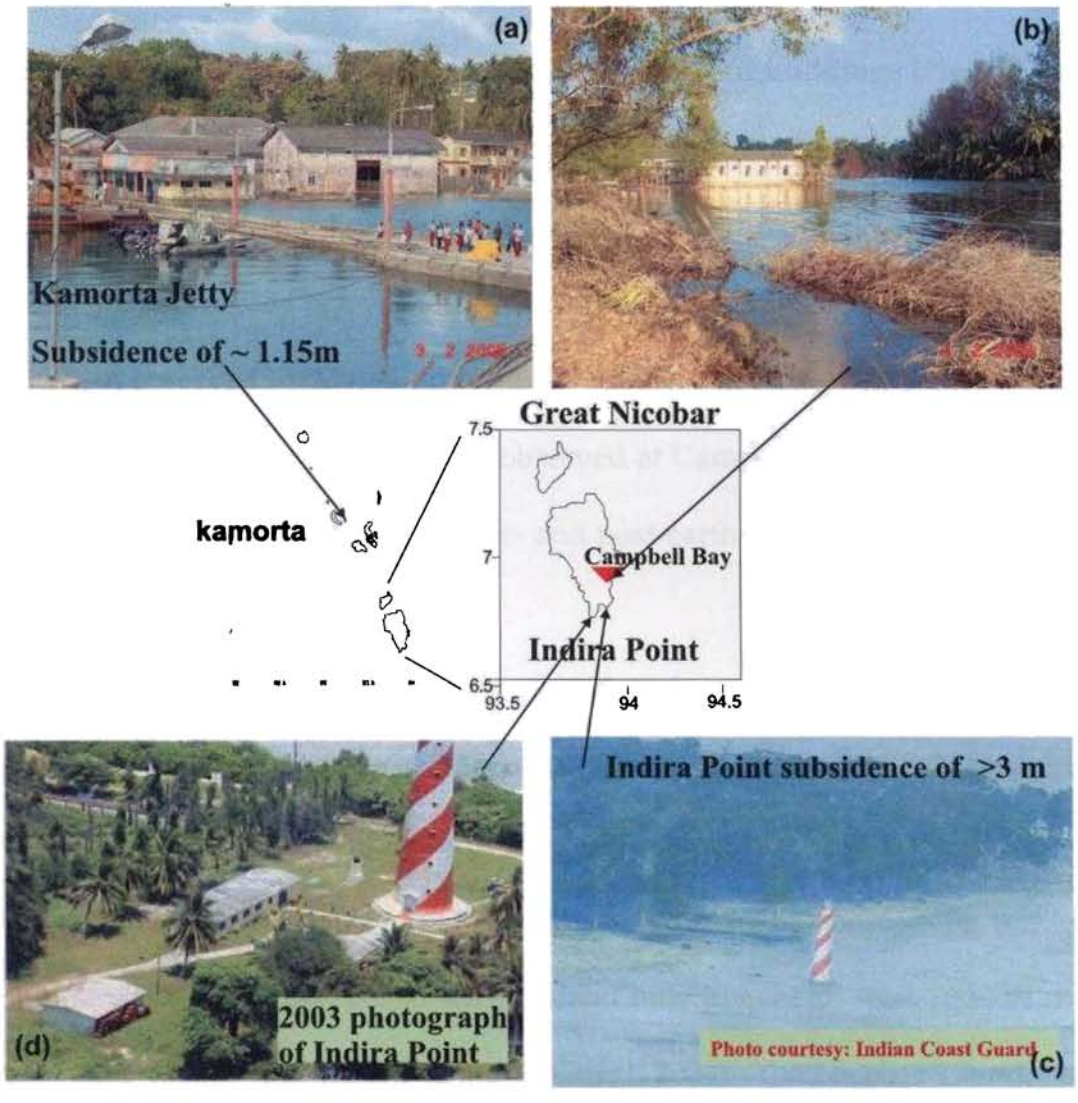

Figure 5.5: Co-seismic deformational features observed, as part of this study, in and around Great Nicobar. Respective locations are marked by arrows on the map. a) Post-earthquake photograph of Indira Point, basement of the light house completely submerged in sea. b) Pre-earthquake photograph of the base of Indira point light house. c) subsided jetty at Kamorta, Nancowry.

by more than a meter was evident in kamorta (Fig. 5.5.a), part of the Nancowry group of islands, from the pre-earthquake and post-earthquake high tide water marks on buildings and jetty pillar. In Campbell Bay evidences of submergence can be seen from subsided coast and partially sinked buildings (Fig. 5.5.b). Further south, at Indira Point, the southern most tip of Indian territory, the entire area subsided heavily. The lighthouse at Indira Point submerged by more than three meters, with its base below the post-earthquake sea level (Fig. 5.5.c and d). This was also observed by Mallik and Murthy (2005). Submergence of land leading to permanent water logging was also observed at Campbell Bay and Gandhi Nagar from measurements done on the pre- and post-earthquake high tide water marks on buildings in the Great Nicobar.

Submergence of Katchall Island is evident from the beach level changes observed from pre- and post-earthquake satellite images as well as field observations . Satellite images reveal maximum subsidence along the west coast of the island, which is more or less flat land of low relief and covered by dense mangrove forests, compared with the east coast, where island hills in general start 300-700 m from the coast (Thakkar, 2005; Thakker and Goyal, 2006). The Nicobar Islands, constituting the Car Nicobar, Nancowrie group, and the Great Nicobar showed effect of subsidence, maximum being at Indira Point (3 m), the southern most observation point of this study.

Table 5.1: Summary of the co-seismic changes recorded as part of this study from the field observations on ground level changes along the Andaman-Nicobar Islands.

Location	Long. (^{0}E)	Lat. (^{0}N)	Up/Down(m)	Feature
Landfall Isl.	93.05	13.62	0.65	Mangroves
Landfall Isl.	93.05	13.62	0.65	Microatolls
Diglipur	93.06	13.35	0.63	Beach
Interview Isl.	92.66	12.89	1.4	Coast
Interview Isl.	92.66	12.89	1.5	Microatolls
Avis Isl.	92.95	12.94	0.80	Beach
M.bandar	92.93	12.85	0.69	Microatoll
M.bandar	92.93	12.85	0.62	Mussels
Wandoor	92.61	11.58	-0.80	Beach
P.Blair	92.70	11.48	-0.95	Mangroves
P.Blair	92.76	11.68	-1.00	Tide gauge
N.Sentinel	92.26	11.47	1.0	Coral bed
H.Bay	92.54	10.58	0.30	Beach
C.Nicobar	92.85	9.26	-1.25	Buildings
Kamorta	93.54	8.15	-1.25	Jetty
C.Bay	93.95	6.92	-1.5	Houses
I.Point	93.85	6.80	-3.5	Lighthouse

5.3 Effects of ground shaking

In most part of the Andaman-Nicobar Islands, the earthquake started as a mild shaking that turned violent, lasting 4-5 minutes. The shaking resulted in damage to man-made structures as well as ground failure and liquefaction. At Port Blair, ground shaking was so severe that people found it difficult to stand. Overhead water tanks toppled and some poorly constructed cement structures were damaged in this part of the island. In many parts of Diglipur, severe shaking resulted in prominent ground fissures oriented in N-S direction. Horizontal shift in structures were also observed here as seen in the span of the Panighat Bridge (Fig. 5.1.d), 50 km south of Diglipur, which showed an E-W shift of 15-20 cm. North-south trending ground fissures were observed along the Andaman Trunk Road (ATR) which connects Port Blair to Diglipur. Ground fissures were also observed at Port Blair and surroundings.

Ground shaking generated sand blows along the Malacca coast and Kakkana (Car Nicobar), where water mixed with white sand gushed out of the vent coseismically. Liquefaction and sand-blow features (vents measuring up to 30 cm across) were also observed in Magar Nalla (Fig. 5.1.e), Krishnapuri and Kalipur areas of Diglipur. Jain et al., (2005) have discussed the pattern of damage to the built environment around Andaman Islands.

5.4 Effects of Tsunami inundation

Some of the most beautiful beaches along the archipelago were damaged by the tsunami. The impact of the tsunami was more severe in the southern Nicobar Islands and minimal in Diglipur, where only occasional seiches were reported. Wave height reached $\sim$ 3.5 m from the ground level at the Chidiya Tau and Munda Pahar beaches of Port Blair. A 10-15 cm thick tsunami sand deposition was observed in this part of the island. Eyewitness reports suggest that the tsunami waves first hit the Port Blair coast by around 7.30 am and the run-up height at Jawaharlal Nehru Rastriya Mahavidyalaya (JNRM) college was about 3 m. The tsunami deposited about 10 cm thick silty sand at Chidiyatapu, Port Blair (Fig. 5.1.d). Waves of height 6 m high hit the Hut Bay coast and deposited 15-20 cm thick sand layers along its coast. In Great Nicobar the maximum effect was reported from the western coast, where the waves advanced as far as 3 km landward. Maximum thickness of tsunami deposits of $\sim$70 cm was observed from Car Nicobar. Eastern coast of North Andamans, Middle Andamans and Havelock Islands were not hit by the tsunami waves, but reported occasional sei ches were there at Ariel Bay on 26^{th} December, 2004 morning after the earthquake.

5.5 Geodetic studies on near field deformation

The control points established for this study along the islands have been systematically re-occupied from time to time (see, Section 3.4.1, Table 3.1, Fig. 3.1 for details). With the December earthquake causing significant horizontal and vertical

shift, the pre-earthquake data could be used to model the co-seismic deformation. During the post-earthquake survey, started on January 13th, 2005, only five of these points could be re-ocuppied due to logistical reasons.

5.5.1 Co-seismic displacements

For the campaign sites in the Andaman Islands, the data is averaged over the time periods of the last pre-earthquake campaign (September 2004) and the first post-earthquake campaign (January 13 to February 2, 2005). For the campaign sites, the steady pre-seismic motion is corrected by projecting all data to the date of the earthquake assuming the velocity of PBLR, Port Blair GPS site. This is a small correction and its uncertainty is insignificant relative to other uncertainties in the co-seismic displacements. Coordinate repeatability was computed and the time series of station coordinates were generated (Fig. 5.6 - 5.8) using GAMIT/GLOBK software over the available campaign period.

For each set of displacements several daily GPS solutions were averaged together to get estimates of the pre- and post-earthquake positions. The uncertainty in each set of positions was scaled based on the misfit to the adjustment, assuming that the reduced chi-square statistic should be equal to unity in each case. This resulted in scaling the uncertainties by a factor of $\sim$2.5. The displacement uncertainties were calculated directly from the uncertainties in the pre- and post-earthquake positions; typical values were 1-2 mm horizontal and 2-4 mm vertical. This accounts for daily random errors, but not for systematic errors that may vary slowly over time, such as seasonal variations in position, or other variations

Table 5.2: Co-seismic horizontal and vertical offsets, in meters, of the Andaman-Nicobar GPS control points.

Site	North Offset	error (±)	East Offset	error (±)	Up Offset	error (±)
DGLP	-2.697	0.002	-4.008	0.004	0.602	0.010
PBLR	-1.055	0.001	-2.983	0.001	-0.867	0.002
HBAY	-2.939	0.003	-3.584	0.004	0.364	0.010
CARN	-2.994	0.004	-5.746	0.006	-1.125	0.010
CBAY	-2.382	0.003	-4.137	0.003	-1.394	0.010

that have longer timescales than a week. These campaign site occupations were months apart, and seasonal or other systematic variations from linear motion may be significant. With no reliable estimate of the magnitude of these effects available, somewhat arbitrarily the uncertainties were increased for the campaign sites by a factor of 4.

Pre- and post-earthquake GPS campaigns in the Andaman region suggest that the co-seismic displacement for all the control points is towards south west direction (Fig. 5.9). Their magnitudes are nonuniform along the arc (Table 5.2), Car Nicobar having registered the maximum shift of 6.479±0.007 m. Diglipur showed a displacement of 4.83±0.004 m, Port Blair 3.164±0.001 m, Hut Bay 4.635±0.005 m and Campbell Bay 3.132±0.004 m. Diglipur and Hut Bay showed signals of uplift of 60.2±1 cm and 36.4±1 cm respectively. Port Blair subsided by 86.70±0.2 cm and Car Nicobar by 1.125±0.01 m. Maximum amount of subsidence occurred for the Cambell Bay control point registering a 1.394±0.01 m of submergence. Independent GPS constraints on the co-seismic deformation from the region also show comparable results (Jade et al., 2005 and Gahalaut et al., 2006).

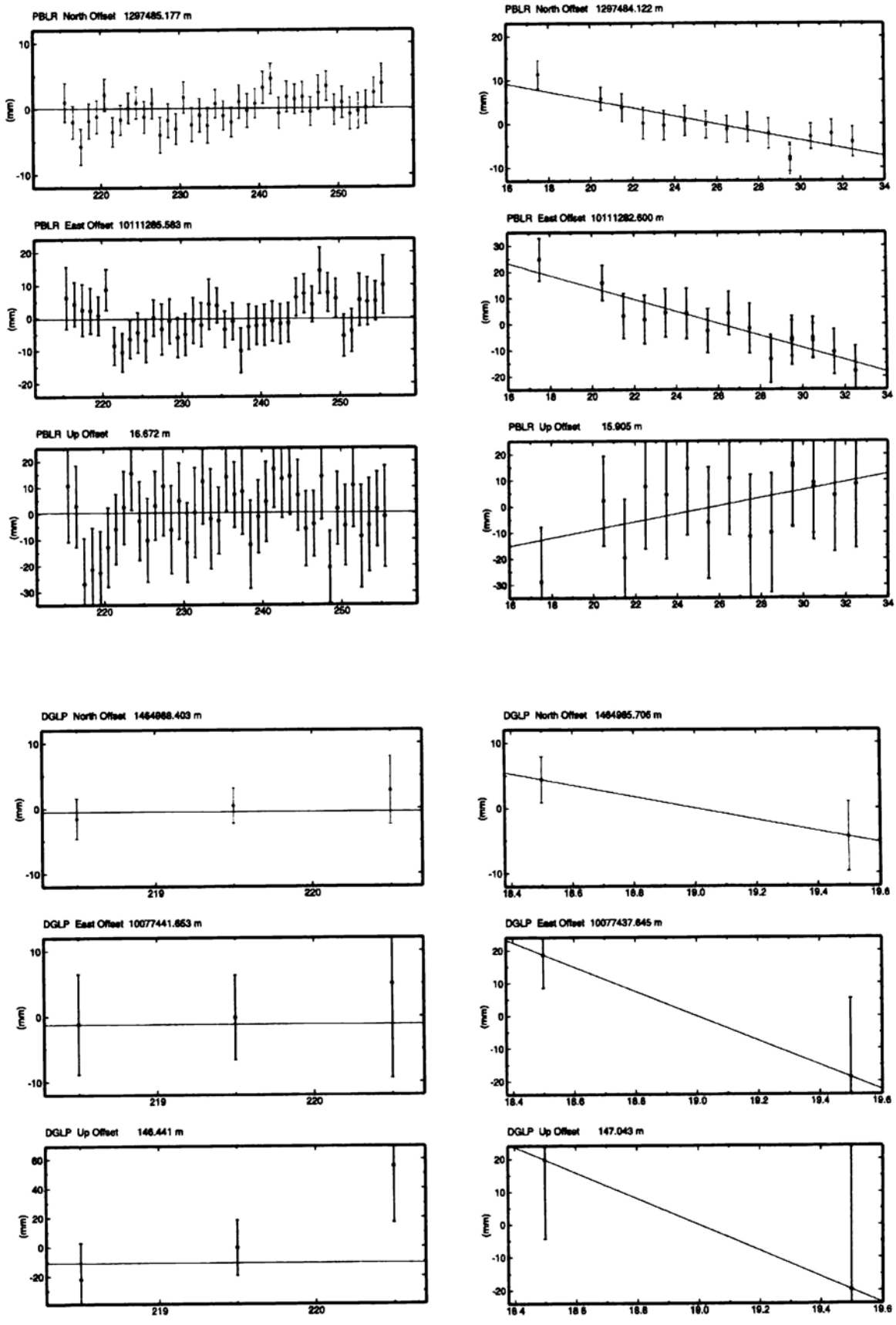

Figure 5.6: Time series plot of North, East and vertical offsets of PBLR, Port Blair; and DGLP, Diglipur GPS sites from September, 2004 (left panel) and January, 2005 (right panel) campaigns.

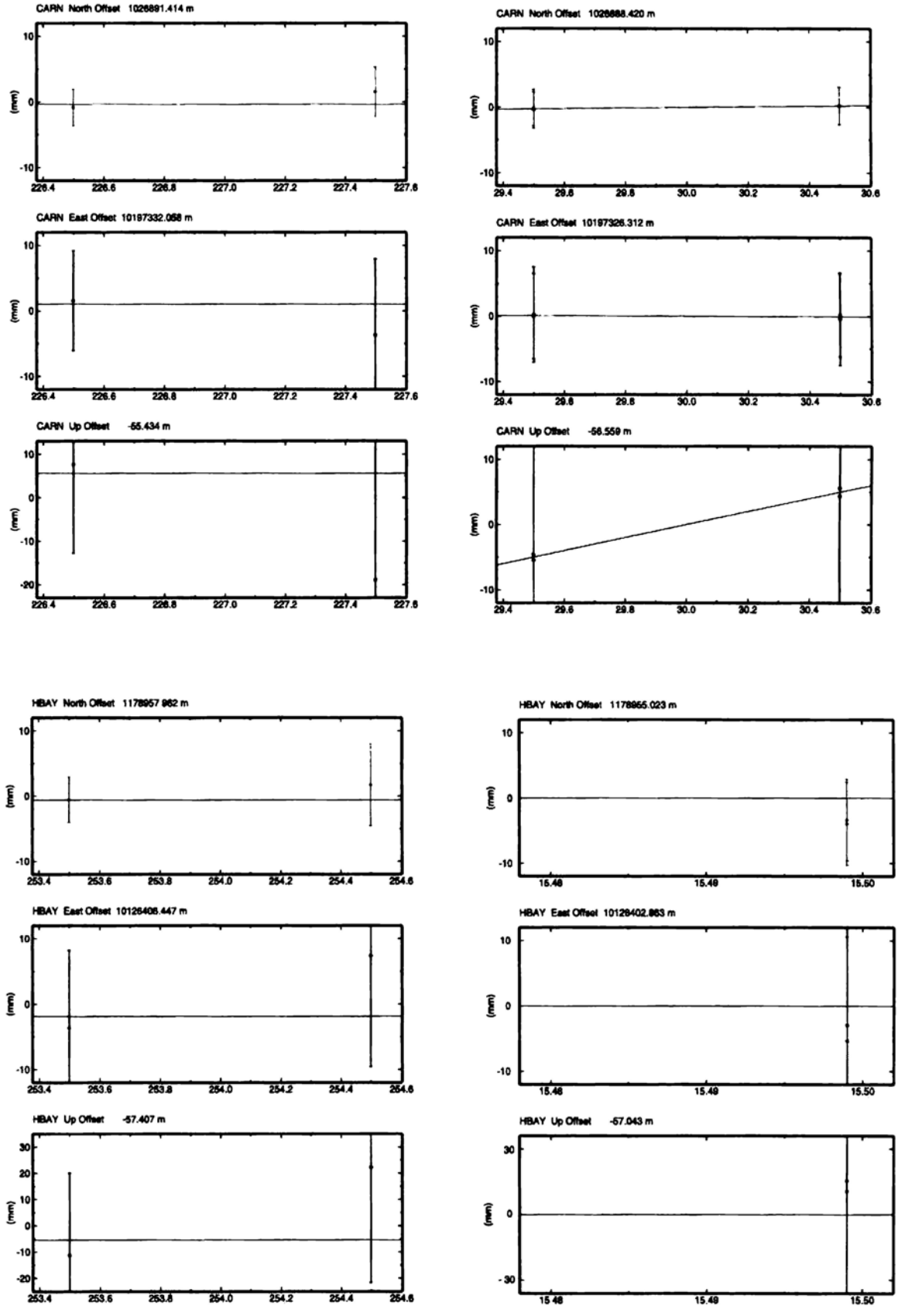

Figure 5.7: Time series plot of HBAY, Hut Bay, Little Andamans and CARN, Car Nicobar, GPS points from september, 2004 (left panel) and January, 2005 (right panel) campaigns.

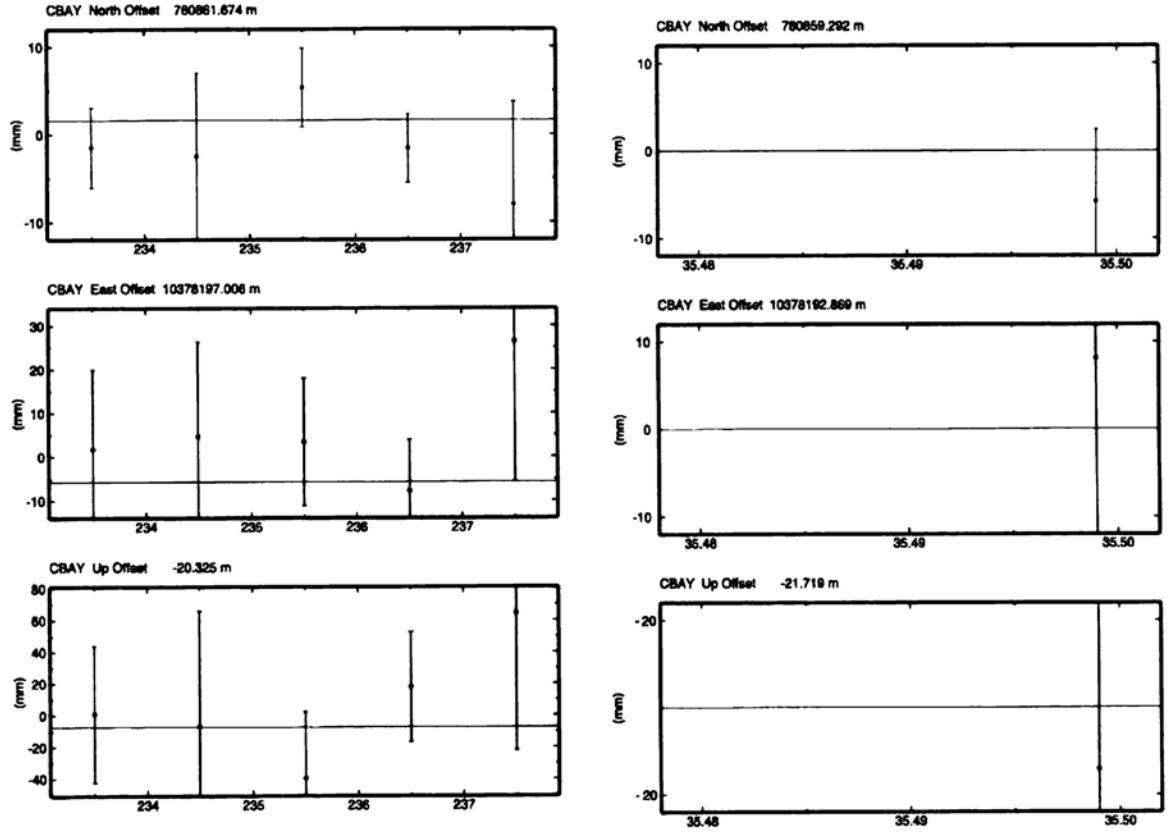

Figure 5.8: Time series plot of CBAY, Campbell Bay, Great Nicobar control point from September, 2004 (left panel) and January, 2005 (right panel) campaigns

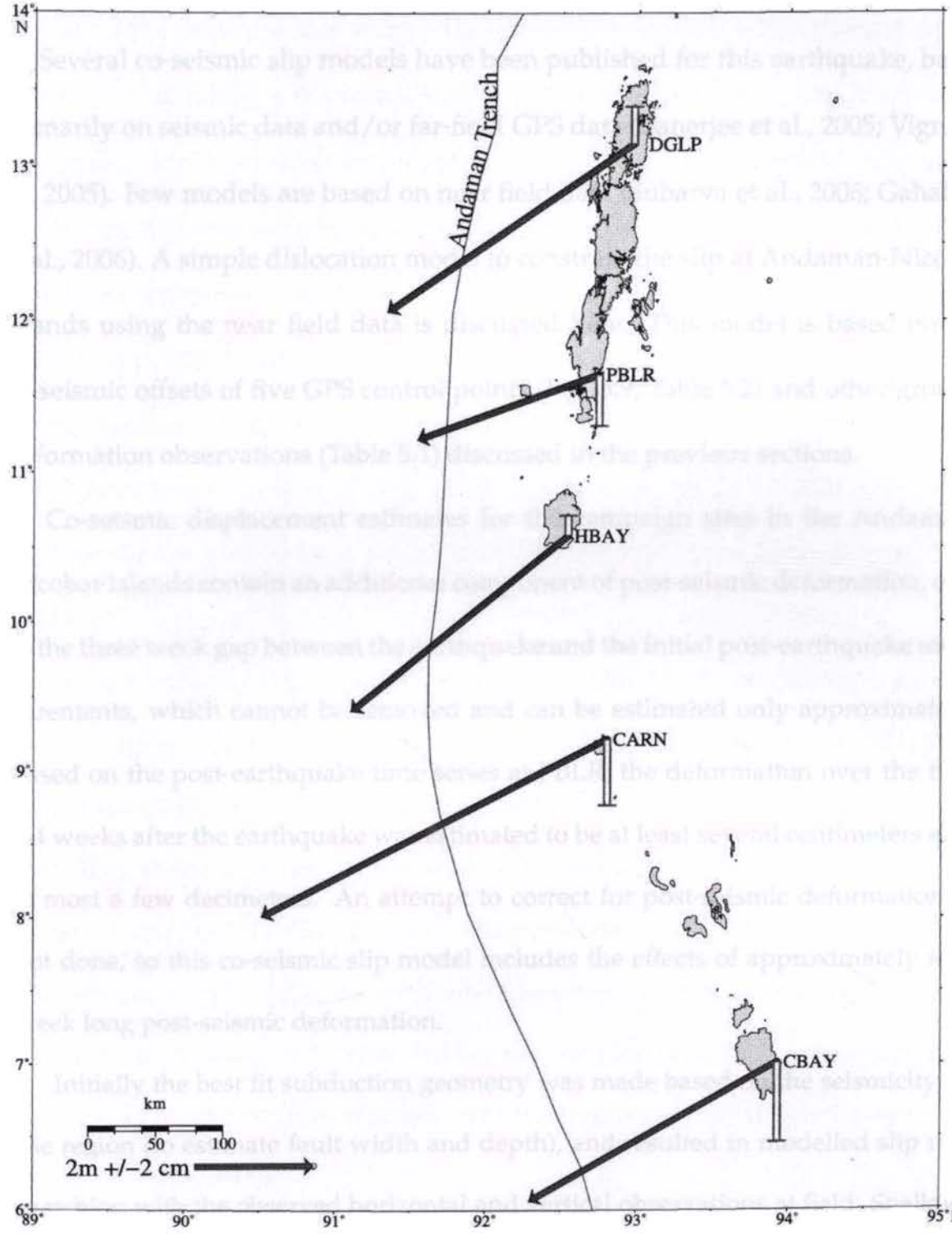

Figure 5.9: Computed scaled co-seismic horizontal and vertical offsets of Andaman-Nicobar GPS control points.

5.6 A simple co-seismic slip model

Several co-seismic slip models have been published for this earthquake, based primarily on seismic data and/or far-field GPS data (Banerjee et al., 2005; Vigny et al., 2005). Few models are based on near field data (Subarya et al., 2006; Gahalaut et al., 2006). A simple dislocation model to constrain the slip at Andaman-Nicobar Islands using the near field data is discussed here. This model is based on the co-seismic offsets of five GPS control points (Fig. 5.9, Table 5.2) and other ground deformation observations (Table 5.1) discussed in the previous sections.

Co-seismic displacement estimates for the campaign sites in the Andaman-Nicobar Islands contain an additional component of post-seismic deformation, due to the three week gap between the earthquake and the initial post-earthquake measurements, which cannot be removed and can be estimated only approximately. Based on the post-earthquake time series at PBLR, the deformation over the first 3-4 weeks after the earthquake was estimated to be at least several centimeters and at most a few decimeters. An attempt to correct for post-seismic deformation is not done, so this co-seismic slip model includes the effects of approximately few week long post-seismic deformation.

Initially the best fit subduction geometry was made based on the seismicity of the region (to estimate fault width and depth), and resulted in modelled slip not matching with the observed horizontal and vertical observations at field. Shallow dip angles of the multiple point source model of Tsai et al., (2005) shows dip angle of 6-8 degrees but was again inconsistant with the field observations. Finally the

ratio of vertical to horizontal displacements was taken to constrain the dip angle and slip zone width in this work. This is applicable even when there is only a single GPS site along a rupture segment, and is independent of slip magnitude. The fault model is divided into segments based on changes in strike. The strike of the model planes were made to match the strike of the trench. The model is divided into segments along the strike, based on changes in strike needed to match the trench position and orientation or clear variations in the displacements. Two segments were defined, viz., the Andaman segment, striking N10^{0}E and the Nicobar segment, striking N20^{0}W (Fig. 5.10). Andaman segment is 440 km long and Nicobar segment is 385 km long, covering almost 65% of the December 26, 2004 rupture.

Using horizontal displacements alone, it is possible to fit the data well, using a range of dip angles. For example, in an early version of the model used the fit of the horizontal displacements from our near-field with a model that had dip angles of 6-8^0. Such shallow dip angles would be consistent with the multiple point source model of Tsai et al., (2005). However, this model did not fit the near-field vertical displacements well. Using the horizontal displacements alone, there is also a very strong tradeoff between the width of the rupture plane and the average slip (this is a tradeoff that preserves moment, which remains well constrained even with minimal geodetic data).

The vertical displacements provided critical information to the model. The ratio of vertical to horizontal displacements constrains the dip angle and slip zone width, even where there is only a single GPS site along a rupture segment, and

is independent of the slip magnitude. In general, two families of models can be found that give the same vertical to horizontal displacement ratio, one family in which the maximum vertical displacement lies trenchward of the site, and another family in which it lies farther from the trench than the site. For many of the sites, the two families of models have separate dip angles, while intermediate dip angles cannot fit the both vertical and horizontal displacements. This ratio is used to narrow down the search of the model space.

With the range of dip angles restricted, the displacements from other near-field sites or from far-field data could have used to resolve the large rupture width - slip magnitude tradeoff . Gahalaut et al., (2006) independently derived a similar conclusion from the difference between the horizontal and vertical displacements. Additional information comes from qualitative or semi-quantitative observations of uplift or subsidence along the coastlines of many of the islands, in some cases only the sign of this vertical coastal motion is certain, but even knowing only the sign of the vertical motions is a powerful constraint on the possible location of the zero line separating uplift and subsidence. The observed surface displacements are modelled (Fig. 5.10) using Okada's formulation of a dislocation buried in an infinite half-space (Okada, 1985).

5.7 Discussion

Co-seismically the upper plate overlying the locked subduction interface recovers the elastic strain and experiences sudden co-seismic uplift while the regions above the down-dip end of the rupture will subside (e.g., Plafker and Savage,

Table 5.3: Slip Model parameters. Long - logitude is ^{0}E, Lat - Latitude is ^{0}N, Length - Length of the fault (km), Width - Width of the slip plane (km) Depth - Depth of the up-dip edge (km), Dip - Dip angle of the slip plane in decimal degrees (^{0}), Strike - Strike of the fault in decimal degrees (^{0}), Slip - Slip in meters (m), Rake - Rake of the fault in decimal degrees (^{0}). The latitude and longitude specifies the location of the GPS sites along which the slip distribution was computed, and dip angles indicate planes that dip downward from the surface.

Long	Lat	Length	Width	Depth	Dip	Strike	Slip	Rake
92.97^{0}E	13.16^{0}N	140	80	11	13	18	9.5	134
92.74^{0}E	11.65^{0}N	150	65	6	9	6	6	124
92.54^{0}E	10.59^{0}N	150	75	7	11	0	8	120
92.80^{0}E	09.25^{0}N	195	115	5	9	357	13	104
93.92^{0}E	07.01^{0}N	190	120	5	11	338	17	103

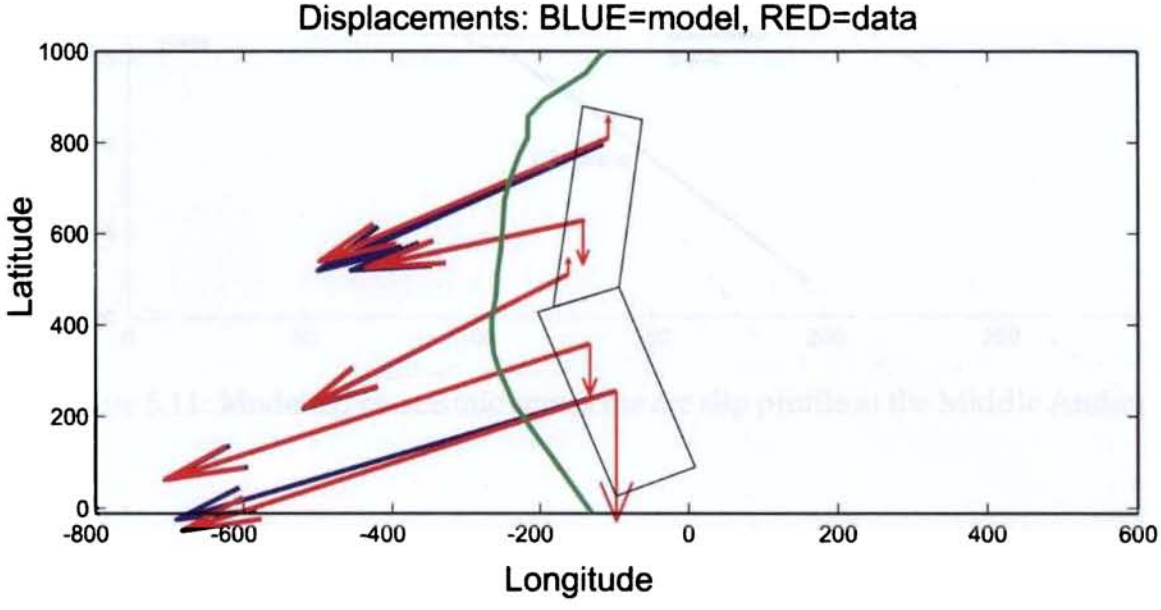

Figure 5.10: Best fit modelled fault geometry and slip distribution (see, Table 5.3), for the co-seismic displacement vectors observed. Red vectors are from observed GPS data and blue ones are modelled.

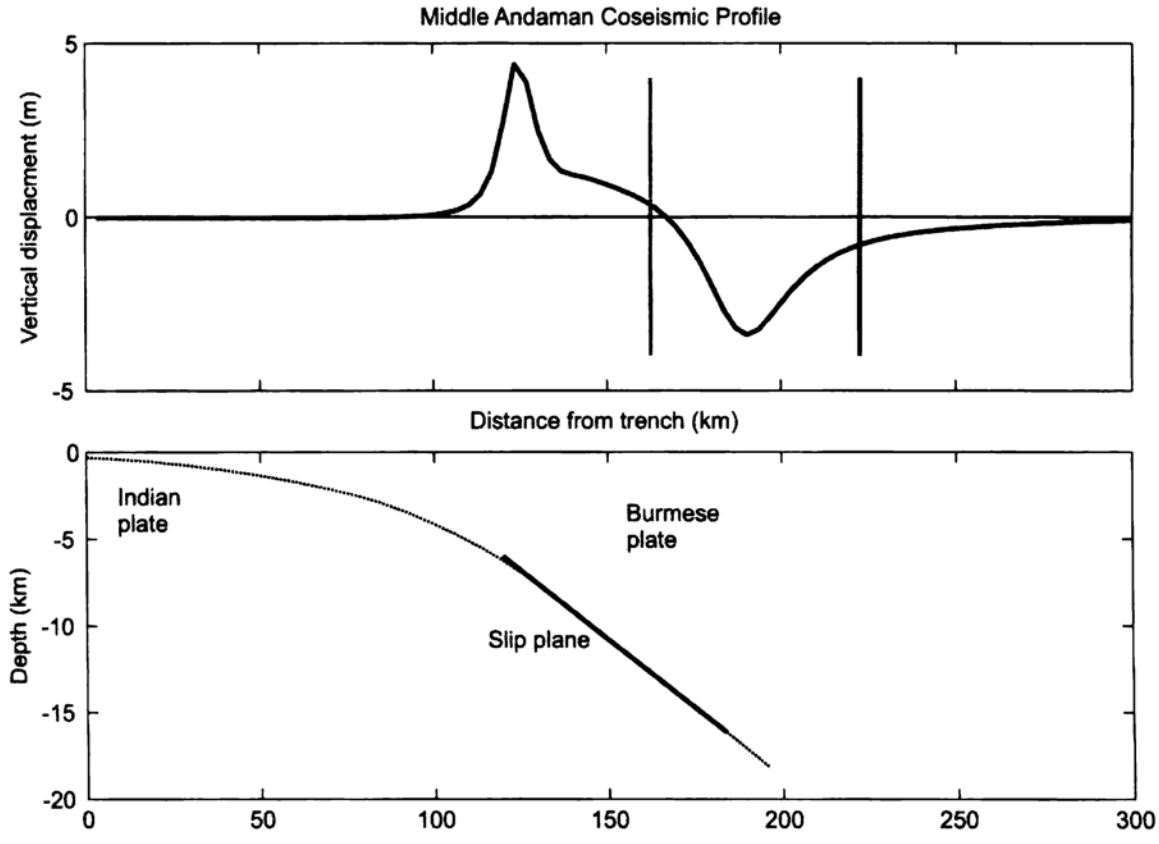

Figure 5.11: Modelled co-seismic across the arc slip profile at the Middle Andaman.

1970; Plafker, 1972). Field observations and GPS results from this study shows, co-seismically Port Blair, Car Nicobar and Campbell Bay recorded subsidence and Diglipur and Hut Bay recorded uplift. These co-seismic vertical movements were expected by the their respective locations above the up-dip or down-dip extensions of the fault except at Diglipur. Altogether the North Andamans showed signs of uplift, possibly because of the proximity to the zone of transition between subduction to collision north of it. The southern groups of islands show greater horizontal displacement compared to the Andaman segment. The fact that the Car Nicobar Island shows the largest displacement (co-seismic slip) remains to be explained, as this patch had generated a large earthquake in 1881 and a large aftershock (M_W 7.1, 26^{th} January, 2004). This possibly indicates that there existed a slip deficit in spite of the 1881 earthquake. Ground deformation at North Andamans was considerable comparing with Port Blair. Around Diglipur ground fissures and secondary features like sand blows were seen more, a depiction on the intense co-seismic deformation within the wedge in this region.

The fault model used in this study (Table 5.3) takes care of almost 65% of the December 26, 2004 earthquake rupture, extending upto north of the island archipelago. The estimated range of dip angles for the slip plane varies from 9-13^0. The rupture plane is wider in the Nicobars, 115-120 km wide, and 65-80 km wide through the Andaman segment. Whole along the Andaman-Nicobar arc, a rupture area extending beneath and east of the islands is required to explain the observed vertical displacements. But in Nicobar segment a deeper rupture misfits the near field data. Significant amount of slip extends to near the trench axis over

most of the southern part of the rupture in the Nicobar Islands, but in most of the Andaman Islands the rupture did not extend close to the trench.

However, in the case of Car Nicobar the rupture plane in this alternate case would need to have a much shallower dip, in the order of 4 degrees in order to match the GPS vertical displacement. Given the dip angles, it is inferred that the rupture did not extend deeper than 30 km at any point. A deeper rupture significantly misfits the near-field data. It is inferred, a rupture to 30 km depth for the segments off the southern Nicobar Islands, but only 19-22 km for the northern Nicobar segment. The maximum depth of rupture through the Andaman Islands was even shallower, 16-20 km except for slip to 30 km depth for the North Andaman. The data in the southern half of the rupture can be fit well by rupture planes that extend to the trench or close to it. North of about 8^0N, the data again fit better by a model in which the up-dip limit of the rupture was somewhat down-dip of the trench.

In the northernmost segment, corresponding to North Andaman Island, the GPS site and ground observations show very high uplift relative to their horizontal motions, which means that they must lie much closer to the up-dip limit of rupture than to the down-dip limit. This data could be satisfied either by a very wide rupture zone (150 km wide) with the up-dip limit of rupture near the trench, or by a narrower zone in which the up-dip limit is well back from the trench and close to the island. In both cases, the dip angle is relatively steep. It is prefered that the model with a lack of slip near the trench, although the fit to the GPS data is about the same in both cases, as the model with the wide rupture zone requires

slip extending to a much greater depth than any other part of the rupture.

Estimation of an earthquake recurrence time from plate convergence rate is complicated by the large variation in slip along-strike. This comes with a caveat, it may be premature to define a recurrence interval based on the limited data available, especially because many subduction zones exhibit variable patterns of rupture such as the Colombia-Ecuador trench (Kanamori and McNally, 1982) and the Kurile and Aleutian arcs (Nanayama et al., 2003). With the limited amount of the available data, a preliminary and segment specific recurrence intervals may be computed, assuming a uniform earthquake cycle. Assuming a uniform subduction and Indo/Andaman converegence of ~40 mm/yr (see, section 4.5), the replenishment time for a 6 m of slip at Port Blair is ~150 years. Similarly for North Andaman such a renewal time for 9.5 m slip is around ~235 years. Assuming a similar convergence vector for Car Nicobar the renewal time for a 13 m slip is around ~325 years.

Taking the present day along-arc convergence rates as representative of long-term deformation, the replenishment time for a 2004 type slippage can be computed. It comes ~1100 years for the Port Blair segment for a convergence of ~5.5 mm/yr. Also similar calculation for North Andaman and Car Nicobar segments show ~630 (for a 15 mm/yr convergence) and ~840 (for 15.5 mm/yr convergence) years respectively. The paleo-tsunami observations reported by Rajendran et al. (2007) suggest that 900-1000 years ago is a plausible date for the predecessor to the 2004-type earthquakes, and is almost in agreement with the renewal time calculated from this study.

Chapter 6

Summary and conclusions

The Andaman Islands lie on the Burma Plate, a narrow fore-arc sliver lying between the Indian plate and the Sunda block, bounded by the Andaman trench to the west and the Andaman Sea transform on the east. Spatio temporal analysis of the pre-seismic era earthquakes showed that there is a higher amount of seismicity in the back-arc side and almost negligible amount of activity in the fore-arc side, indicating a locked up-dip edge of the plate interface. Focal mechanism solutions also support this inference.

Along the arc the major orientation of stress is NNE-SSW, due to the under-thrusting of the Indian lithosphere. Opening up of the Andaman basin do have an azimuth of $\sim 320^0$. A general sense of compression is there on the Sumatra-Andaman trench in NE-SW to N-S direction at the shallower portions. In the ASR region, the general trend of stress is in NNW-SSE. In a transition zone between the ASR and SF, the stress orientations change to E-W direction. In intermediate depths, the trend of east of Sunda-Andaman trench is NE-SW to N-S.

Pre-earthquake GPS measurements at Port Blair show slow convergence between the Burma plate and the Indian plate, 5 mm/yr directed almost purely westward. Similar, but less precise, velocities are estimated for Car Nicobar and Diglipur. The uncertainty in this velocity is primarily due to the large uncertainty in the motion of India with respect to the ITRF2000 reference frame. This veloc-

ity is a lower bound on the long-term motion of the Burma Plate relative to India, as it includes a component of eastward motion due to elastic strain from the locked shallow plate interface that ruptured in the earthquake. This suggests that the Andaman Trench is part of a purely slip partitioned plate boundary, with the strike-slip component of India-Sunda relative plate motion being taken up on the transform fault in the Andaman Sea or on the West Andaman Fault, and the convergent component on the Andaman Trench.

GPS observations prior to the earthquake show nearly pure convergence across the Andaman trench, consistent with the previous and independent GPS results of Paul et al., (2001), although the present study obtained almost less than half of the earlier rate. Given the uncertainties, the GPS velocities from a relatively short time series, and the various model assumptions, this difference is not significant. Paul et al., (2001) estimated a higher convergence velocity for Port Blair relative to India, but their India-fixed frame was based on the NNR-NUVEL-1A velocity of India, and the NUVEL-1A velocity of India is too fast in both the northward and eastward directions. The difference between Port Blair velocity of this study and that of Paul et al., (2001) (14 mm/yr) is probably attributable to a bias in their India-fixed frame, although their velocity is about equally consistent with the model and velocity from this study. A re-analysis of the Paul et al., (2001) data with careful attention to the definition of an Indian frame would help to resolve this discrepancy.

A vector closure model (Fig. 5.12) based on these assumptions predicts an arc-normal convergence, that in the pre-earthquake period PBLR was converging ~15 % towards India, with the remaining ~85% being accomadated by the unknown

amount of seismic coupling there. Along the arc, North Andamans and Car Nicobar showed almost comparable results of 37% and 37.5% respectively. These results show, pre-semically, Andaman-Nicobar arc was almost 65-85% locked for a uniform convergence to take place.

Field observations and GPS results from this study shows, co-seismically Port Blair, Car Nicobar, Campbell Bay recorded subsidence and Diglipur and Hut Bay recorded uplift. These co-seismic vertical movements are expected by the there respective locations above the up-dip or down-dip extensions of the fault except at Diglipur. Altogether the North Andamans showed signs of uplift, possibly because of the proximity to the zone of transition between subduction to collision north of it. The southern group of islands show greater displacement compared to the Andaman segment. Car Nicobar island showed the largest displacement and a larger co-seismic slip. This patch had generated a large earthquake in 1881 and a large aftershock following the 2004 rupture. This possibly indicates that there existed a slip deficit in spite of the 1881 earthquake and still it is active.

The estimated co-seismic dip angles ranged from 9-13^0. The width of the rupture plane is wider in the Nicobars, 115-120 km wide, and 65-80 km wide through the Andaman segment. Whole along the Andaman-Nicobar arc, a rupture area extending beneath and east of the islands is required to explain the observed vertical displacements.

For Indo/Andaman convergence rates obtained from this study, renewal rates of ~630-1100 years are observed. These values are almost comparable with paleoseismic results from Rajendran et al., (2007). The GPS convergence rates represent

the present day deformation, and they may vary over the entire seismic cycle. As an avarage, a value of ~1000 years may be appropriate for a 2004 type meagthrust recurrence along the Andaman-Nicobar margin.

References

Abercombie, R. E., M. Antolik, G. Ekstorm. The June 2000 Mw 7.9 earthquakes south of Sumatra: Deformation in the India Australia plate, *Jour. Geophys. Res.*, 108, B1, 2018, doi:10.1029-2001JB000674, 2003.

Aki, K. Characterization of barriers on an earthquake fault., *Jour. Geophys. Res.*, 84, pp. 6140-6148, 1979.

Alcock, A. W. A naturalist in Indian seas, *John Murray Pub. Co., London*, 328 pp, 1902.

Ammon C.J., Chen Ji, Hong-Kie Thio, D. Robinson, S. Ni, V. Hjorleifsdottir, H. Kanamori, T. Lay, S. Das, D. Helmberger, G. Ichinose, J. Polet, D. Wald. Rupture Process of the 2004 Sumatra-Andaman Earthquake, *Science*, 308(5725), pp. 1133-1139, doi: 10.1126/science.1112260, 2005.

Ando, M. Source mechanisms and tectonic significance of historical earthquakes along the Nankai trough, Japan, *Tectonophysics*, 27, pp. 119-140, 1975.

Aung Khin, Aung Tin U, Aung Soe, Khin Khan. A study on the gravity indication of the Shan scarp fault, *Jour. Sci and Tech.*, 1, pp. 241-251, 1968.

Aung Khin, Aung Tin U, Aung Soe, Khin Khan. Geology and hydrocarbon prospects of the Burma Tertiary geosyncline, *Jour. Sci and Tech.*, 2, pp. 53-81, 1969.

Ball, V. Notes on geology of the vicinity of Port Blair, *Jour. Asiat. Soc. Ben.*, 39, pp. 231-239, 1870.

Banerjee, P., F. F. Pollitz, and R. Burgmann. The size and duration of the Sumatra-Andaman earthquake from far-filed static offsets, *Science*, 308, pp. 1769-1772, 2005.

Banerjee, P., F. Pollitz, B. Nagarajan, and R. Burgmann. Coseismic slip distributions of the 26 December 2004 Sumatra-Andaman and 28 March 2005 Nias earthquakes from GPS static offsets, *Bull. Seis. Soc. Am.*, 7, S86-S102, 2007.

Bandopadhyay, P. C., M. Ghosh. Facies, petrology and depositional environment of the Tertiary sedimentary rocks, *Jour. Geol. Soc. Ind.*, 52, pp. 53-66, 1998.

Banghar, A. R. Seismo-tectonics of the Andaman-Nicobar Islands, *Tectonophysics*, 133, pp. 95-104, 1987.

Bapat. A., R. C. Kulkarni, and S. K. Guha. Catalogue of earthquakes in india and neighborhood from historical period up to 1979 and references therein, *Indian Society of Earthquake Technology, Roorkee*, 211 p., 1983.

Bender, F. Geology of Burma, *Borntraeger, Berlin*, 260 pp., 1983.

Bilham, R., E. R. Engdahl, N. Feldl, and S. P. Satyabala. Partial and complete rupture of the Indo-Andaman plate boundary, 1847-2004, *Seism. Res. Lett.*, 76, pp. 299-311, 2005.

Bird, P. An updated digital model of plate boundaries, *Geoche. Geophys., Geosys.*, 4, 3, doi:10.1029-GC000252, 2003.

Borrero, J.C. Field Data and Satellite Imagery of Tsunami Effects in Banda Aceh , *Science*, 308, pp. 1596, 2005.

Braitenberg, C. and M. Zadro. Comparative Analysis of the Free Oscillations Generated by the Sumatra- Andaman Islands 2004 and the Chile 1960 Earthquakes, *Bull. Seis. Soc. Am.*, 97, S6-S17, 2007.

Briggs, R. W., K. Sieh, A. J. Meltzner, D. Natawidjaja, J. Galetzka, B. Suwargadi, Y. Hsu, M. Simons, N. Hanato, I. suprihanto, D. Prayudi, J. Avouac, L. Prawirodirdjo, Y. Bock. Deformation and slip along the Sunda megathrust in the great 2005 Nias-Simeulue earthquake, *Science*, 311, pp. 1897-1901, 2006.

Brunnschweiler, R. O. On the geology of the Indoburman ranges, *Jour. Geol. Soc. Aust.*, 13, pp. 127-194, 1966.

Brunnschweiler, R. O. Indoburman ranges, Mesozoic-Cenozoic orogenic belts, *Jour. Geol. Soc. Lond.*, 4, pp. 279-299, 1974.

Burgmann, R., M. G. Kogan, G M. Steblov, G. Hilley, V. E. Levin, and E. Appel. Interseismic coupling and asperity distribution along the Kamchatka subduction zone, *Jour. Geophys. Res.*, 110, B07405, doi:10.1029-2005JB003648, 2005.

Byrne, D. E., D. M. Davis, and L. R. Sykes. Loci and maximum size of thrust earthquakes and the mechanics of the shallow region of subduction zones, *Tectonics*, 7, pp. 833-857, 1988.

Chamot-rooke, N. and X. Le Pichon. GPS determined eastward Sundaland motion with respect to Eurasia confirmed by earthquakes slip vectors at Sunda and Philippine Trenches, *Earth. Planet. Sci. Lett.*, 173, 439-455, 1999.

Chandra, U. Tectonic segmentation of the Burmese-Indonesian arc, *Tectonophysics*, 105, pp. 279-290, 1984.

Chibber, H. L. The geology of Burma, *McMillan and Co. Ltd., St. Martin's street, London*, pp. 47-70, 1934.

Chlieh, M., J.P. Avouac, V. Hjorleifsdottir, T.-R. A. Song, C. Ji, K. Sieh, A. Sladen, H. Hebert, L. Prawirodirdjo, Y. Bock, and J. Galetzka. Coseismic Slip and Afterslip of the Great Mw 9.15 Sumatra-Andaman Earthquake of 2004, *Bull. Seis. Soc. Am.*, 97, S152-S173, 2007.

Choy, G. L. and J. Boatwright. The Energy Radiated by the 26 December 2004 Sumatra-Andaman Earthquake Estimated from 10-Minute P-Wave windows, *Bull. Seis. Soc. Am.*, 97, S18-S24, 2007.

Chatterjee, P. K. The invisible bank fault and geotectonics of the Andaman-Nicobar islands, *Quat. Jour. Geol. Min. Metal. Soc.*, 56, pp. 28-40, 1984.

Chen, Z., B. C. Burchfiel, Y. Liu, R. W. King, L. H. Royden, W. Tang, E. Wang, J. Zhao, and X. Zhang. GPS measurements from eastern Tibet and their implications for India/Eurasia intercontinental deformation, *Jour. Geophys. Res.*, 105, pp. 16,215 - 16,227, 2000.

Conrad, C.P., S. Bilek, C. L. Bertellloni. Great earthquakes and slab pull: interaction between seismic coupling and plate-slab coupling, *Earth planet. Sci. Lett.*, 218, pp. 109-122, 2004.

Curray, J. R., D. G. Lawyer, F. J. Emmel, R. W. Raitt, M. Henry, R. Kieckhefer. Tectonics of the Andaman Sea and Burma, Geological and geophysical investigations of continental margins, *Mem. Am. Asso. Pet. Geol.*, 29, pp. 189-198, 1979.

Curray, J. R., D. G. Lawyer, F. J. Emmel, D. G. Moore, R. W. Raitt. Structure, tectonics and geological history of the northeastern Indian Ocean, *The Oceans Basins and Margins, 6, The Indian Ocean, Plenum Press, New York*, 399-450, 1982.

Curray, J.R. Tectonics and history of the Andaman sea region, *Jour. Asian Earth Sci.*, 25, 187-204, 2005.

DeMets, C., R. G. Gordon, D. F. Argus, and S. Stein. Current plate motions, *Geophys. Jour. Int.*, 101, pp. 425-478, 1994a.

DeMets, C., R. G. Gordon, D. F. Argus, and S. Stein. Effect of recent revisions to the geomagnetic reversal time scale on estimates of current plate motions, *Geophys. Res. Lett.*, 21, pp. 2191-2194, 1994b.

Dziewonski, A.M., T.-A. Chou and J.H. Woodhouse. Determination of earthquake source parameters from waveform data for studies of global and regional seismicity, *Jour. Geophys. Res.*, 86: 2825-2852, 1981.

Earnest, A., Rajendran, C. P., Rajendran, K., Anu, R., Arun, G. M., and P.M. Mohan. Near-field observations on the coseismic deformation associated with the 26 December 2004 Andaman-Sumatra earthquake, *Cur. Sci.*, 89, 7, pp. 1237- 1244, 2005.

Eguchi, T., S. Uyeda, and T. Maki. Seismotectonics and tectonic history of the Andaman Sea, *Tectonophysics*, 57, pp. 35-51, 1979.

Engdahl, E. R., A. Villasenor, H. R. DeShon, and C. H. Thurber. Teleseismic relocation and assessment of seismicity (1918-2005) in the region of the 2004 Mw 9.0 Sumatra-Andaman and 2005 Mw 8.6 Nias Island great earthquakes, *Bull. Seis. Soc. Am.*, 97, S43-S61, 2007.

Fitch, T. J. Plate convergence, transcurrent faults and internal deformation adjacent to southeast Asia and the western Pacific, *Jour. Geophys. Res.*, 77, pp. 4432-4462, 1972.

Frerichs, W. E. Paleobathymetric trends of Neogene foraminiferal assemblages and sea floor tectonism in the Andaman Sea area, *Mar. Geol.*, 11, pp. 159-173, 1971.

Gahalaut, V. K., B. Nagarajan, J. K. Catherine, and S. Kumar. Constraints on 2004 Sumatra-Andaman earthquake rupture from GPS measurements in Andaman-Nicobar Islands, *Earth Planet. Sci. Lett.*, 242, 365-374, 2006.

Genrich, . F., Y. Bock, R. McCaffrey, L. Prawirodirdjo, C. W. Stevens, S. S. O. Puntodewo, C. Subarya, and S. Wdowinski. Distribution of slip at the northern Sumatran fault system, *Jour. Geophys. Res.*, 105, B12, pp. 28,327-28,341, 2000.

Gomberg, J., N.M. Beeler, M.L. Blanpied, and P. Bodin. Earthquake triggering by transient and static deformations, *Jour. Geophys. Res.*, 103 , pp. 24411-24426, 1998.

Gordon, R. G., C. DeMets, and D. F. Argus. Kinematic constraints on distributed lithospheric deformation in the equatorial Indian ocean from present motion between the Australian and Indian plates, *Tectonics*, 9, pp. 409-422, 1990.

Gordon, R. G., C. DeMets, and J. Royer. Evidence for long-term diffuse deformation of the lithosphere of the equatorial Indian Ocean, *Nature*, 395, pp. 370-374, 1998.

Gupta, H. K., L. Fleitout, and C. Froidevaux.Lithosphere subduction beneath the Arakan-Yoma fold belt: quantitative estimates using gravimetric and seismic data, *Jour. Geol. Soc. Ind.*, 35, pp. 235-250, 1990.

Guzman-Speziale, M., and J. F.Ni. The opening of the Andaman Sea: where is the short-term displacement being taken up?, *Geophys. Res. Lett.*, 20, 24, pp. 2949-2952, 1993.

Haldar, D., T. Lascar, P. C. Bandyopadhyay, N. K. Sarkar. Volcanic eruption of the Barren Island volcano, Andaman Sea, *Jour. Geol. Soc. Ind*, 39, pp. 411-419, 1992.

Hamilton, W. Tectonics of the Indonesian region, *USGS Prof. Paper*, 1078, p. 345, 1979.

Harjono, H., M. Diament, J. Dubois, and M. Larue. Seismicity of the Sunda strait: evidence for crustal extension and volcanological implications, *Tectonics*, 10, 1, pp. 17-30, 1991.

Herring, T. GLOBK: Global Kalman Filter VLBI and GPS analysis program, v.10.2, *Massachusetts Institute of Technology*, 2005.

Hill, D. P., F. Pollitz, and C.Newhall. Earthquake-Volcano interactions, *Physics Today*, 55, pp. 41-47, 2002.

Hochstetter, F. Von. Contributions to the Geology and Physical Geography of the Nicobar Islands, (translated by F. Soliczka) from the "Voyage of the Austrain Frigate Novara, round the world in 1857-1859. Geological part, 2, 85-112, Vienna, 1866. reproduced in *Mem. Geol. Surv. India.*, 4. 59-73, 1870, 1866.

Hochstetter, F. Von. Geological evolution of South-East Asia, *Clarendon Press, London*, 368 pp., 1869.

Hyndman, R. D., M. Yamano, D. A. Oleskevich. The seismogenic zone of subduction thrust faults, *The Island Arc*, 6, pp. 244-260, 1997.

Ishii, M., P. M. Shearer, H. Houston, and J.E. Vidale. Extent, duration, and speed of the 2004 Sumatra-Andaman earthquake imaged by the Hi-Net array, *Nature*, 435, pp. 933-936, 2005.

Iyengar, R. N., D. Sharma, and J. M. Siddiqui. Earthquake history of Indian medieval times, *Indian. Jour. Hist. Sci.*, 34, pp. 181-237, 1999.

Jade, S., M. B. Ananda, P. D. Kumar and S. Banerjee. Co-seismic and post-seismic displacements in Andaman and Nicobar Islands from GPS measurements, *Current Science*, 88, 1980-1984, 2005.

Jain, S. K., C. V. R. Murty, D. C. Rai, J. N. Malik, A. R. Sheth, A. Jaiswal, S. A. Sanyal, H. B. Kaushik, P. Gandhi, G. Mondal, S. R. Dash, J. S. Sodhi, and G. S. Kumar. The great Sumatra Earthquake and Indian Ocean tsunami of December 26, 2004, Report 3: The effects in mainland India and in the Andaman-Nicobar Islands, *EERI Special Earthquake Report*, April 2005, 112, 2005.

Jhingran, A. G. A note on an earthquake in the Andaman Islands (26^{th} June 1941), *Rec. Geol. Sur. Ind.*, 82, pp. 300-307, 1953.

Kanamori, H. The energy release in great earthquakes, *Jour. Geophys. Res.*, 82, 20, pp. 2981-2987, 1977.

Kanamori H., and E. E. Brodsky. The physics of earthquakes, Reports on progress in Physics, *Institute of Physics Publishing*, 67, pp. 1429- 1496, 2004.

Kanamori, H., and K. C. McNally. Variable rupture mode of the subduction zone along the Ecuador-Colombia coast, *Bull. Seis. Soc. Am.*, 72, 4, pp. 1241-1253,1982.

Karunakaran, C., K. K. Ray, C. R. Sen, S. S. Saha, S. K. Sarkar. Tertiary sedimentation in the Andaman-Nicobar geosyncline, *Jour. Geol. Soc. Ind.*, 9, pp. 32-39, 1968.

Karunakaran, C., K. K. Ray, C. R. Sen, S. S. Saha, S. K. Sarkar. Geology of Great Nicobar Island, *Jour. Geol. Soc. Ind.*, 16, pp. 135-142, 1975.

Kayal, J. R., S. G. Gaonkar, G. K. Chakkraborty, and O. P. Singh. Aftershocks and seismotectonic implications of the 13 September 2002 earthquake (Mw 6.5) in Andaman sea basin, *Bull. Seis. Soc. Am.*, 94, pp. 326-333, 2004.

Kayenne, H., Y. Ikeda, T. Echigo, M. Shishikura, T. Kamataki, K. Satake, J. N. Malik, S. R. Basir, G. K. Chakrabortty, and A. K. G. Roy. Coseismic and post seismic creep in the Andaman Islands associated with the 2004 Sumatra-Andaman eartquake, *Geophys. Res. Lett.*, 34, doi: 10.1029/2006GL028200, 2007.

Kelleher, J., and W. McCann. Buoyant zones, great earthquakes, and unstable boundaries of subduction, *Jour. Geophys. Res.*, 89, pp. 10233-10248, 1976.

Kennett, B. L. N., and P. R. Cummins. The relationship of seismic source and subduction zone structure for the 2004 December Sumatra-Andaman eartquake, *Earth. Planet. Sci. Lett.*, 239, pp. 1-8, 2005.

King, R., and Y. Bock. Documentation for the GAMIT GPS analysis program, v.10.2, *Massachusetts Institute of Technology*, 2005.

Kreemer, C., W. E. Holt, and A. J. Haines. An integrated global model of present-day plate motions and plate boundary deformation, *Geophys. Jour. Int.*, 154, pp. 8-34, 2003.

Kruger, F. and Ohrnberger, M. Tracking the rupture of the Mw=9.3 Sumatra earthquake over 1150km at teleseismic distance. Nature, 435, 2005.

Kumar, K. V., T. R. Martha, P. S. Roy. Detection of volcanic eruption in Barren Island using IRS P6 AWiFS data, *Cur. Sci.*, 91, 6, pp. 752-753, 2006.

Lallemand, S., A. Heuret, and D. Boutelier. On the relationships between slab dip, back-arc stress, upper palte absolute motion, and crustal nature in subduction zones, *Geochem. Geophys. Geosys.*, 06, Q09006, doi:10.1029/2005GC000917, 2005.

Lay, T., H. Kanamori, C. J. Ammon, M. Nettles, S. N. Ward,, R. Aster, S. L. Beck, S. L. Bilek, M. R. Brudzinski, R. Butler, H. R. DeShon, G. Ekstorm, K. Satake, and S. Sipkin. The Great Sumatra-Andaman earthquake of 26 December 2004, *Science*, 308, pp. 1127-1133, 2005.

Lay, T., H. Kanamori,and L. Ruff. An asperity model of large earthquake sequences, *Earthquake Prediction: An International Review, Maurice Ewing Ser.*, 4 , pp. 579-592, 1981.

Le Dain, A. Y., Tapponnier, P. and Molnar, P. Active faulting and tectonics of Burma and surrounding regions, *Jour. Geophys. Res.*, 89:453-472, 1984.

Liu, C. S., J. R. Curray, and J. M. McDonald. New constraints on the tectonic evolution of the Eastern Indian Ocean, *Earth. Planet. Sci. Lett.*, 65, pp. 331-342, 1983.

Liu, P. L.-F., P. Lynett, H. Fernando, B. E. Jae, H. Fritz, B. Higman, R. Morton, J. Go, and C. Synolakis. Observations by the International Tsunami Survey Team in Sri Lanka, *Science*, 308, 1595, 2005.

Lomax. A. Rapid estimation of rupture extent for large earthquakes: Application to the 2004, M9 Sumatra-Andaman mega thrust, *Geophys. Res. Lett.*, 32, L10314, doi:10.1029-2005GL0022437, 2005.

Lu, Z., M., Wyss, and H. Pulpan. Details of stress directions in the Alsaka subduction zone from fault plane solutions, *Jour. Geophys. Res.*, 102, B3, pp. 5385 - 5402, 1997.

Malik, J. N., and C. V. R. Murty. Landscape changes in Andaman and Nicobar Islands (India) due to M_W9.3 tsunamigenic Sumatra earthquake of 26 December 2004, *Cur. Sci.*, 88, pp. 1384-1386, 2005.

Mallet, F. R. Some early allusions to Barren Island, with a few remarks thereon, *Mem. Geol. Surv. India.*, 28, pp. 22-34, 1895.

Malod, J. A., Komar karta, M. O. Beslier, and Jr. M. T. Zen. From normal to oblique subduction: Tectonic relationships between Java and Sumatra, *Jour. South East Asia. Earth. Sci.*, 12, pp. 85-93, 1995.

Maung, H. Transcurrent movments in the Burma-Andaman region, *Geology*, 15, p.911-912, 1987.

McCaffrey, R. Active tectonics of the eastern Sunda and Banda arcs, *Jour. Geophys. Res.*, 93, B12, 15,163-15,182, 1988.

McCaffrey, R., P. C. Zwick, Y. Bock, L. Prawirdodirdjo, J. F. Genrich, C.W. Stevens, S. S. O. Puntodewo, and C. Subarya. Strain partitioning during oblique plate convergence in northern Sumatra: Geodetic and seismologic constraints and numerical modeling, *Jour. Geophys. Res.*, 105, B12, 28,363- 28,376, 2000.

McKenzie, D. P. The relationship between fault palne sloutions for earthqaukes and directions of the principal stresses, *Bull. Seis. Soc. Am.*, 59, pp. 591-601, 1969.

Meltzner, A. J., K. Sieh, M. Abrams, D. C. Agnew, K. W. Hudnut, J. Avouac, and D.H.Natawidjaja. Uplift and subsidence associated with the great Aceh- Andaman earthquake of 2004, *Jour. Geophys. Res.*, 111, B02407, doi:10.1029-2005JB003891, 2006.

Michell, G. W., Y. Q. Yu, S. Y. Zhu, C. Reigber, M. Becker, e. reinhart, W. Simons, B. A. C. Ambrosius, C. Vigny, N. Chamot-Rooke, X. Le Pichon, P. Morgan and S. Matheussen. Crustal motion and block behaviour in SE-Asia from GPS measurments, *Earth. Planet. Sci. Lett.*, 187, pp. 239-244, 2001.

Mishra, O. P., J. R. Kayal, G. K. Chakrabortty, O. P. Singh, and D. Ghosh. Aftershock Investigation in the Andaman-Nicobar Islands of India and Its Seismotectonic Implications., *Bull. Seis. Soc. Am.*, 97, S71-S85, 2007.

Mitchell, A. H. G. and W. S. McKerrow. Analogous evolution of the Burma orogen and the scottish Caldonides, *Geol. Soc. Am. Bull.*, 86, pp. 305-315, 1975.

Mukhopadyay, M. Seismotectonics of subduction and back-arc rifting under the Andaman Sea, *Tectonophysics*, 108, pp. 229-239, 1984.

Mukhopadyay, M. On earthquake focal mechanism studies for the Burmese arc, *Cur. Sci.*, 62, pp. 72-85, 1992.

Mukhopadyay, M., and S. Dasgupta. Deep structure and tectonics of the Burmese arc: constraints from earthquake and gravity data, *Tectonophysics*, 149, pp. 299-322, 1988.

Mukhopadyay, M. Gravity anomalies and deep structure of the Andaman arc, *Mar. Geophys. Res.*, 9, pp. 197-210, 1988.

Mukhopadyay, M., and M. R. Krishna. Gravity field and deep structure of the Bengal fan and its surrounding continental margins, northeast Indian Ocean, *Tectonophysics*, 186, pp. 365-386, 1991.

Murray, J. R., and P. Segall. Testing time-predictable earthquake recurrence by direct measure of strain accumulation and release, *Nature*, 419, 287-291, 2002.

Nanayama, F., K. Satake, R. Furukawa, K. Shimokawa, B. F. Atwater, K. Shigeno, and S. Yamaki. Unusually large earthquakes inferred from tsunami deposits along the Kuril trench, *Nature*, 424, pp. 660-663, 2003.

Natawidjaja, D., K. Sieh, S. Ward, H. Cheng, R. L. Edwards, J. Galetzka, and B. Suwargadi. Paleogeodetic records of seismic and aseismic subduction from central Sumatran microatolls, Indonesia, *Jour. Geophys. Res.*, 109, doi 10.1029/2003JB0002398, 2004.

Natawidjaja, D., K. Sieh, M. Chlieh, J. Galetzka, B. W. Suwargadi, H. Cheng, R. L. Edwards, J. P. Avouac, and S. N. Ward. Source parameters of the gret Sumatra megathrust earthquakes of 1797 and 1833 inferred from coral microatolls, *Jour. Geophys. Res.*, 111, doi 10.1029/2005JB004025, 2006.

Nelson, A. R., I. Shennan and A. J. Long. Identifying coseismic subsidence in tidal-wetland stratigraphic sequences at the Cascadi subduction zone of western North America, *Jour. Geophys. Res.*, 101, pp. 6115-6135, 1996.

Neetu, S., I. Suresh, R. Shankar, D. Shankar, S. S. C. Shenoi, S.R. Shetye, D. Sundar, B. Nagarajan. Comment on "The Great Sumatra-Andaman Earthquake of 26 December 2004", *Science*, 310, 5753, p. 1431, doi: 10.1126/science.1118950, 2005.

Ni, J. F., Guzman-Speziale, M. Bevis, W. E. Holt, T. C. Wallace, and W. Seager. Accretionary tectonics of Burma and three dimensional geometry of the Burma subduction zone, *Geology*, 17, pp. 68-71, 1989.

Ni, S., H. Kanamori, and D. Helmberger. Energy radiation from the Sumatra earthquake, *Nature*, 434, p. 582, 2005.

Ohtake, M., T. Matumoto, and G. Latham. Evaluation of the forecast of the 1978 Oaxaca, Southern Mexico earthquake based on a precurusory seismic quiescence. In *Earthquake Prediction, an International Review.*, M. Eving Ser. 4, ed. D. Simpson and P. Richards. Washington, D. C.: American Geophysical Union, pp. 53-62, 1981.

Okada, Y. Surface deformation due to shear and tensile faults in an elastic half space, *Bull. Seis. Soc. Am.*, 75, pp. 1135-1154, 1985.

Oldham, R. D. Note on the geology of the Andman islands, *Rec. Geol. Surv. India*, 17(2), pp. 47-53, 1884.

Oritz, M., R. Bilham. Source area and rupture parameters of 31 December 1881Mw = 7.9 Car Nicobar earthquake from tsunamis recorded in the Bay of Bengal, *Jour. Geophys. Res.*, 108, B4, 2215, doi:10.1029-2002JB001941, 2003.

Pacheco, J. F., L. R. Sykes, C. H. Scholz. Nature of seismic coupling along simple plate boundaries of the subduction type, *Jour. Geophys. Res.*, 98, pp. 14133-14159, 1993.

Pal, T., P. P. Chakraborty, T. D. Gupta, and C. D. Singh. Geodynamic evolution of the outer-arc forearc belt in the Andaman Islands, the central part of the Burma-Java subduction complex, *Geo. Mag*, 140, 3, pp. 289-307, 2003.

Park J., T. R. A. Song, J. Tromp, E. Okal, S. Stein, G. Roult, E. Clevede, G. Laske, H. Kanamori, P. Davis, J. Berger, C. Braitenberg, M. Van Camp, X. Lei, H. Sun, H. Xu, and S. Rosat. Earth's Free Oscillations Excited by the 26 December 2004 Sumatra-Andaman Earthquake, *Science*, 308, pp. 1139-1144, 2005.

Paul, D. D. and H. M. Lian. Offshore basins of southwest Asia-Bay of Bengal to South Sea, *Proc. 9th World Petro. Cong.*, 3, pp. 1107-1121, 1975.

Paul, J., R. Burgmann, V. K. Gaur, R. Bilham, K. M. Larson, M. B. Ananda, S. Jade, M. Mukul, T. S. Anupama, G. Satyal and D. Kumar. The motion and active deformation of India, *Geophys. Res. Lett.*, 28, 4, pp. 647-650, 2001.

Peter, G., L. A. Weeks, R. E. Burns. A reconnaisance geophysical survey in the Andaman Sea and across the Andaman arc/back-arc basin, Salin subbasun, Myanmar (Burma), *Am. Assoc. Petro. Geol. Bull.*, 82, pp. 1837-1856, 1966.

Plafker, G. Alaskan earthquake of 1964 and Chilean earthquake of 1960-Implications for arc tectonics, *Jour. Geophy. Res.*, 77, pp. 901-925, 1972.

Polachan, S., and A. Racey. Stratigraphy of the Mergui Basin, Andaman Sea: implications for petroleum exploration, *Jour. Petrol. Geol.*, 17, pp. 373-406, 1994.

Radhakrishna, M., and T. D. Sanu. Shallow seismicity, stress distribution and crustal deformation pattern in the Andaman-West Sunda arc and Andaman Sea, northeastern Indian Ocean, *Jour. Seis.*, 6, pp. 25-41, 2002.

Rajendran, K., and H. K. Gupta. Seismicity and tectonic stress field of a part of the Burma-Andaman-Nicobar arc, *Bull. Seis. Soc. Am.*, 79, pp. 989-1005, 1989.

Rajendran, C. P., A. Earnest, K. Rajendran, R. Devdas, and S. Kesavan. The 13 September 2002 North Andaman (Diglipur) earthquake: An analysis in the context of regional seismicity, *Cur. Sci.*, 84, 7, pp. 919-924, 2003.

Rajendran, C. P., K. Rajendran, R. Anu, A. Earnest, T. Machado, P. M. Mohan, and Jeffrey Freymueller. Crustal deformation and seismic history associated with the 2004 Indian Ocean earthquake: A perspective from the Andaman-Nicobar islands, *Bull. Seis. Soc. Am.*, 97, pp 174-191, 2007.

Raju, K. K. A., T. Ramprasad, P. S. Rao, B. R. Rao, J. Varghese. New insights into the tectonic evolution of the Andaman basin, northeast Indian Ocean, *Earth Planet. Sci. Lett.*, 221, pp. 145-162, 2004.

Raju, K. K. A. Three-phase tectonic evolution of the Andaman back-arc basin, *Cur. Sci.*, 89, 11, pp. 1932-1937, 2005.

Rao, N. P., and M. R. Kumar. Uplift tectonics of the Shillong Plateau, northeast India, *Jour. Phys. Earth.*, 45, pp. 167-176, 1997.

Reid, H.F. The Mechanics of the Earthquake, The California Earthquake of April 18, 1906, *Report of the State Investigation Commission, 2, Carnegie Institution of Washington, Washington, D.C.*, pp. 16-28, 1910.

Rhie, J., D. Dreger, R. Burgmann, and B. Romanowicz. Slip of the 2004 Sumatra-Andaman Earthquake from Joint Inversion of Long-Period Global Seismic Waveforms and GPS Static Offsets, *Bull. Seis. Soc. Am.*, 97, S115-S127, 2007.

Rink, P. H. Die Nicobar Inseln. Eine Geographische Skizze, mit speciieller Beruksichtigung der Geognosie - translated sections, Kopenhagen, *Records of Government of India, LXXVII*, p. 540, 1847.

Rodolfo, K. S. Bathymetry and marine geology of the Andaman basin, and tectonic implications for southeast Asia, *Geol. Soc. Am. Bull.*, 80, pp. 1203-1230, 1969a.

Rodolfo, K. S. Sediments of the Andaman basin northeastern Indian Ocean, *Mar. Geol.*, 7, pp. 371-4-2, 1969b.

Rogers, R. E. Memorandum on the earthquake of the 31st December 1881 and the great sea-waves resulting threform, as shown in the diagrams of tidal observatories in the Bay of bengal, in *General Report on the Operations of the Survey of India 1881-1882.*, 70-73, Government Printing Office, Calcutta, 1883.

Roy, T. K., and N. N. Chopra. Wrench faulting in Andaman fore-arc basin, India, *Proc. Offshore Tech. Conf.*, 19, pp. 393-404, 1987.

Ruff, L., and H. Kanamori. Seismicity and the subduction process, *Phys. Earth Planet. Inter.*, 23, pp. 240-252, 1980.

Savage, J.C. A dislocation model of strain accumulation and release at a subduction zone, *Jour. Geophy. Res.*, 88, B6, pp. 4984-4996, 1983.

Scholz, C. H. The Mechanisms of Earthquakes and Faulting, *Cambridge Univ. Press*, p. 439, 1990.

Scholz, C. H. Earthquakes and friction laws, *Nature*, 391, pp. 37-42, 1998.

Schwartz, S. Y. Noncharacteristic behaviour and complex recurrence of large subduction zone earthquakes, *Jour. Geophys. Res.*, 104, B10, pp. 23,111-23,125, 1999.

Shen, Z. K., C. Zhao, A. Yin, Y. Li, D. D. Jackson, P. Fang, and D. Dong. Contemporary crustal deformation in east Asia constrained by Global positioning system measurments, *Jour. Geophys. Res.*, 105, pp. 5721 - 5734, 2000.

Sieh, K., and D. Natawindjaja. Neotectonics of the Sumatra fault, Indonesia, *Jour. Geophys. Res.*, 105, B12, pp. 28,295-28,326, 2000.

Simones, W. J. F., B. A. C. Ambrosius, R. Noomen, D. Angermann, P. wilson, M. Becker, E. Reinhart, A. Walpersdorf, and C. Vigny. Observing plate motions in SE Asia: geodetic results of the GEODYSSEA project., *Geophys. Res. Lett.*, 26, pp. 2081-2084, 1999.

Sinvhal, H., K. N. Khattri, K. Rai, and V. K. Gaur. Neo-tectonics and timespace seismicity of the Andaman-Nicobar region, *Bull. Seis. Soc. Am.*, 68, 2, pp. 399-409, 1978.

Sewell, R. B. S. The geography of the Andaman sea basin, *Jour. Asia. Soc. Bengal*, 9, pp 1-26, 1925.

Shimazaki, K., and T. Nakata. Time-predictable recurrence for large earthquakes, *Geophys. Res. Lett.*, 7, 279-282, 1980.

Singh, S. C., and Sumatra-Aftershocks team. Sumatra earthquake research indicates why rupture propagated northward, *EOS Trans., AGU 86, Fall Meet. Suppl.*, 497, 502, 2005.

Spence, W. Slab pull and the seismotectonics of the subducting lithosphere, *Rev. Geophys.*, 25, 1, pp. 5-69, 1987.

Srivastava, H. N., and H. M. Chaudhury. Seismcity and focal mechanism of earthquakes in Andaman Islands, *Mausam*, 30, 23, pp. 213-220, 1979.

Stein, S., and E. A. Okal. Speed and size of the Sumatra earthquake, *Nature*, 434, pp. 581-582, 2005.

Stern, R. J. Subduction zones, *Rev. Geophys.*, 40, 4, doi:10.1029-2001RG000108, 2002.

Subarya, C., M. Chlieh, L. Prawirodirdjo, J.-P. Avouac, Y. Bock, K. Sieh, A. Meltzner, D. H. Natawidjaja, and R. McCaffrey. Plate boundary deformation of the great Sumatra-Andaman earthquake, *Nature*, 440,doi:10.1038/nature04522, 2006.

Surendara Kumar. Geodynamics of Burma and Andaman-Nicobar region on the basis of tectonic stresses and regional seismicity, *Tectonophysics*, 79, pp. 75-95, 1981.

Temple, R.C. The diaries of Streyansham Master:1675-1680, The Indian Record Series, *John Murray, London*, 1911.

Thakkar, M. G. Preliminary documentation of ground deformation and tsunami effects at Andaman and Nicobar Islands and eastern coast of India, *Project completion report submitted to the Department of Science and Technology*, 77 pp, 2005.

Thakkar, M. G., and B. Goyal. Historic submergence and tsunami destruction of Nancowry, Kamorta, Katchal and Trinket Islands of Nicobar: consequences of 26 December 2004 Sumatra-Andaman earthquake, *Cur. Sci.*, 90, pp. 989-994, 2006.

Thatcher,W., J. B. Rundle. A model for earthquake cycle in underthrust zones, *Jour. Geophys. Res.*, 84, B10, pp. 5540-5556, 1979.

Tipper, G. H. The geology of the Andaman Islands, *Mem. Geol. Soc. Ind.*, 35, pp. 1-269, 1911.

Titov, V., A. B. Rabinovich, H. O. Mofjeld, R. E. Thomson, and F. I. Gonzalez. The Global Reach of the 26 December 2004 Sumatra Tsunami, *Science*, 309, pp. 2045-2048, 2005.

Tsai, V. C., M. Nettles, G. Ekstorm, and A. M. Dziewonski. Multiple CMT source analysis of the 2004 Sumatra earthquake, *Geophys. Res. Lett.*, 32, L17304,doi:10.1029-2005GL023813, 2005.

Uyeda, S., and H. Kanamori. Back-arc opening and the mode of subduction, *Jour. Geophys. Res.*, 84, pp.1049-1061, 1979.

Van Linschoten. Itinerario voyage ofte Schipvaert, *Van Jan Huygen Van Lindschoten naer ooste ofte Portugaels Indien*, Amsterdam, 1595.

Venkataraman, A., and H. Kanamori. Observational constraints on the frac93 ture energy of subduction zone earthquakes, *Jour. Geophys. Res.*, 109, B05302, doi:10.1029-2003JB002549, 2004.

Verma, R. K., M. Mukhopadhyay, and N. C. Bhuin. Seismicity, Gravity and ectonics in the Andaman Sea, *Jour. Phys. Earth*, 26,Suppl., pp. 233-248, 1978.

Vigny, C., A. Socquet, C. Rangin, N. Chamot-Rooke, M. Pubellier, M. N., Bouin, G. Bertrand, and M. Becker. Present-day crustal deformation around Sagaing fault, Myanmar, *Jour. Geophys. Res.*, 108, doi: 10.1029/2002JB001999, 2003.

Vigny, C.,W. J., F. Simons, S.Abu, R. Bamphenyu, C. Satirapod, N. Choosakul, C. Subarya, A. Socquet, K. Omar, H. Z. Abidin, and B. Ambrosius, A. C. Insight into the 2004 Sumatra-Andaman earthquake from GPS measurements in southeast Asia., *Nature*, 436, pp. 201-206, 2005.

Wang, K., R.Wells, S.Mazzotti, R. D. Hyndman, and T. Sagiya. A revised dislocation model of interseismic deformation of the Cascadia subduction zone, *Jour. Geophys. Res.*, 108, B1, doi:10.1029-2001JB001227, 2003.

Weeks, L. A., Harbison, R. N., Peter, G. Island arc system in the Andaman Sea, *Am. Assoc. Petrol. Geol.*, 51, pp. 1803-1815, 1967.

Wegner, A. The origin of continents and oceans, *Doveeer Publications, New York*, 246 pp., 1966.

Zoback, M. L. and M. D. Zoback. Tectonic stress field of the continental United States, in L. Palaiser and W. Mooney, Editors, Geophysical Framework of Continental United States, *Geol. Soc. Am. Mem.*, 1987.

Annexure

Papers published from this doctoral work in peer reviewed journals:-

C.P. Rajendran, Kusala Rajendran, Anu. R, Anil Earnest, Terry Machado, and Jeffrey Freymueller. 2006. Crustal deformation and seismic history associated with the 2004 Indian Ocean earthquake: A perspective from the Andaman-Nicobar Islands, Bull. Seism. Soc. America, 97, pp. 174-190, 2007.

Anil Earnest, Rajendran, C.P., Rajendran, K., Anu. R and Arun, G.M. 2005. Near-field observations on the co-seismic deformation associated with the 26 December 2004 Andaman-Sumatra earthquake, Current Science,Vol.89, No.7, 1237-1244.

Rajendran, K., Rajendran, C.P. and Anil Earnest. 2005. The great Sumatra-Andaman earthquake of 26 December 2004, Current Science, Vol. 88, No.1, pp. 11-12.

C.P.Rajendran, Kusala Rajendran, B.P.Baruah, S.Baruah and Anil Earnest. Interpreting the style of faulting and paleoseismicity associated with the 1897 Shillong, northeast India, earthquake, Tectonics, 23, 2004.

C.P.Rajendran, Anil Earnest, Kusala Rajendran, R.Devdas and Sreekumari Kesavan.2003, The 13th September 2002 North Andaman (Diglipur) earthquake: An analysis in the context of regional seismicity, Current Science, Vol.84, No.7, 10 April.

Abstracts Submitted for Conferences/Seminars from this doctoral work (2004-2006)

C P. Rajendran, Kusala Rajendran, Anil Earnest, Anu R, and Jeffrey Freymueller 2006. The deformational characteristics and the recurrence pattern of the December 26 2004 Indian Ocean earthquake, Chapman conference on Active tectonics and seismic potential of Alaska Alyeska Resort, Girdwood, Alaska, USA, 11-14 May 2006.

C.P. Rajendran, Kusala Rajendran, Anil Earnest, Anu, R and Terry Machado. 2006. The style of crustal deformation and seismic history associated with the 2004 Indian Ocean earthquake: A perspective from the Andaman-Nicobar Islands, AOGS, Singapore, 2006.

Rajendran, C.P., Rajendran, K and Anil Earnest. 2005. The spatio-temporal context of the December 26, 2004 Aceh-Andaman earthquake: AGU Fall meeting, December 05-09, 2005 at San Francisco, USA.

Rajendran, K., Rajendran, C.P., Anil Earnest and Jeff Freymueller. 2005. Co-seismic ground level changes associated with the great Andaman-Sumatra earthquake: A tour from Nicobar to North Andaman: AGU Fall meeting, December 05-09, 2005 at San Francisco, USA.

Anil Earnest, Rajendran, C.P., Rajendran, K., Anu, R and Ratheesh R. 2005. Post-seismic Deformation Measurements from the Andaman and Nicobar Islands, AGU Fall meeting, December 05-09, 2005 at San Francisco, USA.

Rajendran, C.P., Rajendran, K and Anil Earnest. 2005. Spatial and temporal context of the December 26, 2004 Sumatra-Andaman Earthquake: Accepted for the 2nd AOGS (Asia Oceania Geo-sciences) Meeting 2005, (20-24 June 2005), Suntec, Singapore.

Anil Earnest and Rajendran, C.P. 2005. The deformation characteristics along the Andaman-Nicobar arc associated with the December 26, 2004 megathrust earthquake: insights from GPS data : Accepted for the 2nd AOGS (Asia Oceania Geo-sciences) Meeting 2005, (20-24 June 2005), Suntec, Singapore.

Appendix A

Introduction

Geodetic measurements provide very accurate determinations of positions of points on the surface of Earth. When measured over a few years, the change in positions of points are representative of strain accumulation in a region. The rapid growth of usage of GPS devices over the last decade has occurred primarily because of comparatively low cost and high accuracy of GPS receivers.

A.1 The Global Positioning system (GPS) - a brief overview

GPS is a passive, all weather, 24-hour global navigation satellite system (GNSS) operated and maintained by the Department of Defense, United States. It consists of a nominal constellation of 24 satellites in high altitude orbits. The whole system consists of three distinct segments: the space segment (satellites), the control segment (ground tracking and monitoring stations), and the user segment (air, land, and seabed receivers). The space segment consists of all GPS satellites in orbit, at an average altitude of 20,200 km and have 11-hour 58-minute orbital periods. Other-than GPS, Russia maintains a similar global orbiting satellite navigation system (GLONASS) and European GALILEO, a proposed 30 satellite system. Control segment consists of master control stations and six monitoring stations located over the world and the user segment represents the ground based GPS receiver units that process the satellite signals and compute the position and/or velocity of the user. Each satellite transmits signals ranging signals on two L-band frequencies, designated as L1 and L2. The L1 carrier frequency is 1575.42Mhz and has a wavelength of approximately 19 cm. The L2 carrier frequency is 1227.60 Mhz and has a wavelength of approximately 24 cm. The L1 signal is modulated with a 1.023MHz Coarse/Acquisition (C/A) code and a 10.23 MHz precision code P-code. Both codes can be used to determine the range between the user and satellite. A 50 Hz navigation message is also transmitted on both the P(Y)-code and C/A-code. This message contains satellite clock bias data, satellite ephemeris data, orbital information, ionospheric signal propagation correction data, health and status of satellites, satellite almanac data for entire constellation, and other general information.

A.2 GPS observables

A.2.1 The pseudorange

The GPS receiver measures the distance (pseudorange) between the satellite and the antenna by measuring the time the signal takes to propagate from the satellite to the receiver. The psuedorange is this time offset multiplied by the speed of light. The pseudorange is biased by the lack of tie synchronization between

the clock in the GPS satellite and the clock in the GPS receiver. Other bias effects include the ionosphere and troposphere delay, multipath and receiver noise.The receiver coordinates are hidden in the geometric range 'p'.

A.2.2 Carrier phase

A more precise observable than the pseudorange is the phase of the received carrier with respect to the phase generated by an oscillator in the GPS receiver. The difference between the received carrier and the receiver generated one is called the carrier beat phase. The problem is that the GPS receiver cannot distinguish one cycle of a carrier from another. The receiver measures the fractional phase, and keeps track of changes to the phase. The initial phase is undetermined, or ambiguous, by an integer number of cycles 'N'.

A.2.3 Linear combinations

We can form what are known as between receivers (or between satellites) differences to obtain new observable with significantly reduced errors.

The between receivers single difference (two different receivers tracking the same satellite) - eliminates the satellite clock offset. The between satellites single difference (one receiver tracking two satellites) - eliminates the receiver clock offset.

A.3 GPS error budget

Both systematic errors (biases) and random noise affect the code pseudoranges 'p' and phase pseudoranges 'phi'. The error sources can be classified into three groups.

A.3.1 Orbital errors/Clock Bias/Measurement Noise

As mentioned earlier, GPS signals contain information about the ephemeris (orbital position) errors, and about the rate of clock drift for the broadcasting satellite. The data concerning ephemeris errors may not exactly model the true satellite motion or exact rate of clock drift. Distortion of the signal by measurement noise can further increase positional error. The disparity in ephemeris data can introduce 1-5 meters of positional error, introduce 0-10 meters of positional error.

A.3.2 Signal propagation

The ionosphere and troposphere both refract the GPS signals. This causes the speed of the GPS signal in the ionosphere and the troposphere to be different from the speed of the GPS signal in space. Therefore, the distance calculated from signal speed x time will be different for the portion of the GPS signal path that passes

through the ionosphere and troposphere and for the portion that passes through space.

A.3.3 Multipath

A GPS signal bouncing off a reflective surface prior to reaching the GPS receiver antenna is referred to as multipath. Because it is difficult to completely correct multipath error, even in high precession GPS units, multipath error is a serious concern

A.3.4 Selective Availability

Ephemeris errors should not be confused with selective availability (SA), which is the intentional alteration of the time and ephemeris signal by the Department of Defense, United States. Recently (January 2000), they turned off this alteration. fortunately, positional errors caused by SA can be removed by differential correction.

A.3.5 Dilution of Precision (DOP)

The UERE is mapped into the computed position by a geometrical factor scaled DOP. The DOP is a mathematical function involving the relative coordinates of the receiver and the satellite and can be easily computed for a particular satellite arrangement. the more spread out the satellites are in th sky, the smaller the DOP value. A typical value for horizontal dilution of precision (HDOP), assuming that a receiver is processing the signals of 4 satellites only is 2.0.

A.4 GAMIT/GLOBK GPS data processing schema

GAMIT is a comprehensive GPS analysis package developed by MIT and Scripps Institute for the estimation of three dimensional relative positions of ground station and satellite orbits. The primary output of GAMIT is a loosely constrained solution file (H-file) of parameter estimates and covariances that can be passed to GLOBK for combinations of data to estimate station positions, velocities, orbital and Earth orientation parameters. GAMIT is composed of distinct modules, which prepare the data for processing.

A.4.1 Computing loosely constrained solutions using GAMIT modules

First an estimate of the GPS station coordinate for each day in a loosely constrained frame is made (h-file). That means the coordinates of the tracking sites, not the satellites are tightly constraint and the orbits of GPS satellites and station coordinates are not in a well determined reference frame. Baseline lengths are

determined very precisely in the loosely constrained solution and the entire GPS network and constellation can be rotated and translated as a rigid body.

A.4.2 Combining global and local quasi observations GLOBK

To use the coordinates derived from the GAMIT solutions, all the loosely constrained solution are transformed into a consistent reference frame so that deformation rates can be derived from the time series of the station coordinates. The reference frame defines the origin, scale and orientation of our geodetic coordinates. A reference frame is realized through the coordinate and the covariance of a number of reference stations. The information about the reference stations of the adopted geodetic reference (in this work the latest realization of ITRF2000) is included by combining the loosely constrained solutions with the local or global h-files. Finally the the reference frame constraints are applied and the deformation velocities of the sites are computed.

A.5 GPS Antenna Calibration

The vertical positions of the phase centers of all GPS antennas show significant elevation dependent motions, which if not modelled make estimated station heights dependent on the elevation cutoff angle of the observation at each station. Accurate and consistent modelling of the Antenna phase centers continues to be one of the most vexing problems in GPS analysis. GAMIT computes the instantaneous position of an antennas phase center from the geodetic monument in three pieces. From station.info configuration file it records the vertical or slant distance from an accessible point on the antenna structure to the monument, and also any horizontal offsets of the center of antenna from the monument deriving from a setup error. Subroutine hi-sub converts this to an IGS specification with respect to an antenna reference point. Information used in this thesis comes from the National Geodetic Survey - Antenna calibration project, where details of antenna reference and dimensions are properly documented.